MANUFACTURE OF FERROFLUID: BASIC ASPECTS AND THE INFLUENCE OF KEY PARAMETERS ON THE PROCESS

by

Laura Lisa Vatta

A dissertation submitted in partial fulfillment of the requirements for the degree of

Master of Engineering (Chemical)

in the Faculty of Engineering, Built Environment and Information Technology
University of Pretoria
Pretoria

October 2002

Supervisor:
Prof. P. de Vaal

ABSTRACT

Title: Manufacture of ferrofluid: Basic aspects and the influence of key parameters on the process

Author: Laura Lisa Vatta

Supervisor: Prof. P. de Vaal

Department: Faculty of Engineering, Built Environment and Information Technology

Degree: Master of Engineering (Chemical)

Keywords: ferrofluid, ferromagnetic fluid, precipitation, saponification, peptization, magnetite, sedimentation funnels, wet high intensity magnetic separator, surfactant stabilisation, mathematical optimisation

A ferromagnetic liquid or ferrofluid refers to a stable colloidal dispersion or suspension of single domain magnetic particles coated by a surfactant and suspended in a carrier liquid. The ferrofluid as referred to in this dissertation is produced in three main stages: oxide precipitation and magnetite formation, saponification of the surfactant and peptization of the coated particles. Magnetite (Fe_3O_4), a ferrimagnetic material, is produced in a precipitation reaction from ammonium hydroxide and iron salt solutions. The magnetite is coated with oleic acid as the surfactant and is suspended in kerosene as the carrier liquid.

From this brief description, it appears that the process for the synthesis of ferrofluids is quite simple. However, some of the basic aspects and key manufacturing parameters are not understood fully. In this dissertation an attempt is made to explain and offer a more detailed understanding of some of the steps in the manufacture of ferrofluid.

Magnetite formation is vital for the production of ferrofluids. The formation and transformation pathways of iron oxides required to form magnetite are, however, more complex. There are many pathways that could lead to the formation of incorrect species. Possible mechanisms for the formation of magnetite are discussed. Parameters that could affect the production of magnetite are discussed and an investigation conducted to confirm what the preferred conditions are for its production. The investigations appear to provide evidence that magnetite is produced through the formation of green rust complexes. The green rust complexes are produced from ferrihydrites and iron (II) ions. Magnetite is then produced by the dehydroxylation of the green rusts. The following parameters favour the formation of magnetite: high pH, rapid addition of ammonium hydroxide solution, a rapid stirrer speed and sufficient ammonium hydroxide to ensure that the pH is in the correct range for the dehydroxylation of green rusts and for the prevention of formation of non-magnetic oxides.

After precipitation, the aqueous solution in which the precipitate is suspended contains dissolved salts. Often, in the production of ferrofluids in the laboratory, a third phase has been produced. It is suspected that organic-inorganic phase interactions that may cause this third phase are promoted in some cases by the salts in the mixture containing the precipitate. This may hinder the final organic/aqueous phase separation. In addition, the salts in solution may increase the viscosity of the product. It would therefore be beneficial to wash the precipitate to remove these salts. For water-based ferrofluid production (where the carrier liquid is water), concentration of the magnetite suspension is essential for the production of a fluid of suitable magnetic properties. Washing is also important to ensure stability of the water-based fluids.

Two methods for the washing of the precipitate were suggested. The first makes use of what have been termed sedimentation funnels. Precipitate is fed to four cone-shaped vessels in series. The funnels are plastic containers around which copper coils are wound. A direct current is passed through the coils thus generating a magnetic field in the interior of the funnel. When placed in the funnel and exposed to the magnetic field, the magnetite is attracted towards the region of greatest magnetic field and becomes concentrated at the base of the funnel. Wastewater leaves the funnels via an overflow. Computational fluid dynamics (CFD) was used to investigate the suitability of the funnel design and to determine whether the funnel configuration would ensure that the salts would be washed from the precipitate and that the magnetite would be retained in the funnels. From preliminary results obtained from the CFD model, it appears that the inflowing liquid churns up material that may have settled at the base of the funnel. It was initially recommended that the funnel geometry be modified such that the flow into the funnel does not disturb the particles at the base of the funnel. The second concept that was investigated, namely, the wet high intensity magnetic separator (WHIMS) was found to function more effectively and efforts were focused on this new concept instead.

The procedure used for the WHIMS is analogous to that of deep bed filtration with the magnetic force assisting in particle capture. The WHIMS consists of a funnel shaped vessel containing a magnetisable matrix or mesh and surrounded by a magnet e.g. solenoid electromagnet. Magnetic particles (such as the magnetite) fed to the WHIMS are captured in the matrix when the current to the coils is switched on. The liquid in which the magnetite is contained passes through the vessel. Water can be added to the vessel to wash the magnetite. An investigation was conducted on a WHIMS prototype that was built to determine whether or not it would be suitable for the purposes of washing and concentrating the magnetite. Furthermore, a qualitative estimation of the suitability of three mesh types was performed and suggestions made as to which mesh would be most suitable for use in a process to manufacture ferrofluid on a continuous basis.

The particle size of the magnetite which is one of the most important components of the ferrofluid is critical for fluid stability. Particles must be small enough not to settle or agglomerate as a result of gravitational and magnetic interaction forces. In addition to ensuring that the particle size is correct, the coating of the particles is an important factor for maintaining stability. The coating of particles prevents agglomeration that could occur as a result of Van der Waals interaction forces. An investigation into the optimum quantity of surfactant required for steric stabilisation showed that as the percentage oleic acid increases, the volume of magnetite

remaining suspended above the ferrofluid appears to decrease. This was accompanied by an increase in the saturation magnetisation of the fluids.

In order to achieve a more rapid phase transfer in the peptization stage of the fluid production, heat is required to be input into the system. To obtain the maximum heat transfer at the maximum allowable temperature, the surface area in the column should be at a maximum. Mathematical optimisation using the dynamic trajectory method was applied to the formulation of this problem to determine the optimum dimensions of such a column (diameter, height and glass bead diameter) that would result in maximum heat transfer. Various scenarios were investigated. It was found that in the simple case where a recommended residence time for the mixture and a geometric diameter to height constraint are ignored, the solution converges where the height and diameter of the column are a maximum and the bead diameter is a minimum. When including the residence time considerations and the height to diameter ratio as constraints, various valid solutions were obtained for this problem.

Various aspects and key parameters of ferrofluid manufacture were discussed and investigated in this dissertation. Information was provided regarding the preferred parameters for the formation of magnetite, precipitate washing and concentration, the volume of surfactant required for coating magnetite particles and a suggestion of the optimum method for heat transfer in the peptization reaction. This information clarifies some of the aspects in the production of this intriguing substance.

ACKNOWLEDGEMENTS

I would like to express my sincere gratitude towards

- my supervisor, Prof. de Vaal for his guidance and assistance in the completion of the dissertation,
- my colleagues for their advice on the work and assistance with the editing of the dissertation,
- and very specially to my family and friends for their constant encouragement and support throughout my studies.

Furthermore, I would like to thank DebTech, a division of De Beers Consolidated Mines for its financial support of my studies.

CONTENTS

LIST OF FIGURES

LIST OF TABLES

LIST OF ABBREVIATIONS

CFD	Computational Fluid Dynamics
FHS	ferrohydrostatic separation
VSM	Vibrating Sample Magnetometer
WHIMS	wet high intensity magnetic separator

CHAPTER 1

PROBLEM STATEMENT AND INTRODUCTION

A ferromagnetic liquid or ferrofluid refers to a stable colloidal dispersion or suspension of single domain magnetic particles in a carrier liquid. The suspension of particles is coated by a surfactant and suspended in a carrier liquid. The ferrofluid as referred to in this dissertation is produced in three main stages: oxide precipitation and magnetite formation, saponification of the surfactant and peptization of the coated particles. Figure 1.1 gives the schematic representation of a potential method for manufacturing ferrofluid. Magnetite (Fe_3O_4), a ferrimagnetic material, is produced in a precipitation reaction in reactor 3 from ammonium hydroxide (from storage tank 1) and iron salt (from storage tank 2) solutions. The magnetite is coated with oleic acid (from storage tank 4) as the surfactant and is suspended in kerosene (from storage tank 5) as the carrier liquid in the peptization stage. This occurs in reactor 6. Storage tank 7 is a vessel for housing the final product.

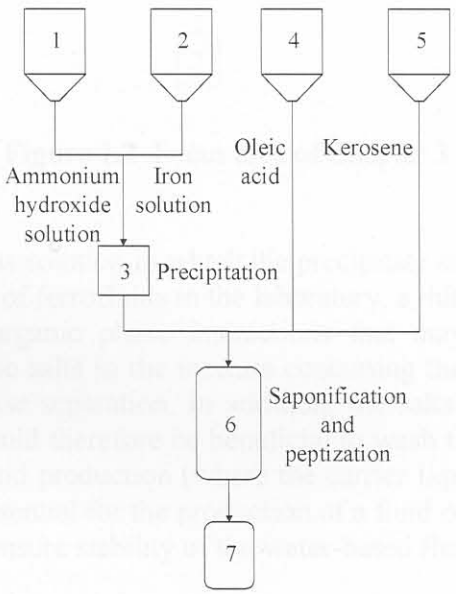

Figure 1.1 Schematic representation of a potential method for manufacturing ferrofluid

From this brief description, it appears that the process for the synthesis of ferrofluids is quite simple. However, some of the basic aspects and key manufacturing parameters are not understood fully. This dissertation attempts to explain and offer a more detailed understanding of some of these aspects.

Magnetite formation is vital for the production of ferrofluids. The formation and transformation pathways of iron oxides required to form magnetite are, however, complex. There are many

pathways that could lead to the formation of incorrect species. In Chapter 3, possible mechanisms for the formation of magnetite are discussed. Parameters that could affect the production of magnetite are discussed and an investigation is then conducted to confirm what the preferred conditions are for the production of magnetite and whether or not these parameters are of importance in ferrofluid production. Chapter 3 focuses on the section as highlighted in Figure 1.2.

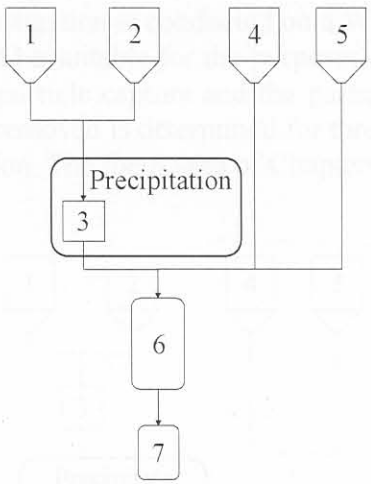

Figure 1.2 Focus area of Chapter 3

After precipitation, the aqueous solution in which the precipitate is suspended contains dissolved salts. Often, in the production of ferrofluids in the laboratory, a third phase has been produced. It is suspected that organic-inorganic phase interactions that may cause this third phase are promoted in some cases by the salts in the mixture containing the precipitate. This may hinder the final organic/aqueous phase separation. In addition, the salts in solution may increase the viscosity of the product. It would therefore be beneficial to wash the precipitate to remove these salts. For water-based ferrofluid production (where the carrier liquid is water), concentration of the magnetite suspension is essential for the production of a fluid of suitable magnetic properties. Washing is also important to ensure stability of the water-based fluids.

In Chapter 4, a method for the washing of the precipitate is suggested, making use of what have been termed sedimentation funnels. Precipitate is fed to four cone-shaped vessels in series. The funnels are plastic containers around which copper coils are wound. A direct current is passed through the coils thus generating a magnetic field in the interior of the funnel. When placed in the funnel and exposed to the magnetic field, the magnetite is attracted towards the region of greatest magnetic field and becomes concentrated at the base of the funnel. Wastewater leaves the funnels via the overflow. Computational fluid dynamics (CFD) is used to investigate the suitability of the funnel design and to determine whether the funnel configuration would ensure that the salts would be washed from the precipitate and that the magnetite would be retained in the funnels.

Chapter 5 investigates an alternative to the method of the sedimentation funnels to improve the washing and concentration of the magnetite precipitate. This concept is entitled the wet high intensity magnetic separator (WHIMS). The procedure used for the WHIMS is analogous to that of deep bed filtration with the magnetic force assisting in particle capture. The WHIMS consists of a funnel shaped vessel containing a magnetisable matrix or mesh and surrounded by a magnet e.g. solenoid electromagnet. Magnetic particles (such as the magnetite) fed to the WHIMS are captured in the matrix when the current to the coils is switched on. The liquid in which the magnetite is contained passes through the vessel. Water can be added to the vessel to wash the magnetite. In this chapter, an investigation is conducted on a WHIMS prototype that was built to determine whether or not it would be suitable for the purposes of washing and concentrating the magnetite. The efficiency of the particle capture and the particle retention on the magnetisable matrix once the magnetic field is removed is determined for three types of mesh in order to select the most suitable mesh for operation. The focus area of Chapters 4 and 5 is shown in Figure 1.3.

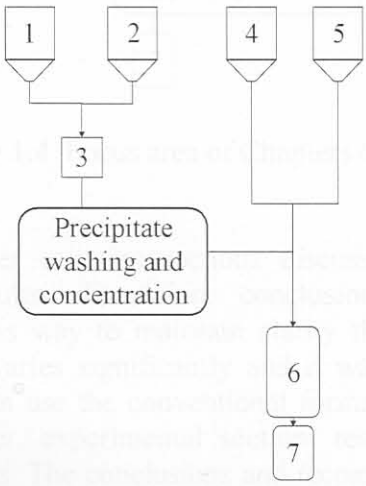

Figure 1.3 Focus area of Chapters 4 and 5

The particle size of the magnetite which is one of the most important components of the ferrofluid is critical for fluid stability. Particles must be small enough not to settle or agglomerate as a result of gravitational and magnetic interaction forces. In addition to ensuring that the particle size is correct, the coating of the particles is an important factor for maintaining stability. The coating of particles prevents agglomeration that could occur as a result of Van der Waals interaction forces. In Chapter 6, the stability requirements in terms of coating of particles are discussed briefly. An investigation is conducted to obtain an indication of the optimum quantity of surfactant required for steric stabilisation by varying the percentage surfactant added.

Chapter 7 investigates the use of a packed column for the saponification and peptization stages of the ferrofluid production. In order to achieve a more rapid phase transfer, heat is required to be input into the system. To obtain the maximum heat transfer at the maximum allowable temperature, the surface area in the column should be at a maximum. This chapter documents the procedure of mathematical optimisation using the dynamic trajectory method to determine the

optimum dimensions of such a column that would result in maximum heat transfer. The focus area of Chapters 6 and 7 is shown in Figure 1.4.

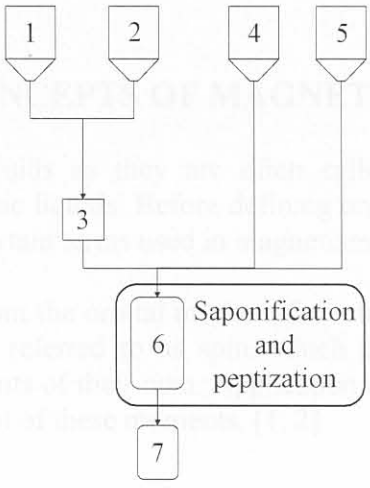

Figure 1.4 Focus area of Chapters 6 and 7

In this dissertation, each chapter contains sections discussing the theoretical background, experimental investigation, results, discussion, conclusions and recommendations. The dissertation was structured in this way to maintain clarity through the chapters. The subject matter from chapter to chapter varies significantly and it was decided to rather separate and discuss concepts individually than use the conventional format usually applied to dissertations i.e. a single introductory chapter, experimental section, results and discussion section and conclusions and recommendations. The conclusions and recommendations from all the chapters are summarised in the final chapter, Chapter 8.

A continuous plant has been designed for the production of ferrofluid on a larger scale. Some of the values used in the chapters relate to the continuous plant design and are not arbitrarily chosen. In many cases the origin of these values is not specified as the mass balance is considered to be confidential information.

CHAPTER 2

BASIC CONCEPTS OF MAGNETIC LIQUIDS

1. INTRODUCTORY CONCEPTS OF MAGNETISM

Ferromagnetic fluids, or ferrofluids as they are often called, are suspensions of magnetic particles that behave like magnetic liquids. Before defining and describing ferrofluids, however, it may be necessary to explain certain terms used in magnetism.

Magnetic moments may arise from the orbital motion of electrons in atoms. Electrons also have an intrinsic angular momentum referred to as spin, which causes the electrons to behave as though they had magnetic moments of their own. Application of an external magnetic field to an atom may influence the alignment of these moments. [1, 2]

1.1 Ferromagnetism

When an external magnetic field is applied to a ferromagnetic material, the alignment of moments is parallel to the field. French physicist Pierre-Ernest Weiss proposed that ferromagnetic materials are subdivided into areas known as domains. [1] In an unmagnetised sample, the moments of the domains are randomly orientated. When a magnetic field is applied to the sample, the moments of the domains tend to orient themselves in the direction of the field. This phenomenon occurs below a certain temperature known as the Curie temperature (above the Curie temperature, the ferromagnetic property disappears as a result of thermal agitation). Figure 2.1 (a) gives a schematic representation of this phenomenon. In the top picture of Figure 2.1 (a), there is no applied field. In the bottom picture, there is a strong field applied to the right causing the moments of the domains to orientate themselves in the direction of the applied field. [1, 2] The transition of moments between domains is gradual. The region over which the transition occurs is known as the Bloch wall. This is shown in Figure 2.1 (b) for the area circled in Figure 2.1 (a). [3]

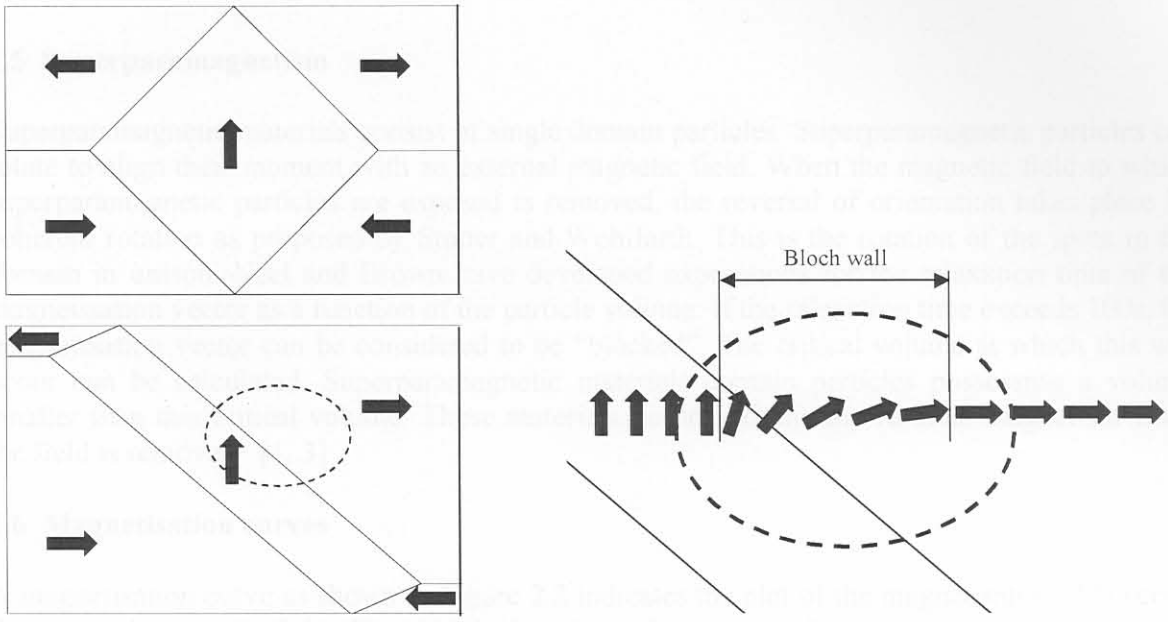

Figure 2.1 (a) Domains with no field (top) and applied field directed to the right (bottom) and (b) schematic of Bloch wall

1.2 Antiferromagnetism

Antiferromagnetic materials consist of sublattices possessing antiparallel moments. These moments are of the same size and result in no net magnetic moment. [1]

1.3 Ferrimagnetism

Ferrimagnetic materials also consist of interpenetrating sublattices. When a magnetic field is applied to a ferrimagnetic material, some of the moments of the domains are orientated in the direction of the field whilst other moments are aligned in the opposite direction to the field. Either the number or size of the moments aligned in the direction of the field is greater than that in the opposite direction to the field resulting in a net magnetic moment. The net magnetic moment for ferrimagnetic materials is smaller than that for ferromagnetic materials. [1, 4, 5]

1.4 Paramagnetism

A paramagnetic material is a material containing atoms with permanent magnetic dipole moments. In the absence of an external magnetic field, the moments point in random directions. When placed in a magnetic field, the moments tend to align with the magnetic field as a result of the field exerting a torque on these moments. The atoms align in their position of minimum potential energy. The alignment, however, is not complete, due to the disruptive effect of thermal vibrations. Paramagnetic substances are therefore only weakly attracted by a magnet. [1, 2]

1.5 Superparamagnetism

Superparamagnetic materials consist of single domain particles. Superparamagnetic particles can rotate to align their moment with an external magnetic field. When the magnetic field to which superparamagnetic particles are exposed is removed, the reversal of orientation takes place by coherent rotation as proposed by Stoner and Wohlfarth. This is the rotation of the spins in the domain in unison. Néel and Brown have developed expressions for the relaxation time of the magnetisation vector as a function of the particle volume. If the relaxation time exceeds 100s, the magnetisation vector can be considered to be "blocked". The critical volume at which this will occur can be calculated. Superparamagnetic materials contain particles possessing a volume smaller than this critical volume. These materials do not exhibit any residual magnetism when the field is removed. [1, 3]

1.6 Magnetisation curves

A magnetisation curve as shown in Figure 2.2 indicates the plot of the magnetisation (M) versus the external magnetic field (H) as applied to ferromagnetic and ferrimagnetic materials. As this external field is increased, the magnetisation of the material will gradually increase. A point is reached where the magnetisation is constant and no further magnetisation can take place (B in Figure 2.2), however strong the field. This condition is called the saturation magnetisation (M_s). If the field is decreased, the magnetisation does not retrace the original curve B-A-O. When the field is decreased to zero, the magnetisation has a non-zero value (C). The magnetisation now increases in the direction in which the field is applied. When the field is sufficiently large applied in the opposite direction, the magnetisation passes through zero (D) and begins to increase in the direction in which the field is applied until the magnetisation reaches the saturation magnetisation value again (E). If the field is decreased again, the magnetisation follows the curve through F and G to the saturation magnetisation (B) again. If the field is continuously varied in this manner, the magnetisation will vary repeatedly along the closed loop B-C-D-E-F-G-B. This loop is called the hysteresis loop. Curve O-A-B is called the initial magnetisation curve. [1]

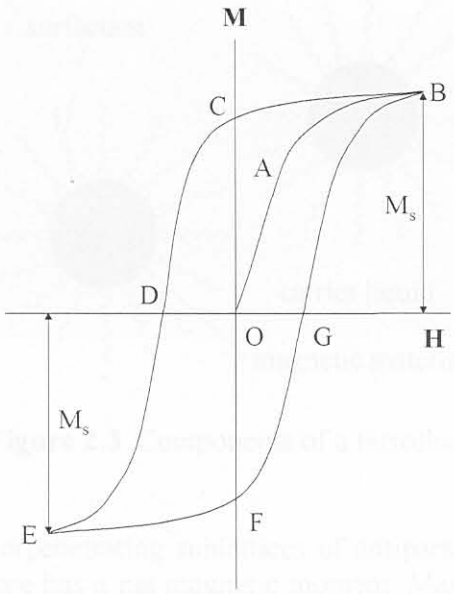

Figure 2.2 Magnetisation curve showing hysteresis loop

2. DEFINITION AND DESCRIPTION OF FERROFLUID

2.1 Structure of magnetic liquids

The existence of intrinsic ferromagnetism in the liquid state is not known to exist. There is no mathematical reason for this state not to exist and it is therefore suggested that other factors which make its existence impossible or unlikely have not been considered. [6] Reports of ferromagnetism in the liquid state probably refer to liquids containing ferromagnetic particles. The ferromagnetic liquid or ferrofluid as discussed in this dissertation refers to a stable colloidal dispersion or suspension of single domain ferrimagnetic particles in a carrier liquid. [7] The suspension of particles is coated with a surfactant and is suspended in a carrier liquid. In this dissertation, magnetite (Fe_3O_4) is the ferrimagnetic material coated with oleic acid as the surfactant and suspended in kerosene as the carrier liquid.

The components of a ferrofluid are indicated schematically in Figure 2.3.

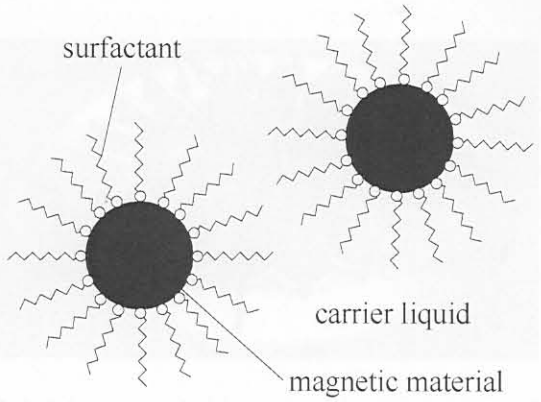

Figure 2.3 Components of a ferrofluid

Magnetite consists of two interpenetrating sublattices of antiparallel spins. These moments are unequal and magnetite therefore has a net magnetic moment. Magnetite is an iron (II)-iron (III) ion mixed oxide possessing an inverse spinel structure. This means that the two cations of different valence (Fe^{2+} and Fe^{3+}) share octahedral sites. [8] This can have an important influence on the magnetic and electrical properties of the compound.

Other magnetic particles that are often used in ferrofluids are γ-Fe_2O_3 (maghemite), Fe, Co or Ni. [9] Carrier liquids could be, for example, different types of oils, fluorocarbons or even water. (Water-based fluids usually exhibit a lower saturation magnetisation as it is more difficult to stabilise a concentrated water-based fluid.)

The magnetite particle size, which is important for stability, is approximately 10 nm. This particle size is small enough to ensure that the kinetic energy imparted to the particle by the motion of solvent molecules (Brownian motion) is sufficient to overcome both magnetic interactions and the effects of gravity thereby preventing agglomeration and settling. [7] This property is discussed further in Section 4. The stability of the ferrofluid also arises from the fact that each magnetite particle is coated with a monolayer of surfactant. This surfactant inhibits the agglomeration of particles which could occur as a result of Van der Waals interactions. This property is discussed further in Section 4 and in Chapter 6.

Each magnetite particle in the ferrofluid behaves like a spherical permanent magnet. In the absence of a magnetic field, the particles exhibit a random distribution of magnetic moments and the fluid has no net magnetisation. In an applied field, the moments experience a torque and align in the direction of the field. The critical volume for single domain particles for magnetite, is calculated to be approximately 50 nm, however, superparamagnetism is often only displayed at room temperature when the particle size is in the region of 10 nm. [3] Seeing as ferrofluid exhibits superparamagnetic properties, the fluid does not retain any residual magnetisation once the magnetic field is removed and the particles randomise quickly. The fluid shows no hysteresis in its magnetisation curve. [9] Figure 2.4 shows a magnetic fluid exposed to a magnetic field. The ferrofluid forms spikes as the fluid aligns itself with the external magnetic field gradient.

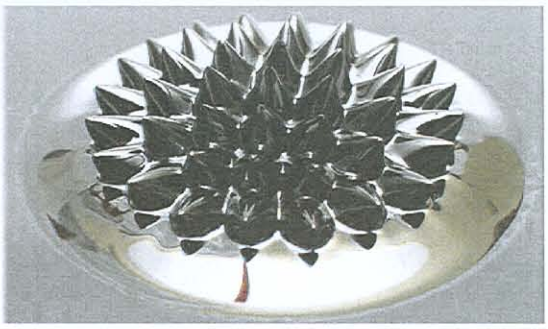

Figure 2.4 Magnetic fluid exposed to a magnetic field [10]

Figure 2.5 shows a permanent magnet being brought close to a vessel containing ferrofluid and water. The ferrofluid is pulled towards the magnet.

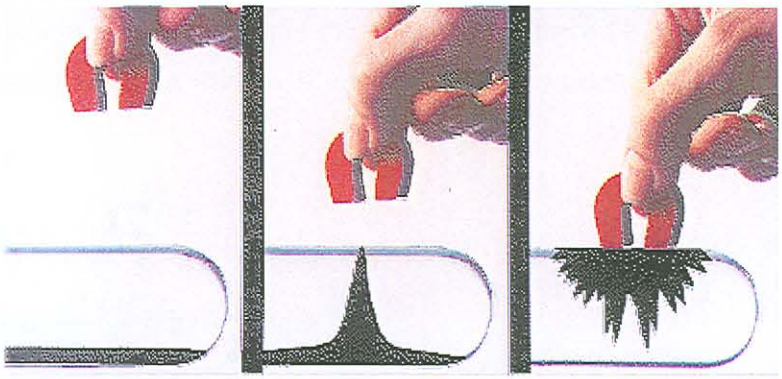

Figure 2.5 Effect of a magnetic field on a magnetic fluid exposed to the field [11]

2.2 The history of ferrofluids

The history of ferrofluids dates back to the 1700s when Gowan Knight in 1779 attempted to disperse iron filings in water. He obtained a suspension of small particles after several hours of mixing, but the fluid was not stable over long periods of time. In 1932, Bitter produced a suspension of magnetite of particle size 10^3 nm in water. Elmore (in 1938) as well as Craik and Griffiths (in 1958) produced suspensions containing smaller particles (20 nm) which closely resembled ferrofluids. Ultrastable ferrofluids containing ferrite particles in a non-conducting liquid carrier were first prepared by Papell at NASA in the 1960s. [6, 9]

Magnetic suspensions were first used to detect microscopic-magnetic patterns on ferromagnetic tools (through deposition of the fluid on the surface and evaporation of the carrier liquid) and later for the identification of flux change on magnetic tapes. NASA manufactured ferrofluids for investigations into its use as a pumpable rocket propellant in microgravity conditions (controlling

fuel flow under conditions of weightlessness). Ferrofluids can be manipulated to flow or remain immobilized via application of an external magnetic field. One of the most common applications is the use of ferrofluid in the voice coils of loudspeakers. In this case, the ferrofluid functions as a coolant and damping medium and keeps the voice coil concentric with the magnet. Ferrofluid has also been used to form airtight seals in rotating machinery. The performance of such a seal is impressive: the seal is able to withstand a differential pressure of greater than 4 MPa at 10 000 rpm or 100 000 rpm for a shorter period of time. Most conventional O-ring seals function at approximately 300 rpm. [6, 12]

The use of ferrofluid has been investigated as a variable density fluid for the separation of scrap metals. Magnetic paints have been developed and magnetisable liquids have found application in the fields of biology and medicine (e.g. enzyme fixing, immunoanalysis, cell separation of bacteria cultures and drug delivery to specific points in the body by application of a magnetic field). [9, 12]

2.3 Forces acting on a volume of ferrofluid and on a particle suspended in the ferrofluid

Two fundamental forces act on a given volume (V, in m^3) of ferrofluid when it is placed in a magnetic field gradient. These forces are the gravitational force ($\mathbf{F}_g$) and the magnetic traction force ($\mathbf{F}_m$). The total force on a volume of ferrofluid can be written as: [13]

$$\begin{aligned}\mathbf{F} &= \mathbf{F}_g + \mathbf{F}_m \\ &= \rho_f V\mathbf{g} + \mu_0 MV\frac{\partial H}{\partial z}\frac{\mathbf{g}}{g} \\ &= (\rho_f + \mu_0\frac{M}{g}\frac{\partial H}{\partial z})V\mathbf{g}\end{aligned} \qquad (2.1)$$

where ρ_f is the density of the ferrofluid (kg/m^3), μ_0 is the magnetic permeability of a vacuum ($4\pi*10^{-7}$ Tm/A), M is the magnetisation of the fluid (A/m), H is the magnetic field strength (A/m), $\frac{\partial H}{\partial z}$ is the vertical magnetic field gradient (A/m^2) and g is the gravitational acceleration (m/s^2).

(1 T = 1 N/A m)

The expression in parenthesis in eq. (2.1) can be viewed as the apparent density (ρ_a, in kg/m^3) of the fluid if it is assumed that the magnetic field gradient is parallel to gravity and of the same sense. [13]

$$\rho_a = \rho_f + \frac{\mu_0 M}{g}\frac{\partial H}{\partial z} \qquad (2.2)$$

When the field gradient makes an angle with gravity, eq. (2.2) can be written as: [13]

$$\rho_a = \rho_f + \frac{\mu_0 M}{g}\frac{\partial H}{\partial z}\cos(\mathbf{g}\frac{\partial \mathbf{H}}{\partial z}) \qquad (2.3)$$

As can be seen from eq. 2.2, it is possible to control the apparent density of the magnetic fluid by changing the magnetic field gradient to which the fluid is exposed.

The production of ferrofluid has become increasingly important in the diamond industry as a result of developments in ferrohydrostatic separation (FHS). FHS making use of a ferrohydrostatic separator is used for the recovery of diamonds. The ferrohydrostatic separator consists of an electromagnet and a separation chamber in which a pool of ferrofluid is held. Material is introduced into the separation chamber via a vibratory feeder. A photograph of such a separator is shown in Figure 2.6 with a close-up of the separation chamber shown in Figure 2.7.

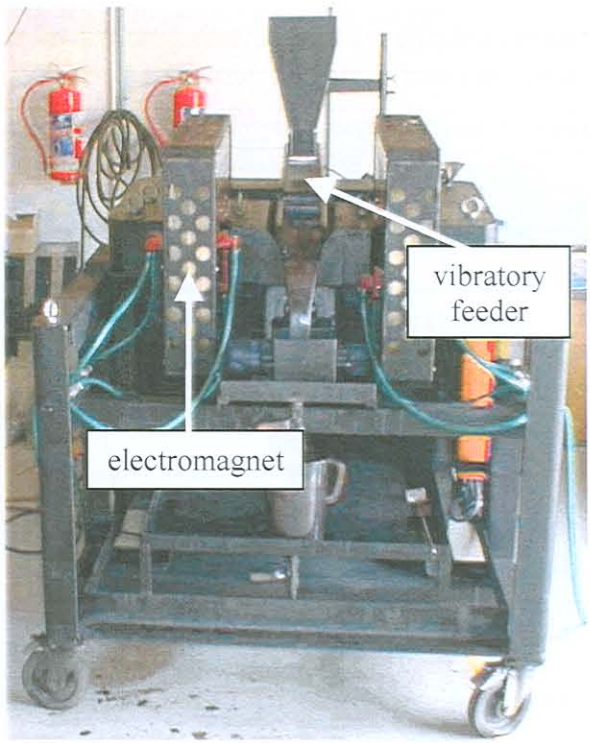

Figure 2.6 Ferrohydrostatic separator

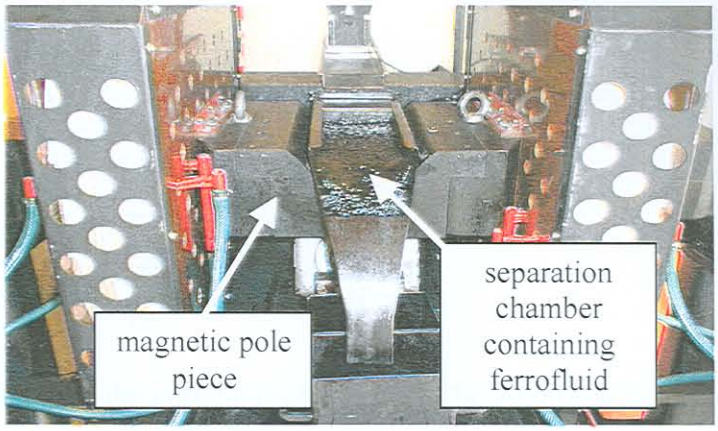

Figure 2.7 Ferrohydrostatic separator chamber

A particle entering the ferrohydrostatic separator chamber is suspended in ferrofluid and is acted upon by the gravitational force ($\mathbf{F}_{gp}$), the magnetic traction force ($\mathbf{F}_{mp}$), a gravity-related buoyancy force ($\mathbf{F}_{bg}$) and a magnetically induced buoyancy force ($\mathbf{F}_{bm}$). This is shown schematically in Figure 2.8. [14]

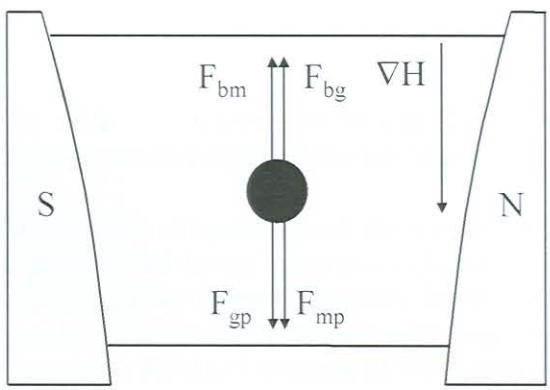

Figure 2.8 Forces acting on a particle in a separation chamber

These forces acting on the particle are given in eqs (2.4) to (2.7) with the net vertical force on the particle given in (2.8) (in cgs units). [13]

$$\mathbf{F}_{gp} = \rho_p V_p \mathbf{g} \tag{2.4}$$

$$\mathbf{F}_{mp} = V_p \chi_p H \frac{\partial \mathbf{H}}{\partial z} \tag{2.5}$$

$$\mathbf{F}_{bg} = \rho_f V_p \mathbf{g} \tag{2.6}$$

$$\mathbf{F}_{bm} = V_p M \frac{\partial \mathbf{H}}{\partial z} \tag{2.7}$$

$$\begin{aligned} \mathbf{F} &= \mathbf{F}_{gp} + \mathbf{F}_{mp} + \mathbf{F}_{bg} + \mathbf{F}_{bm} \\ &= \rho_p V_p \mathbf{g} + V_p \chi_p H \frac{\partial \mathbf{H}}{\partial z} - \rho_f V_p \mathbf{g} - V_p M \frac{\partial \mathbf{H}}{\partial z} \end{aligned} \tag{2.8}$$

where ρ_p is the density of the particle (kg/m^3), V_p is the volume of the particle (m^3) and χ_p is the volume magnetic susceptibility of the particle.

When the resultant force acting on a particle is zero, eq. (2.8) reduces to eq. (2.9) to where ρ_{sp} is defined as the effective cut point density of separation.

$$\rho_{sp} = \rho_f + \frac{1}{g}[M \frac{\partial \mathbf{H}}{\partial z} - \chi_p H \frac{\partial \mathbf{H}}{\partial z}] \tag{2.9}$$

For non-magnetic particles, χ_p =0 and (2.9) reduces to (in SI units):

$$\rho_{sp} = \rho_f + \frac{\mu_0 M}{g} \frac{\partial H}{\partial z} \tag{2.10}$$

Eq. (2.10) is equivalent to eq. (2.2). It can therefore be seen that for non-magnetic particles, the density cut point is equal to the apparent density of the ferrofluid.

These equations describe the principle of operation of the ferrohydrostatic separators. If the sum of the forces exerted on a particle fed to the separation chamber is such that the sum of the magnetic buoyancy force and the gravity-related buoyancy force is greater than the gravitational and magnetic forces, the particle will float. (The particle will float when its density is lower than the apparent density of the magnetic fluid.) If the sum of the forces exerted on a particle is such that the sum of the magnetic buoyancy force and the gravity-related buoyancy force is less than the gravitational and magnetic forces, the particle will sink. (The particle will sink when its density is higher than the apparent density of the magnetic fluid.) [15]

3. MANUFACTURE OF FERROFLUIDS

The production of ferrofluid can be according to a variety of methods. The magnetic liquids can contain either a suspension of fine metal particles or fine particles of ferrites. The early magnetic fluids were unstable owing to their large particle size and inadequate surfactant stabilisation. [9]

Metal particles of diameter less than 10^3 nm have been produced by evaporation of the metal in the presence of an inert gas. Single domain ferromagnetic metal particles have also been

produced by electrodeposition techniques. This involves using the salts of the ferromagnetic metals dissolved in water or alcohol and the metal carrier liquid as the cathode. Papell and Rosensweig investigated the method of grinding ferrites in a ball mill and then suspending the particles in a carrier liquid. [6] One of the preferred methods for the economic production of magnetite-based ferrofluid is to obtain the magnetite colloids by precipitation of magnetite from a solution of ferric and ferrous ions using an excess of an alkali hydroxide.

The ferrofluid as referred to in this dissertation is produced in three main stages: oxide precipitation and magnetite formation, saponification of the surfactant and peptization of the coated particles.

3.1 Oxide precipitation and magnetite formation

A solution of ferric and ferrous ions (from ferric chloride ($FeCl_3$) and ferrous sulphate ($FeSO_4.7H_2O$) respectively) is reacted with ammonium hydroxide solution (NH_4OH) to form magnetite. An ammonium chloride and ammonium sulphate solution forms as a result of the precipitation reactions. A very simplified representation of this process is given by eqs (2.11) to (2.13). [12]

$$2FeCl_3 + 6NH_4OH \rightarrow 2FeO(OH) + 6NH_4Cl + 2H_2O \qquad (2.11)$$

$$FeSO_4 + 2NH_4OH \rightarrow Fe(OH)_2 + (NH_4)_2SO_4 \qquad (2.12)$$

$$2FeO(OH) + Fe(OH)_2 \rightarrow Fe_3O_4 + 2H_2O \qquad (2.13)$$

A volumetric packing fraction (volume of magnetite per volume of ferrofluid) of approximately 0.1 is commonly selected for ferrofluid production. According to the stoichiometry of the reactions (eqs (2.11) to (2.13)), a ratio of 2:1 of iron (II):iron (III) ions is required. However, to compensate for the oxidation of iron (II) to iron (III) ions during oxide formation, a ratio of 3:2 (iron (II):iron (III) ions) is used. The ammonium hydroxide should be added rapidly to the iron solution with good mixing to result in the precipitation of the required precursors for the formation of magnetite. If the alkali hydroxide is added slowly with poor mixing, it may lead to local pH gradients and the subsequent variation in hydrolysed species. An excess of ammonium hydroxide is used so that low values of pH are avoided at the end of the reaction and to provide ammonium hydroxide for the saponification reaction. [16]

3.2 Saponification

The excess ammonium hydroxide reacts with oleic acid to form an ammonium oleate soap.

$$CH_3(CH_2)_7CH{=}CH(CH_2)_7C{=}O + NH_4OH \rightarrow R\text{-}C{=}O + H_2O \qquad (2.14)$$
$$\qquad\qquad\qquad\qquad\qquad\qquad\qquad\qquad\qquad\quad | \qquad\qquad\quad |$$
$$\qquad\qquad\qquad\qquad\qquad\qquad\qquad\qquad\qquad\quad OH \qquad\quad ONH_4$$

3.3 Peptization

This ammonium oleate soap can bond to the magnetite particle through covalent bonding to iron ions on the surface. This results in a coated particle that still retains an affinity for water due to the polar nature of the oleate coating. The ammonium oleate coating is transformed upon heating into oleic acid and ammonia gas without becoming detached from the magnetite surface. The coated particles are now reasonably non-polar and would be more stable in a non-polar liquid like kerosene. A migration therefore takes place to the kerosene phase where they form a stable colloidal suspension.

$$\begin{array}{l} R\text{-}C{=}O + Fe_3O_4 \xrightarrow[\Delta]{} R\text{-}C{=}O + NH_3 \\ \quad\quad | \qquad\qquad\qquad\quad | \\ \quad ONH_4 \qquad\qquad\quad OH(Fe_3O_4) \end{array} \tag{2.15}$$

4. STABILITY REQUIREMENTS FOR FERROFLUIDS AS DICTATED BY MAGNETITE PARTICLE SIZE

The mechanism by which the single domain particles are produced for use in magnetic liquids leads to particle size distributions which influence the magnetic properties of the liquid. A number of different factors come into play when determining the stability against settling of a magnetic liquid. For example, the particles must be sufficiently small so that Brownian motion opposes particle agglomeration. Particle interactions arising from London-type Van der Waals forces may cause particle agglomeration which can destroy the desirable characteristics of the fluid. [6] These and other factors are discussed in more detail in Sections 4.1 to 4.4.

4.1 Stability in a magnetic field gradient

Magnetic particles exposed to a magnetic field are attracted to the higher intensity regions of the magnetic field. The magnetic energy (see eq. (2.16)) is the work required to move a magnetised particle from a point in the fluid where the field strength is H to a point outside the field where the field is equal to 0 [7]. In eq. (2.16) M_s is the saturation magnetisation of magnetite (480000 A/m) and V is the volume. In eq. (2.16), ∇H, the field gradient is equal to (0-H) or $-H$ and therefore, the value for the field strength, H (in the range of 100 to 200 kA/m for ferrohydrostatic separators) can be used.

$$W = -\int_H^0 (\mu_0 M \frac{dH}{ds} V) ds \approx \mu_0 M_s H V \tag{2.16}$$

According to the kinetic theory of matter, a particle that is denser than the fluid in which it is found can remain suspended in the fluid as long as the particle size is sufficiently small. Molecules in the liquid collide continuously with the particles and transfer their kinetic energy to the particles keeping them suspended. The energy carried by these particles is equal to kT where k is the Boltzmann constant ($1.38*10^{-23}$ J/K) and T is the temperature (K). For a particle in a

magnetic field to remain in suspension, the ratio of the thermal energy (kT) to the magnetic energy must be greater than or equal to 1. [17]

$$\frac{thermal\ energy}{magnetic\ energy} = \frac{kT}{\mu_0 M_s HV} \geq 1 \tag{2.17}$$

If the volume of a sphere is substituted in eq. (2.17), the maximum particle size can be determined. [7]

$$\frac{kT}{\mu_0 M_s H}\frac{6}{\pi d^3} \geq 1$$
$$\therefore d \leq (6kT / \pi\mu_0 M_s H)^{1/3} \tag{2.18}$$

At ambient temperature (298 K) the particle size is calculated as follows:

$$d \leq \left[\frac{6(1.38*10^{-23}\ J/K)(298\ K)}{\pi(4\pi*10^{-7}\ Tm/A)(480000\ A/m)(100000\ A/m)}\right]^{1/3} * \frac{1\ nm}{1*10^{-9}\ m} = 5.1\ nm \tag{2.19}$$

The particle size is found to be smaller than or equal to 5.1 nm. This value is used as a guideline for the particle size. Other effects in the environment in which the fluid is located will also influence the allowable particle size perhaps resulting in the allowable particle being larger. Such a small particle size may be detrimental to the fluid. It is thought that particles of too small a size may possess a lower saturation magnetisation and would thus be less effective for use in ferrohydrostatic separators. [18]

4.2 Stability in a gravitational field

The relative effect of the gravitational to the magnetic energy can be calculated to determine whether this force is significant or not.

$$\frac{gravitational\ energy}{magnetic\ energy} = \frac{\Delta\rho VgL}{\mu_0 M_s HV} = \frac{\Delta\rho gL}{\mu_0 M_s H} \tag{2.20}$$

Typical values for the ferrofluid are substituted into eq. (2.20) with L equal to 0.1 m (as the approximate height in a magnetic separation chamber), and the difference in density between the solid and liquid equal to 4400 kg/m^3 (with magnetite density equal to 5180 kg/m^3 and kerosene density equal to 780 kg/m^3) to give:

$$\frac{gravitational\ energy}{magnetic\ energy} = \frac{(4400\ kg/m^3)(9.81\ m/s^2)(0.1\ m)}{(4\pi*10^{-7}\ Tm/A)(480000\ A/m)(100000\ A/m)} = 0.072 \tag{2.21}$$

Gravity is therefore less of a threat than the magnetic energy to the settling out of particles in ferrofluid. [7] This is further confirmed by checking what the size of a magnetite particle can be

to prevent settling in a gravitational field. For a particle in a gravitational field to remain in suspension, the ratio of the thermal energy (kT) to the gravitational energy must be greater than or equal to 1:

$$\frac{thermal\ energy}{gravitational\ energy} = \frac{kT}{\Delta\rho VgL} \geq 1 \tag{2.22}$$

If the volume of a sphere is substituted in eq. (2.22), the maximum particle size can be determined.

$$\frac{kT}{\Delta\rho gL}\frac{6}{\pi d^3} \geq 1$$
$$\therefore d \leq (6kT / \pi\Delta\rho gL)^{1/3} \tag{2.23}$$

At ambient temperature (298 K) the particle size is calculated as follows:

$$d \leq \left[\frac{6(1.38*10^{-23}\ J/K)(298\ K)(1\ nm)}{\pi(5180\ kg/m^3)(9.81\ m/s^2)(0.1\ m)}\right]^{1/3} * \frac{1\ nm}{1*10^{-9}\ m} = 11.56\ nm \tag{2.24}$$

For the ratio of the thermal to the gravitational energy to be greater than or equal to one, the particle size should be smaller than or equal to 11.56 nm. The magnetic field gradient is of more of a threat to the settling out of particles than the gravitational energy as the gravitational energy allows for a larger particle size before settling will take place. The magnetic field gradient allowed for a maximum particle size of 5.1 nm.

4.3 Stability against magnetic agglomeration

Collisions between particles are frequent in a typical colloidal magnetic fluid as such a fluid contains in the order of 10^{23} particles per cubic metre. A magnetic attractive force can exist between two particles that approach one another. Each particle will be treated as a magnetic dipole which generates a magnetic field. The magnetic-dipole magnetic-dipole interaction energy between the particles is given by eq. (2.25). [7]

$$E_{dd} = \frac{1}{4\pi\mu_0}\left[\frac{\mathbf{m}_1 \cdot \mathbf{m}_2}{r^3} - \frac{3}{r^5}(\mathbf{m}_1 \cdot \mathbf{r})(\mathbf{m}_2 \cdot \mathbf{r})\right] \tag{2.25}$$

where $\mathbf{m}$ is a dipole moment and r is the distance between the centres of two particles.

It is assumed that the particles are single domain, spherical and of the same dimensions. If the particles are below the Curie temperature, they will be saturated and it can be assumed that their moments are equal ($\mathbf{m}_1 = \mathbf{m}_2 = \mathbf{m}$). When these moments are aligned, $\mathbf{m}_1 = \mathbf{m}_2 = m^2$ (dot product of parallel vectors) and $(\mathbf{m}_1 \cdot \mathbf{r})(\mathbf{m}_2 \cdot \mathbf{r}) = m^2 r^2$. According to [7], the moment of the particle is given by:

$$m = \frac{\mu_o M \pi d^3}{6} \tag{2.26}$$

s is the distance between the surfaces of the particles) and d is the diameter of a particle as shown in Figure 2.9.

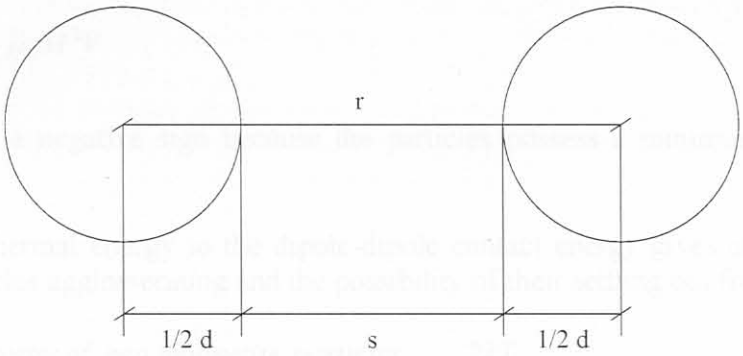

Figure 2.9 Representation of distances between particles

Eq (2.26) is substituted into (2.25) to give:

$$\begin{aligned} E_{dd} &= \frac{1}{4\pi\mu_o}\left[\frac{m^2}{r^3} - \frac{3}{r^5}m^2r^2\right] \\ &= \frac{m^2}{4\pi\mu_o}\left[-\frac{2}{r^3}\right] \\ &= \frac{\mu_o{}^2 M^2\pi^2 d^6}{36(4\pi\mu_o)}\left[-\frac{2}{r^3}\right] \\ &= -\frac{\mu_o M^2 \pi d^6}{72}\left[\frac{1}{(s+d)^3}\right] \end{aligned} \tag{2.27}$$

When the particles are in contact i.e. $s = 0$, and the diameter of the sphere is replaced in terms of its volume, eq. (2.27) reduces to:

$$
\begin{aligned}
E_{dd} &= -\frac{\mu_o M^2 \pi d^6}{72}\left[\frac{1}{(0+d)^3}\right] \\
&= -\frac{\mu_o M^2 \pi d^3}{72} \\
&= -\frac{\mu_o M^2 \pi \frac{6V}{\pi}}{72} \\
&= -\frac{1}{12}\mu_o M^2 V
\end{aligned}
\tag{2.28}
$$

This equation has a negative sign because the particles possess a minimum potential energy when they touch.

The ratio of the thermal energy to the dipole-dipole contact energy gives an indication of the likelihood of particles agglomerating and the possibility of their settling out from suspension.

$$
\frac{thermal\ energy\ of\ two\ magnetite\ particles}{dipole-dipole\ contact\ energy} = \frac{2kT}{\frac{\mu_0 M^2 V}{12}} \tag{2.29}
$$

Solving for d, again with the substitution for the volume of a sphere, gives

$$
\begin{aligned}
&\frac{24kT}{\mu_0 M^2}\frac{6}{\pi d^3} \geq 1 \\
&d \leq (144kT/\pi\mu_0 M^2)^{1/3}
\end{aligned}
\tag{2.30}
$$

For magnetite particles at room temperature:

$$
d \leq \left[\frac{144(1.38*10^{-3}\ J/k)(298\ K)(1\ nm)}{\pi(4\pi*10^{-7}\ Tm/A)(480000\ A/m)^2(1*10^{-9}\ m)}\right]^{1/3} = 8.7\ nm \tag{2.31}
$$

Particles of the order of 9 nm are therefore not likely to experience magnetically induced agglomeration and the subsequent settling of agglomerates is not expected from ferrofluids with particles of diameter of the order of 10 nm.

4.4 London-type Van der Waals attractive forces

Particles in a ferrofluid may be attracted to one another by London-type Van der Waals attractive forces. Fluctuating orbital electrons in one particle may induce dipoles in another and result in Van der Waals forces arising between the particles. According to Fritz London, the energy required to overcome Van Der Waals forces between two particles is inversely proportional to the sixth power of the distance between their centres. For spheres of equal size, the Van der

Waals energy is equal to the thermal energy kT, when two spheres are separated by a distance approximately equal to their radius. To avoid agglomeration, the particles must be kept apart or, as is done in the case of ferrofluids, the particles are coated with a surfactant which then acts as an elastic cushion and provides some sort of "entropic repulsion". [6, 7]

Figure 2.10 shows a plot of the potential energy versus distance between coated particles. [6] As can be seen from Figure 2.10, particles of any size will experience London-type interactions and have a large potential energy when in contact. A repulsive force is required to overcome these interactions. The entropic repulsion is introduced by coating the particles so that, when particles are close together, the repulsion due to steric hindrance overcomes the attractive interaction. For example, the resultant potential energy plots (from entropic repulsion, London attraction and magnetic attraction) for particles of diameter 10 nm are given for particles that are coated to a thickness (δ) of between 0.5 and 2 nm. Through coating of particles, the repulsion owing to steric hindrance of the surfactant long chain molecules is sufficient to overcome the attractive energy. [6]

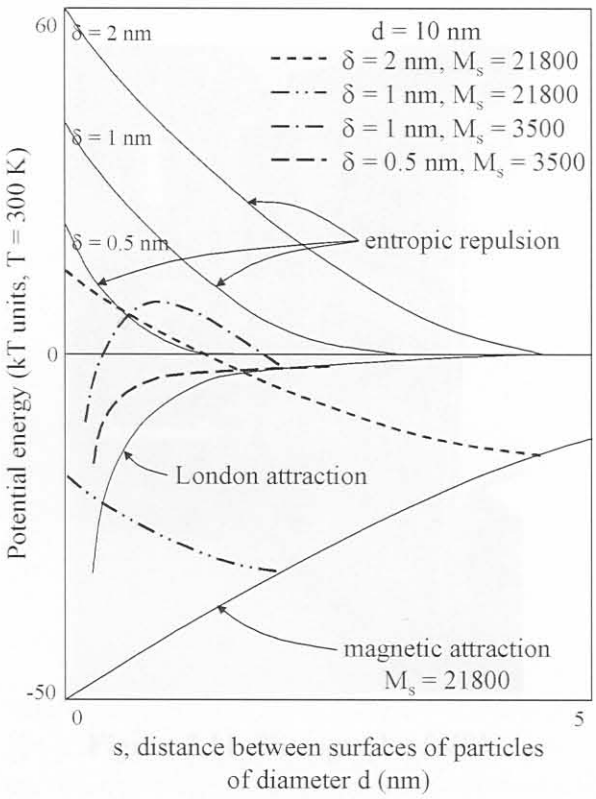

Figure 2.10 Example of a plot of potential energy versus distance between particles for coated particles

In conclusion then, to ensure a ferrofluid remains stable, the particles must be small enough so that thermal agitation can overcome the effect of the magnetic field gradient and gravitational

field and overcome magnetic agglomeration. In addition, a short range repulsive force in the form of coated particles must be present so that the London-type Van der Waals attractive repulsive interaction can be overcome.

5. FERROFLUID QUALIFICATION

A simple method to determine the quality of a ferrofluid that is produced, is by recording a magnetisation curve of the fluid and measuring its saturation magnetisation.

The saturation magnetisation is measured at room temperature using a Vibrating Sample Magnetometer (VSM). A small sample is vibrated in a magnetic field at a constant frequency. The sample is suspended between two coils. When a magnetic field is applied, oscillating magnetic flux lines from the sample induce an oscillating voltage in the coils which are in close proximity to the sample. Using this data, a hysteresis curve can be generated. A photograph of a VSM is shown in Figure 2.11. [19]

Figure 2.11 Photograph of VSM

An approximation of the magnetite particle size can be determined indirectly from the saturation magnetisation measurements. There is evidence that the distribution of particle size $f(y)$ where y is the reduced diameter $\frac{D}{D_v}$ (D is the particle diameter D_v and is the median diameter of the distribution) is given by a log normal distribution.

$$f(y) = \frac{1}{y\sigma\sqrt{2\pi}} \exp\left(\frac{-(\ln(y))^2}{2\sigma^2}\right) \tag{2.32}$$

Ferrofluids usually contain a distribution of particle size and this modifies the magnetic properties of the system. In this case, the total magnetisation is given by the sum of the contribution from each particle size weighted using the distribution function. Chantrell *et al.* have derived formulae for the median diameter of the log normal distribution (D_v) and the standard deviation (σ) of the log normal distribution. [20]

$$D_v = \left[\frac{18kT}{\pi I_s'} \sqrt{\frac{\chi_i}{3\varepsilon I_s'} \frac{1}{H_o}}\right]^{\frac{1}{3}} \tag{2.33}$$

$$\sigma = \frac{\sqrt{\ln\left(\frac{3\chi_i}{\varepsilon I_s' \frac{1}{H_o}}\right)}}{3} \tag{2.34}$$

I_s' (G) is the saturation magnetisation for the bulk magnetic particles, ε is the volumetric particle packing fraction ($\varepsilon I_s'$ is the saturation magnetisation of the ferrofluid), χ_i is the initial susceptibility and $\frac{1}{H_o}$ (Oe^{-1}) is the reciprocal field at I =0. [20] (1 Oe = 1000/4π A/m)

A spreadsheet is used to calculate D_v and σ using the constants k, T, I_s' and π. χ_i and $\varepsilon I_s'$ can be calculated from the parameters read off from the magnetisation curve (from the initial slope and the saturation magnetisation). The linear behaviour between H_1=7000 Oe and $H_2 = H_{max}$ has been determined. $\frac{1}{H_o}$ is determined from inputting H_1, H_2 and the corresponding values of magnetisation. [20]

This method of particle size determination should be considered as an approximate one. The accuracy of the method has been tested against electron microscope measurements and results indicate that the D_v values calculated from the magnetisation curve are lower than the measured ones (17% for the petroleum based ferrofluids). The discrepancy could arise from the assumptions in terms of the validity of the log normal distribution of particle sizes. [20]

CHAPTER 3

THE EFFECT OF KEY PARAMETERS ON THE MECHANISM OF THE PRODUCTION OF MAGNETITE

1. INTRODUCTION

Magnetite formation is vital for the production of ferrofluids. A very simplified representation of the process by which magnetite is produced was given by eqs (2.11) to (2.13). The formation and transformation pathways of iron oxides are, however, more complex. There are many pathways that could lead to the formation of incorrect species. These species (with the exception of maghemite) will result in the production of a non-magnetic fluid. Although maghemite is magnetic, it may be unsuitable for other reasons. Superparamagnetic behaviour requires smaller elongated particles as compared to rounded particles. For the same particle size distribution, a fluid with rounder particles will exhibit less hysteresis than a fluid with elongated particles. When elongated particles are exposed to a magnetic field, the magnetisation vector will have a preference to lie along the elongated axis. When the field is removed, elongated particles will have to overcome an addition to the energy barrier before reversal of the vector can take place. Although maghemite is magnetic, because of shape anisotropy, its more elongated shape may result in inferior magnetic properties when used as a component of a ferrofluid. [3]

In this chapter, mechanisms for the formation of magnetite are proposed. Parameters that could affect the production of magnetite are discussed and an investigation is then conducted to confirm what the preferred conditions are for the production of magnetite and whether or not these parameters are of importance in ferrofluid production.

2. CHEMICAL PRECIPITATION OF MAGNETITE PARTICLES

Although ultrafine magnetite particles can be produced by mechanical methods such as grinding, chemical precipitation of iron oxides is the preferred method of producing magnetite as it is more rapid and offers greater control. Figure 3.1 gives a schematic representation of the possible species that can be produced from iron (III) and iron (II) ions during hydrolysis. [21]

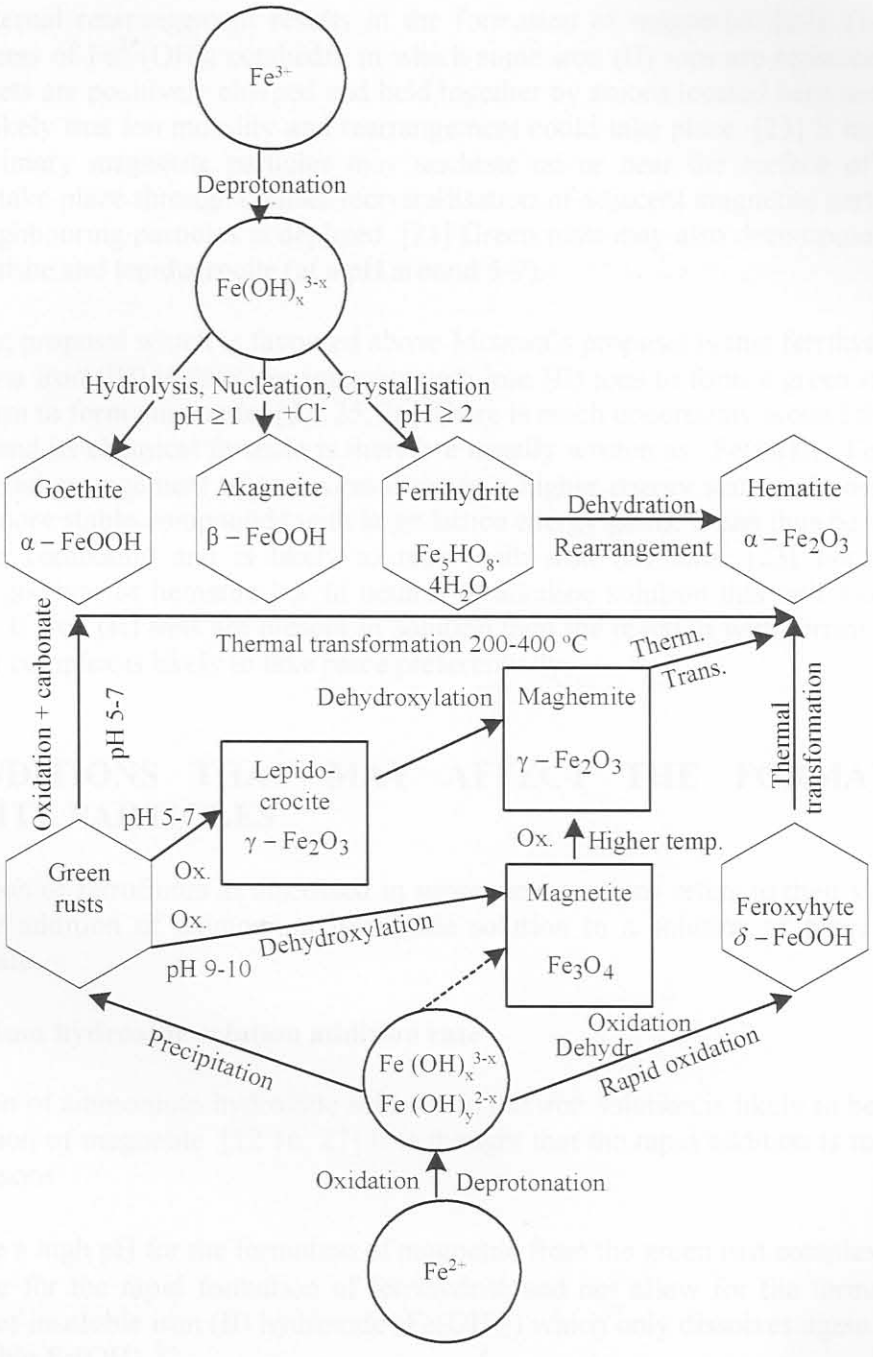

Figure 3.1 The formation of various species from iron (III) and iron (II) ions during hydrolysis

According to Figure 3.1, magnetite can be produced via the hydrolysis of a mixture of iron (III) and iron (II) ions.

Misawa has proposed that when a base is added to a mixture of iron (III) and iron (II) ions, "green rust" complexes form. These green rust complexes then transform to dark red complexes

before an internal rearrangement results in the formation of magnetite. [22] The green rusts consist of sheets of $Fe^{2+}(OH)_6$ octahedra in which some iron (II) ions are replaced by iron (III) ions. The sheets are positively charged and held together by anions located between the layers. It is therefore likely that ion mobility and rearrangement could take place. [23] It has been shown that small primary magnetite particles may nucleate on or near the surface of these plates. Growth may take place through contact recrystallisation of adjacent magnetite particles until the supply of neighbouring particles is depleted. [24] Green rusts may also decompose to form non-magnetic goethite and lepidocrocite (at a pH around 5-7).

A more recent proposal which is favoured above Misawa's proposal is that ferrihydrite, which is precipitated via iron (III) hydroxides interacts with iron (II) ions to form a green rust which can again transform to form magnetite. [22, 25, 26] There is much uncertainty around the structure of ferrihydrites and its chemical formula is therefore usually written as "$Fe(OH)_3$". Ferrihydrite has a poorly ordered arrangement of atoms resulting in a higher energy state and possesses several pathways to more stable compounds with large lattice energy gains. It can thus be assumed to be a very active compound and is likely to react with iron (II) ions. [23] Ferrihydrites may transform to goethite or hematite but in neutral or alkaline solution this will most likely take place slowly. If iron (II) ions are present in solution then the reaction with ferrihydrites to form the green rust complex is likely to take place preferentially.

3. CONDITIONS THAT MAY AFFECT THE FORMATION OF MAGNETITE PARTICLES

The preparation of ferrofluids as discussed in subsequent sections refers to their synthesis in the laboratory by addition of ammonium hydroxide solution to a solution of ferric chloride and ferrous sulphate.

3.1 Ammonium hydroxide solution addition rate

Rapid addition of ammonium hydroxide solution to the iron solution is likely to be preferred for the precipitation of magnetite. [12 16, 27] It is thought that the rapid addition is required for the following reasons:

- to provide a high pH for the formation of magnetite from the green rust complexes,
- to provide for the rapid formation of ferrihydrite and not allow for the formation of large amounts of insoluble iron (II) hydroxide ($Fe(OH)_2$) which only dissolves again at high pH to form soluble $Fe(OH)_x^{2-x}$.
- to prevent the formation of goethite and akagneite which could result from too slow an ammonium hydroxide solution addition.

3.2 Stirrer speed during precipitation

High stirrer speeds are recommended in literature for the precipitation reaction. [12] The stirrer speed is related to the pH experienced in the solution. Neutralisation of the acidic iron solution will take place more quickly if the mixture is agitated rapidly. Rapid stirring should also prevent

the formation of localised areas of high pH. In these areas, the green rust complexes will very likely form, but in other areas of low pH, non-magnetic species may be formed and non-magnetic iron oxides precipitated.

As mentioned in Section 2, small primary magnetite particles may nucleate on or near the surface of the sheets of the green rust complex and growth may take place through contact recrystallisation of adjacent magnetite particles. It is predicted that growth will cease once the supply of neighbouring particles is depleted. There may therefore be an inherent limitation to the size of magnetite crystals forming by chemical precipitation.

3.3 Time between precipitation and peptization reactions

The formation of magnetite crystals from the green rust complex is governed by the kinetics of the formation of the primary particles and the contact recrystallisation. It is therefore expected that allowing some time between the precipitation and peptization reactions will maximise the formation of magnetite. As discussed in Chapter 2, the magnetite particle size is important to ensure the correct magnetic properties and to ensure stability of the fluid (by preventing settling out of particles).

3.4 Temperature of the iron solution before precipitation

The precipitation of magnetite is exothermic and is accompanied by a rise in temperature in the range of 33-48 °C. If the initial iron solution temperature is high, the kinetics of the decomposition of the green rust complex may be enhanced to such an extent that smaller magnetite crystals may form.

3.5 Final pH as a function of the total ammonium hydroxide solution added

According to Figure 3.1, the pH required for the conversion of green rusts to magnetite is in the range of 9-10. The amount of ammonium hydroxide solution added to the iron solution must be such that this required final pH is reached (this is on condition that the green rust complex has been produced). A volume of ammonium hydroxide solution far in excess of the final stoichiometric amount will probably be required to achieve this pH.

4. INVESTIGATION INTO THE PREFERRED CONDITIONS FOR MAGNETITE PRECIPITATION

A set of investigations was designed to determine which of the parameters as discussed in Section 3 are critical for the formation of magnetite. Each of the parameters was investigated at a high and a low level. The high and low values were chosen to be at extreme conditions so that it would be more likely to observe an effect if the parameter were of importance. An attempt would be made to explain observations recorded and final results in terms of the mechanisms as discussed in Section 2.

The ammonium hydroxide solution addition rate was varied from immediate addition (in approximately one second) to addition of the solution over 20 minutes. The stirrer speed during precipitation was varied from 130 to 1300 rpm. The time between the precipitation and peptization reactions was varied from one minute to one hour. The temperature of the iron solution before precipitation was varied from room temperature (approximately 22-25°C) to 80°C. To control the final pH, the amount of ammonium hydroxide solution added to the iron solution was varied from the stoichiometric amount of ammonium hydroxide solution required for precipitation of magnetite to two times excess ammonium hydroxide solution according to eqs (2.11) to (2.13).

Whilst the parameter in consideration was varied, the other parameters were maintained constant. The constants for these parameters were chosen such that they would not adversely influence the ferrofluid production e.g. it is suspected that the ammonium hydroxide solution addition should be rapid and when the four others parameters were being investigated, the ammonium hydroxide solution addition was in one second. Five parameters were investigated at a high and low level. This would imply that ten experiments should be conducted. However, because the "constant" parameters were sometimes the same value as the high or low limit, only six investigations were necessary. This is further explained in Tables 3.1 and 3.2. In Table 3.1, the highlighted cells depict the high and low levels for the parameters.

Table 3.1 Upper and lower limits for investigation of parameters influencing magnetite precipitation

	Ammonium hydroxide solution addition rate	Stirrer speed (rpm)	Time (min)	Temperature of iron solution	pH (final) as function of volume of ammonium hydroxide solution
1	Addition in 1 second	1300	60	Room temperature	2*excess NH_4OH solution
2	Addition over 20 min	1300	60	Room temperature	2*excess NH_4OH solution
3	Addition in 1 second	130	60	Room temperature	2*excess NH_4OH solution
4	Addition in 1 second	1300	60	Room temperature	2*excess NH_4OH solution
5	Addition in 1 second	1300	1	Room temperature	2*excess NH_4OH solution
6	Addition in 1 second	1300	60	Room temperature	2*excess NH_4OH solution
7	Addition in 1 second	1300	60	Room temperature	2*excess NH_4OH solution
8	Addition in 1 second	1300	60	Heat iron solution to 80°C before precipitation	2*excess NH_4OH solution
9	Addition in 1 second	1300	60	Room temperature	Stoichiometric amount of NH_4OH solution
10	Addition in 1 second	1300	60	Room temperature	2*excess NH_4OH solution

Experiments number 4, 6, 7 and 10 consist of the same conditions as number 1. These investigations were eliminated. The final investigations are depicted in Table 3.2.

Table 3.2 Final set of investigations to determine the effect of certain parameters on the precipitation of magnetite

	Ammonium hydroxide solution addition rate	Stirrer speed (rpm)	Time (min)	Temperature of iron solution	pH (final) as function of volume of ammonium hydroxide solution
1	Addition in 1 second	1300	60	Room temperature	2*excess NH_4OH solution
2	Addition over 20 min	1300	60	Room temperature	2*excess NH_4OH solution
3	Addition in 1 second	130	60	Room temperature	2*excess NH_4OH solution
5	Addition in 1 second	1300	1	Room temperature	2*excess NH_4OH solution
8	Addition in 1 second	1300	60	Heat iron solution to 80°C before precipitation	2*excess NH_4OH solution
9	Addition in 1 second	1300	60	Room temperature	Stoichiometric amount of NH_4OH solution

The precipitation temperature, the pH of the initial iron solution and that of the mixture immediately after precipitation, one minute after precipitation and the final pH before the addition of the kerosene and oleic acid and the ferrofluid temperature after heating were recorded.

The saturation magnetisation was measured and magnetisation curves recorded as a response to determine the final quality of the fluid. In order to ensure that the final fluid properties are comparable, the fluids were centrifuged to remove any unpeptized material, large particles and agglomerates and diluted to a density of 0.98 g/cm^3.

The method of ferrofluid production was as follows:

1. Add 200 ml water to 37.3 g $FeSO_4.7H_2O$.
2. Stir for ten minutes at a speed of 1050 rpm.
3. Add 54 ml $FeCl_3$.
4. Rinse out the $FeCl_3$ container with 220 ml water and add this volume to the iron solution.
5. Stir for an additional eight minutes.
6. Measure pH.
7. Set the required stirrer speed for precipitation.
8. Add required volume of NH_4OH at the required addition rate.
9. Measure pH immediately after precipitation and again after one minute.
10. Wait the required time delay.
11. Measure final pH.
12. Reduce stirrer speed to 800 rpm.
13. Add 6 ml oleic acid and 38.5 ml kerosene.
14. Heat the mixture over 21 minutes to approximately 80°C (the final temperatures varied but were recorded).
15. Remove from stirrer and allow the mixture to settle and cool on a barium ferrite magnet. The aqueous and organic layers can then be separated.
16. Centrifuge for 30 minutes.
17. Dilute to 0.98 g/cm^3.

18. Measure the saturation magnetisation.

5. RESULTS AND DISCUSSION

Figure 3.2 gives plots of the magnetisation curves for investigations 1, 2, 3, 5 and 8 as outlined in Table 3.2 (curves 1 and 8 lie almost on top of one another) and Table 3.3 gives the temperatures and pH recorded during the investigations.

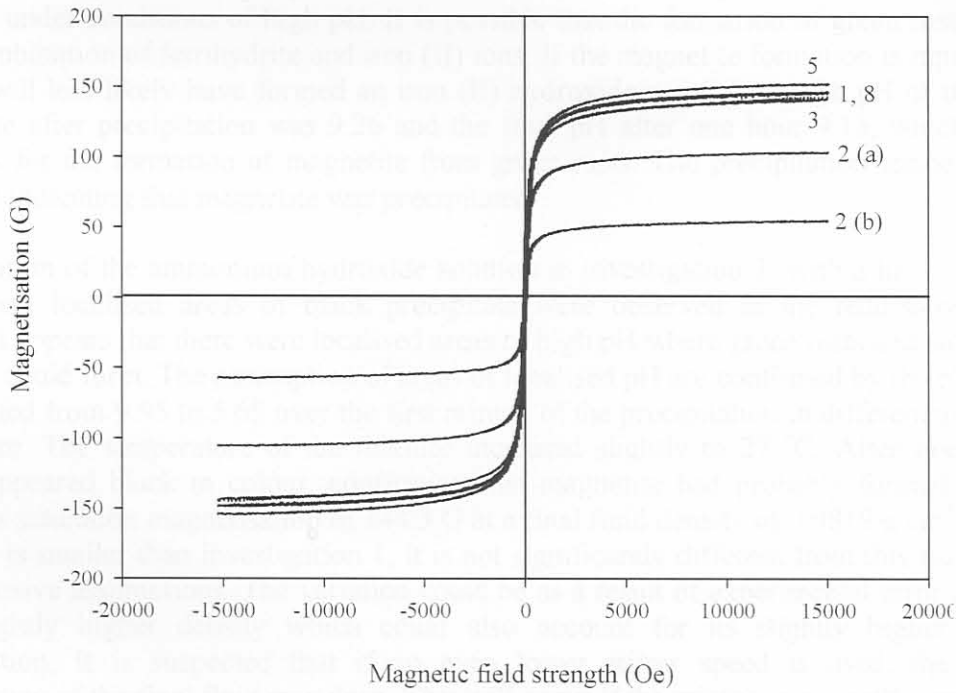

Figure 3.2 Plots of magnetisation curves for the investigations

Table 3.3 Temperatures and pH measured for the various investigations

	Temperature at precipitation (^{0}C)	pH				Temperature of final ferrofluid after heating (^{0}C)
		Iron solution	At precipitation	After 1 minute	Final pH	
1	36	1.32	9.34	9.26	9.13	79
2a	24	1.02	See subsequent discussion		9.21	80
2b	22	1.52	See subsequent discussion		9.18	79
3	27	1.4	Varied from 9.95-5.65		9.4	77
5	34	1.27	9.22	9.15	9.15	79
8	82	1.17	7.49	7.45	8.41	80
9	32	1.06	3.63	4.86	3.95	78

All the magnetisation curves in Figure 3.2 exhibit no hysteresis indicating that the fluids are superparamagnetic.

For investigation 1 where the ammonium hydroxide solution was added rapidly to the iron solutions, a green-black gelatinous viscous mixture was observed immediately. This gelatinous precipitate is then transformed into a black non-viscous crystalline precipitate. The saturation magnetisation of this fluid was 147.6 G at a final fluid density of 0.9853 g/cm^3. These observations are consistent with a mechanism that describes the formation of magnetite via the formation of a green rust complex and the subsequent decomposition of this complex to magnetite under conditions of high pH. It is possible that the formation of green rusts occurred by the combination of ferrihydrite and iron (II) ions. If the magnetite formation is rapid, the iron (II) ions will less likely have formed an iron (II) hydroxide precipitate. The pH of the mixture one minute after precipitation was 9.26 and the final pH after one hour 9.13, which are ideal conditions for the formation of magnetite from green rusts. The precipitation temperature was 36 °C also indicating that magnetite was precipitated.

Upon addition of the ammonium hydroxide solution in investigation 3, with a low stirrer speed of 130 rpm, localised areas of black precipitate were observed in the reddish-orange iron solution. It appears that there were localised areas of high pH where green rusts and subsequently magnetite could form. The assumption of areas of localised pH are confirmed by the pH readings which varied from 9.95 to 5.65 over the first minute of the precipitation in different areas within the mixture. The temperature of the mixture increased slightly to 27 °C. After one hour, the mixture appeared black in colour, confirming that magnetite had probably formed. The final fluid had a saturation magnetisation of 144.3 G at a final fluid density of 0.9819 g/cm^3. Although this value is smaller than investigation 1, it is not significantly different from this fluid to make any conclusive assumptions. The variation could be as a result of experimental error and fluid 1 has a slightly higher density which could also account for its slightly higher saturation magnetisation. It is suspected that if an even lower stirrer speed is used, the saturation magnetisation of the final fluid may drop. This will occur if the mixing is so inefficient that areas of the mixture remain at low pH for an extended period of time.

In investigation 5, the ammonium hydroxide solution was added rapidly to the iron solution and the resultant mixture only stirred for one minute before the addition of oleic acid and kerosene. A precipitation temperature of 34 °C was recorded. The same observations as recorded for investigation 1 were observed. The final saturation magnetisation (at 0.9824 g/cm^3) was 153.6 G.

In investigation 8, the addition of the ammonium hydroxide solution to the iron solution resulted immediately in the precipitation of a black mixture. It is again suspected that the mechanism is the same as for investigations 1 and 5. The final saturation magnetisation was 147.8 G at 0.9802 g/cm^3.

Investigation 9 did not yield a ferrofluid. No magnetic material was precipitated, instead a mixture of a brown rusty colour was precipitated and the appearance of this mixture remained the same throughout the stirring following precipitation (see Figure 3.3). The precipitate later

separated into four layers: a layer containing the brown precipitate at the bottom, a greenish aqueous layer in the middle, a layer with brown precipitate and the oleic acid-kerosene mixture at the top. The reason two layers of brown precipitate are observed is probably because a portion of the precipitate contains trapped kerosene molecules which makes it less dense. [28] The pH at precipitation was 3.63 and that after one minute 4.86. The final pH after an hour was 3.95. According to Figure 3.1, it is likely that at these low pHs, goethite could form. Akagneite is another possible non-magnetic product as the formation of akagneite is likely in solutions containing chlorides. It is possible that some green rusts formed, but at these low pHs, the green rust would probably have been transformed to goethite or lepidocrocite (assuming a pH of just below 5 would be suitable for this reaction to occur). It is also likely that ferrihydrite formed. The iron (II) ions may have formed insoluble iron (II) hydroxide from which the displacement of the iron (II) ions would be difficult at such a low pH for subsequent reaction with ferrihydrite to form magnetite.

Figure 3.3 Brown precipitate produced during investigation 9

The results from investigation 2 proved to be very interesting. Two of these investigations were performed. In the first investigation, the stirrer speed was not increased from 1050 to 1300 for the precipitation reaction and the investigation was therefore repeated. The results were, however, recorded. This investigation was called 2(a) and the subsequent investigation 2(b). The ammonium hydroxide addition rate in 2(a) was 12 ml/min whilst that for 2(b) was 6.8 ml/min.

In investigation 2(a) it was noted that there was a low pH initially. This pH increased over the course of the ammonium hydroxide solution addition to yield a final pH of 9.17 (Figure 3.4). The temperature also increased to 36 °C.

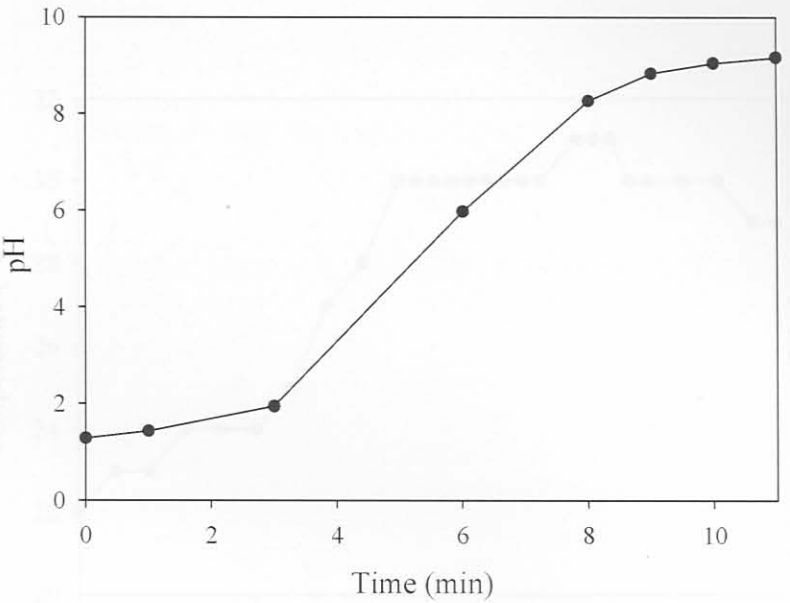

Figure 3.4 Plot of pH versus time for the ammonium hydroxide solution addition rate of 12 ml/min

When the investigation was repeated, a more detailed recording of the pH was performed. The results are shown in Figure 3.5 with the changes in temperature shown in Figure 3.6.

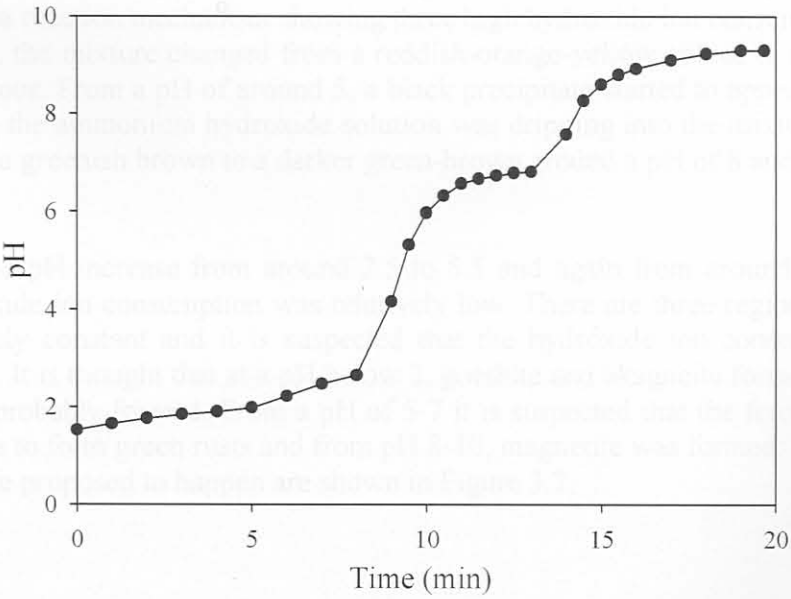

Figure 3.5 Plot of pH versus time for the ammonium hydroxide solution addition rate of 6.8 ml/min

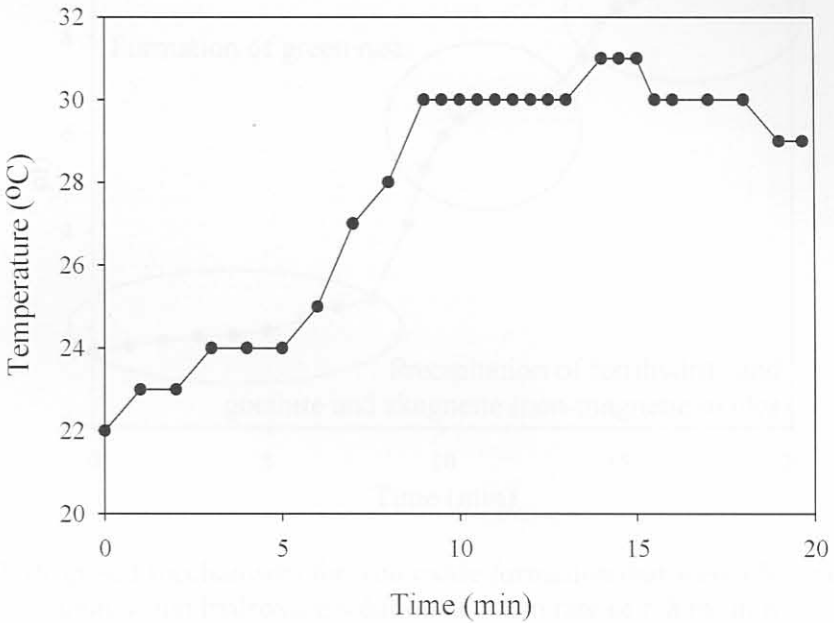

Figure 3.6 Plot of temperature versus time for the ammonium hydroxide solution addition rate of 6.8 ml/min

The plot of pH versus time shows two distinct regions where there was a rapid change in pH. This is typical of a reaction mechanism showing three high hydroxide ion consumption reactions. At a pH below 2, the mixture changed from a reddish-orange-yellow colour to a darker red and then an ochre colour. From a pH of around 5, a black precipitate started to appear at the walls of the beaker where the ammonium hydroxide solution was dripping into the mixture. The mixture then turned from a greenish brown to a darker green-brown around a pH of 8 and then to a glossy black.

There was a rapid pH increase from around 2.5 to 5.5 and again from around 6.5 to 8 during which the hydroxide ion consumption was relatively low. There are three regions where the pH remained relatively constant and it is suspected that the hydroxide ion consumption in these regions was high. It is thought that at a pH below 2, goethite and akagneite formed. Above pH 2, ferrihydrite was probably formed. From a pH of 5-7 it is suspected that the ferrihydrites reacted with iron (II) ions to form green rusts and from pH 8-10, magnetite was formed. The areas where these reactions are proposed to happen are shown in Figure 3.7.

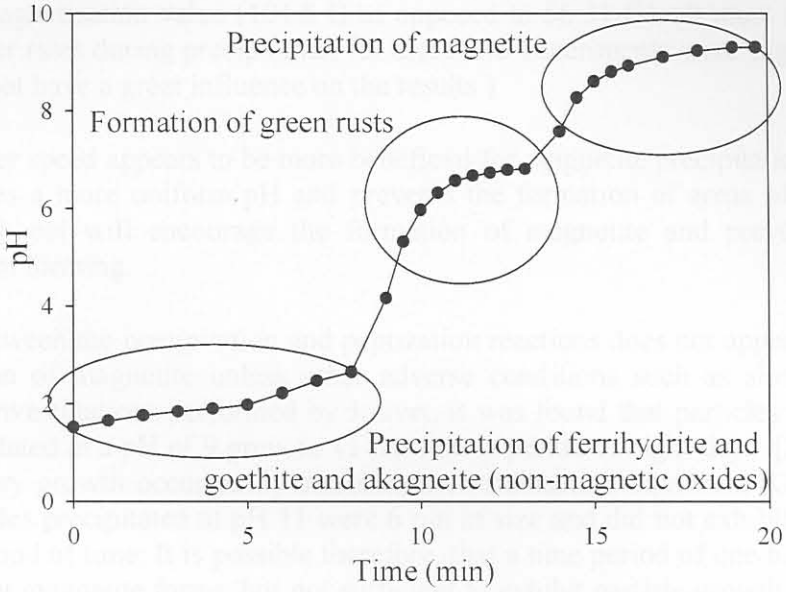

Figure 3.7 Proposed mechanisms for iron oxide formation that were observed with an ammonium hydroxide solution addition rate of 6.8 ml/min

The plot of temperature versus time (Figure 3.6) shows a gradual increase from 22 to 31 °C as the green rust complex forms and magnetite is precipitated. The temperature drops off slightly after 16 minutes and it is believed that the mixture cools slightly while it is being stirred.

The final saturation magnetisations for investigations 2(a) and 2(b) were 104.8 G (0.9827 g/cm^3) and 56.31 G (0.9836 g/cm^3) respectively. The magnetisation was low probably because of the formation of non-magnetic material before the magnetite could precipitate.

6. CONCLUSIONS AND RECOMMENDATIONS

From the investigations conducted into the preferred conditions for the precipitation of magnetite, the following conclusions can be made:

- It appears that magnetite is produced through the formation of green rusts. The green rusts are produced from ferrihydrites and iron (II) ions. Magnetite is then produced by the dehydroxylation of the green rusts. High pH favours the formation of magnetite.

- Rapid addition of ammonium hydroxide solution is recommended. The rapid addition of the solution raises the pH to the range required for magnetite formation and prevents the formation of non-magnetic products. The rapid formation of green rusts through the use of iron (II) ions prevents the formation of insoluble iron (II) hydroxides which are less available for reaction with ferrihydrites. It was observed that adding the ammonium hydroxide at approximately twice the rate (12 ml/min as opposed to 6.8 ml/min) led to almost double the

saturation magnetisation value (104.8 G as opposed to 56.31 G). (It must be borne in mind that the stirrer rates during precipitation for these two experiments were slightly different but this should not have a great influence on the results.)

- A rapid stirrer speed appears to be more beneficial for magnetite precipitation. A rapid stirrer speed ensures a more uniform pH and prevents the formation of areas of localised pH. A uniform high pH will encourage the formation of magnetite and prevent non-magnetic products from forming.

- The time between the precipitation and peptization reactions does not appear to be critical to the formation of magnetite unless other adverse conditions such as slow stirrer rate are present. In investigations performed by Jolivet, it was found that particles of size 9 nm that were precipitated at a pH of 9 grew to 11 nm over a period of eight days. [29] It is proposed that secondary growth occurred by dissolution-crystallisation equilibria (Ostwald ripening). Those particles precipitated at pH 11 were 6 nm in size and did not exhibit any growth over the same period of time. It is possible therefore, that a time period of one hour was sufficient to ensure that magnetite forms, but not sufficient to exhibit particle growth which could lead to improved magnetic properties. On the other hand, it could be that growth is not significant and the mechanism by which growth occurs does not favour large particle sizes.

- The temperature of the iron solution before precipitation did not appear to be critical in the formation of magnetite. The ammonium hydroxide solution addition rate and stirrer speed to ensure correct pH conditions are thought to be more critical.

- The final pH as a function of volume of ammonium hydroxide added is critical to the formation of magnetite. Sufficient ammonium hydroxide should be added to ensure that the pH is in the correct range for the dehydroxylation of green rusts and for the prevention of formation of non-magnetic oxides.

CHAPTER 4

PRECIPITATION: THE WASHING AND CONCENTRATION OF MAGNETITE PARTICLES USING SEDIMENTATION FUNNELS

1. INTRODUCTION

As discussed in Chapter 2, a precipitate of magnetite in an aqueous salt solution is produced during the preparation of ferrofluid. For water-based ferrofluid production, concentration of the magnetite suspension is essential for the production of a fluid of suitable magnetic properties. Washing is also important to ensure stability of the fluid. Although concentration of the magnetite suspension is not vital in the production of hydrocarbon solvent-based ferrofluid (the magnetite is transferred to a specified volume of hydrocarbon carrier liquid), washing the precipitate will very likely improve the quality of the hydrocarbon solvent-based ferrofluid. The salts in solution may adversely affect the production process, hinder the final organic/aqueous phase separation and may increase the viscosity of the product. It was therefore decided to investigate a method for the washing and concentration of the magnetite particles.

Washing and concentrating the ultrafine magnetite particles is extremely difficult. By virtue of their size, the particles cannot be trapped in filter media. In addition, because of their size, they are colloidally stable and settle with difficulty. There is currently no commercially available system to perform this function on production scale. Washing of precipitate in ferrofluid manufacture is performed only on a laboratory scale and is a manual and laborious process.

To achieve the concentration and washing of the magnetite, a concept was developed which involves four cone-shaped vessels in series. These vessels were called sedimentation funnels which are plastic containers of approximately 20 litre volumetric capacity around which copper coils are wound. A direct current is passed through the coils thus generating a magnetic field in the interior of the funnel. The proposed layout of the funnels is given in Figure 4.1. [30]

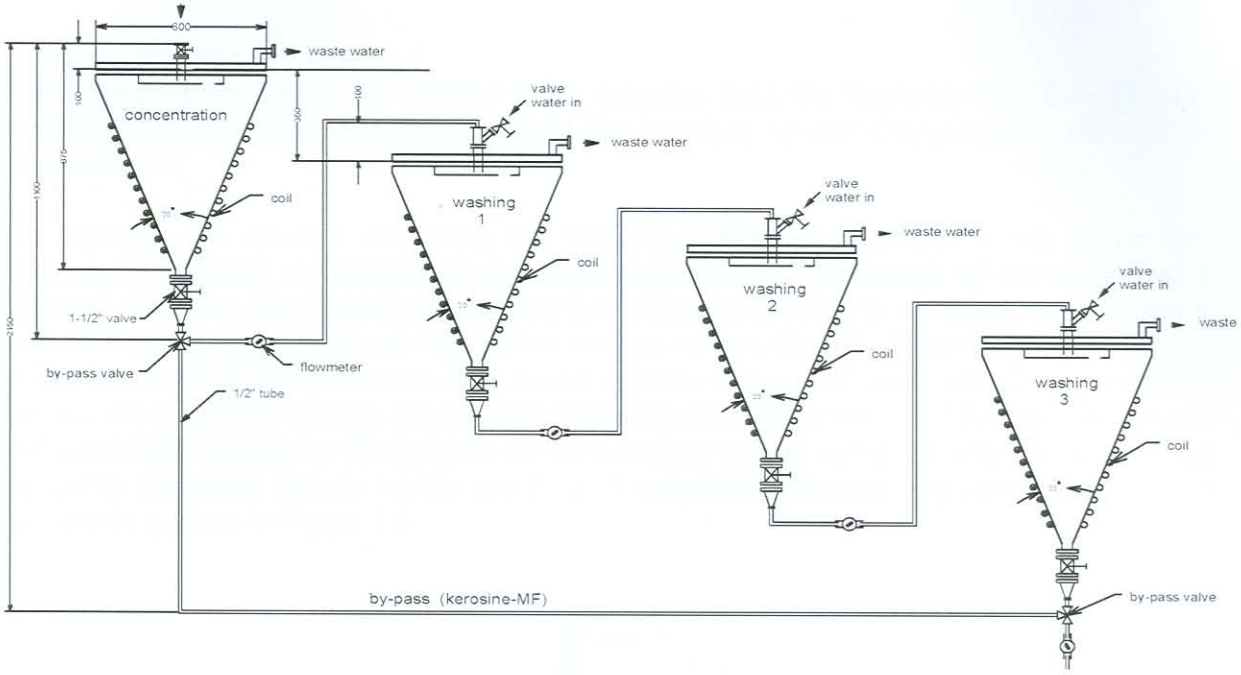

Figure 4.1 Layout of sedimentation funnels

Preliminary modelling using 2D PC Opera (to display the magnetic field strength in one of the funnels) indicated that the magnetic field is strongest towards the base of the funnel as shown in Figure 4.2. [31] The values as given in Figure 4.2 are in Gauss or Oe.

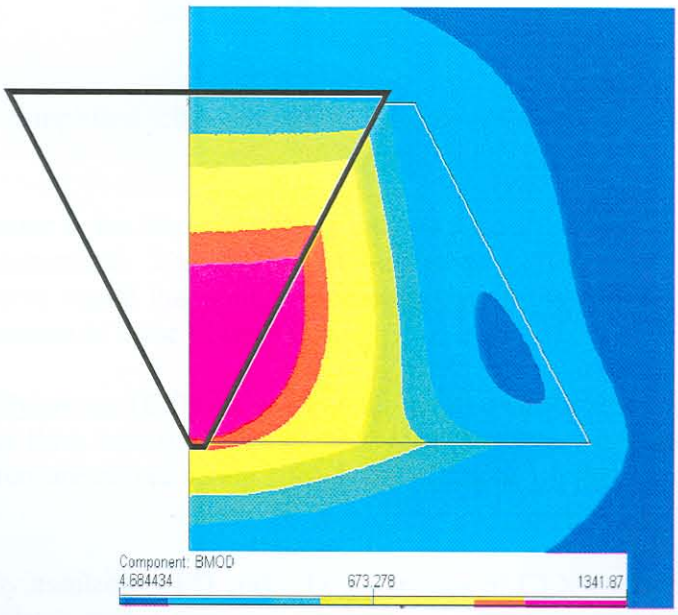

Figure 4.2 Magnetic field strength in one of the sedimentation funnels

When placed in the funnel and exposed to the magnetic field, the magnetite should be attracted towards the region of greatest magnetic field and therefore become concentrated at the base of the funnel.

The aqueous salt solution containing the suspended magnetite particles is fed to the first sedimentation funnel. A volume of the carrier liquid and a percentage of the magnetite is removed from the first funnel via an overflow. This liquid reports to waste. In subsequent funnels, water is added to the mixture before its entry to these funnels. Depending on the volume of wastewater removed from the first funnel and the volume of water added to subsequent funnels, the magnetite fraction can be concentrated to the desired volume. The addition of water to the last three funnels serves to dilute the salts that are present in the salt solution. Wastewater leaves the remaining funnels via the overflow. A simplified schematic representation of one of the funnels is given in Figure 4.3.

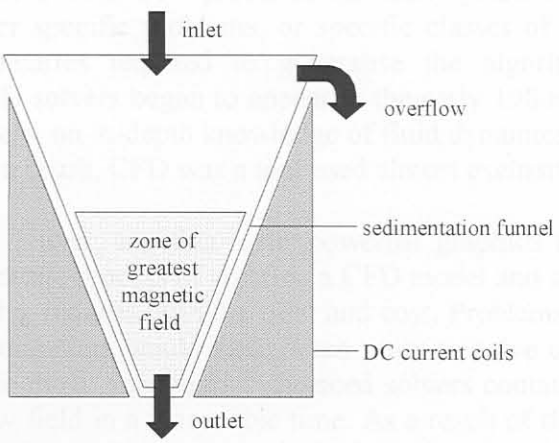

Figure 4.3 Simplified schematic representation of the sedimentation funnel

The most important factor in the funnel design is that the total allowable loss of magnetite to the overflow should be minimised. The volume of magnetite reporting to the overflow will be affected by flow patterns inside the funnel. Modelling the flow of liquid through the funnels would provide an indication of these flow patterns.

Computational Fluid Dynamics (CFD) is a computer-based tool for simulating the behaviour of systems involving fluid flow, heat transfer and other related physical processes. The equations of fluid flow over a region are solved using specified conditions on the boundary of the specific region of interest.

CFX is a commercially available CFD code. Two versions of CFX commonly in use are CFX-4.3 and CFX-5.4.1. These codes vary mainly in the method in which the geometry to be

modelled is meshed. CFX-Build (the pre-processor) is used for geometry creation and meshing while CFX-Visualise or CFX-Analyse is used for visualisation of results (post-processing).

In the CFD study, initially two base case funnels consisting of only water flowing into the funnel were modelled using CFX-4.3. For comparison purposes, the same geometries were meshed in CFX-5.4 which makes use of a different method of meshing (this is explained in subsequent sections). Using multiphase flow, a solid phase was introduced into the funnel to obtain an idea as to the flow of magnetite particles and to determine whether they would be lost in the overflow. The final step would be to model the funnel with the effect of the magnetic field but this was not performed in this investigation.

2. COMPUTATIONAL FLUID DYNAMICS

2.1 The history of Computational Fluid Dynamics

Computers have been used to solve fluid flow problems for many years. Numerous programs have been written to solve either specific problems, or specific classes of problem. From the mid-1970s the complex mathematics required to generalise the algorithms began to be understood. General purpose CFD solvers began to appear in the early 1980s and required what were then very powerful computers, an in-depth knowledge of fluid dynamics and large amounts of time to set up simulations. As a result, CFD was a tool used almost exclusively in research.

Recent advances in computing power, together with powerful graphics and interactive 3D manipulation of models mean that the process of creating a CFD model and analysing the results is much less labour-intensive. This reduces both the time and cost. Problems that can be solved in a few seconds with current computers would have taken years to solve using computational methods and computers available thirty years ago. Advanced solvers contain algorithms which enable robust solution of the flow field in a reasonable time. As a result of these factors, CFD is now an established industrial design tool, helping to reduce design timescales and improving processes throughout the engineering world. CFD provides a cost-effective and accurate alternative to scale model testing, with variations on the simulation being performed quickly. CFD has become an important tool for use in experiment and pure theory. Certain problems with complex physics can be addressed using this technique as long as there is a governing equation describing the physics that can be solved numerically. [32]

2.2 The mathematics of CFD

CFD is the numerical solution of the fluid flow of partial differential equations describing certain models. The equations which describe the processes of mass, momentum and heat transfer are known as the Navier-Stokes equations. These are partial differential equations which were derived in the early nineteenth century. They have no known general analytical solution but can be discretised and solved numerically. The following equations give the Navier-Stokes equations for the conservation of mass (eq. (4.1)), momentum (eq. (4.2)) and energy (eq. (4.3)) respectively. [32]

$$\frac{D\rho}{Dt} + \rho\vec{\nabla} \bullet \mathbf{v} = 0 \tag{4.1}$$

$$\rho\frac{D\mathbf{v}}{Dt} = -\vec{\nabla}P + \rho\mathbf{g} + \mu\vec{\nabla}^2\mathbf{v} \tag{4.2 a}$$

In expanded form, (4.2 a) becomes:

$$\begin{aligned}
\rho\left(\frac{\partial v_x}{\partial t} + v_x\frac{\partial v_x}{\partial x} + v_y\frac{\partial v_x}{\partial y} + v_z\frac{\partial v_x}{\partial z}\right) &= -\frac{\partial P}{\partial x} + \rho g_x + \mu\left(\frac{\partial^2 v_x}{\partial x^2} + \frac{\partial^2 v_x}{\partial y^2} + \frac{\partial^2 v_x}{\partial z^2}\right) \\
\rho\left(\frac{\partial v_y}{\partial t} + v_x\frac{\partial v_y}{\partial x} + v_y\frac{\partial v_y}{\partial y} + v_z\frac{\partial v_y}{\partial z}\right) &= -\frac{\partial P}{\partial y} + \rho g_y + \mu\left(\frac{\partial^2 v_y}{\partial x^2} + \frac{\partial^2 v_y}{\partial y^2} + \frac{\partial^2 v_y}{\partial z^2}\right) \\
\rho\left(\frac{\partial v_z}{\partial t} + v_x\frac{\partial v_z}{\partial x} + v_y\frac{\partial v_z}{\partial y} + v_z\frac{\partial v_z}{\partial z}\right) &= -\frac{\partial P}{\partial z} + \rho g_z + \mu\left(\frac{\partial^2 v_z}{\partial x^2} + \frac{\partial^2 v_z}{\partial y^2} + \frac{\partial^2 v_z}{\partial z^2}\right)
\end{aligned} \tag{4.2 b}$$

$$\frac{\partial}{\partial t}(\rho E) + \vec{\nabla} \bullet (\rho\mathbf{v}E) = \vec{\nabla} \bullet (k\vec{\nabla}T) + \vec{\nabla} \bullet (\overline{\overline{\sigma}} \bullet \mathbf{v}) + W_f + q_H \tag{4.3}$$

There are a number of different solution methods which are used in CFD codes. The most common is known as the finite volume technique. In this technique, the region of interest is divided into small sub-regions, called control volumes. The equations are discretised and solved iteratively for each control volume. As a result, an approximation of the value of each variable at specific points throughout the domain can be obtained. In this way, one derives a full picture of the behaviour of the flow. [32]

The following equations give an example of the discretisation of the first and second derivatives where O indicates the accuracy of the approximation. [32]

$$\begin{aligned}
\frac{\partial f}{\partial x} &= \frac{f(x+\Delta x) - f(x-\Delta x)}{2\Delta x} + O(\Delta x)^2 = \frac{f_{i+1} - f_{i-1}}{2\Delta x} + O(\Delta x)^2 \\
\frac{\partial^2 f}{\partial x^2} &= \frac{f(x+\Delta x) - 2f(x) + f(x-\Delta x)}{\Delta x^2} + O(\Delta x)^2 = \frac{f_{i+1} - 2f_i + f_{i-1}}{\Delta x^2} + O(\Delta x)^2
\end{aligned} \tag{4.4}$$

2.3 Uses of CFD

CFD is used by engineers and scientists in a wide range of fields. Typical applications include:

- Process industry e.g. mixing vessels, chemical reactors
- Building services e.g. ventilation of buildings, such as atria
- Health and safety e.g. investigating the effects of fire and smoke
- Motor industry e.g. combustion modelling, car aerodynamics
- Electronics e.g. heat transfer within and around circuit boards
- Environmental e.g. dispersion of pollutants in air or water
- Power and energy e.g. optimisation of combustion processes

- Medical e.g. blood flow through grafted blood vessels

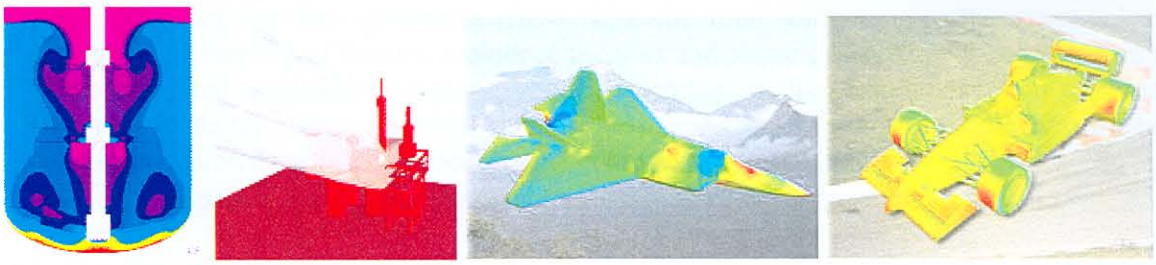

Figure 4.4 Applications of CFD to a stirred tank, to investigate the effects of fire and smoke on an oilrig and in the areas of aeronautical and automotive engineering

2.4 Performing a CFD simulation

In many commercial CFD packages, the process of performing a CFD simulation is split into three stages: the pre-processing, the solving and the post-processing.

2.4.1 The Pre-processor

The pre-processor is the component used to create the input for the solver. Pre-processing involves:

- Defining the geometry of the region of interest
- Selecting the physical models which are to be included in the simulation
- Specifying the properties of the fluid
- Specifying the boundary conditions
- Creating a mesh of control volumes

Pre-processing operations are interactive but are becoming increasingly automated e.g. in some commercial CFD packages, geometry can be imported from a CAD package and the mesh of control volumes is generated automatically. [33]

2.4.2 The Solver

The solver is the non-interactive component which solves the CFD problem and produces the results. The solver proceeds as follows:

- The partial differential equations are integrated over all the control volumes in the region of interest. This is equivalent to applying a basic conservation law (e.g. for mass or momentum) to each control volume.
- These integral equations are converted to a system of algebraic equations by generating a set of approximations for the terms in the integral equations.

- The algebraic equations are solved iteratively. An iterative approach is required because of the non-linear nature of the equations. As the solution approaches the exact solution it is said to converge. For each iteration, an error, or residual, is reported as a measure of the overall conservation of the flow properties. How close the final solution is to the exact solution depends on a number of factors, including the size and shape of the control volumes and the size of the final residuals. Complex physical processes, such as combustion and turbulence are often modelled using empirical relationships, and the approximations inherent in these models also contribute to differences between the CFD solution and the real flow.
- The solver produces a file of results which is then passed to the post-processor. [33]

2.4.3 The Post-processor

The post-processor is the interactive component used to analyse and present the results. Post-processing includes anything from obtaining point values to complex animated sequences.

Examples of some important features of post-processors are:

- Visualisation of the geometry and control volumes
- Vector plots showing the direction and magnitude of the flow
- Visualisation of the variation of scalar variables (such as temperature) through the domain
- Quantitative numerical output
- Hardcopy output [33]

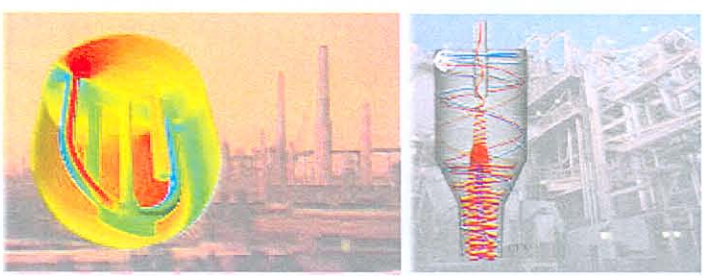

Figure 4.5 Visualisation of CFD modelling using the post-processor

3. APPLICATION OF THE CFD CODE

3.1 CFX-4.3

This section describes the modelling of the sedimentation funnels performed in CFX-4.

3.1.1 CFX-Build

CFX-Build, the pre-processor of CFX, is the main user interface module. It is an interactive program used to specify the CFD problem for input to the Solver. In CFX-Build, a parameterised model geometry must be created, meaning that when the meshlines are constructed on the

geometry they "match up" and create a four-sided element. Figure 4.6 shows an example of a simple circle with unparametrised geometry. This geometry cannot be meshed as the corner elements would only have three sides. The addition of the central element (highlighted in the figure on the right in Figure 4.6) allows the geometry to be parametrised.

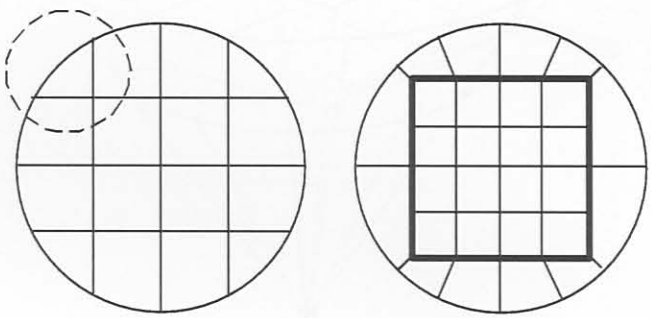

Figure 4.6 Unparametrised circle which can be parametrised with the addition of a square element inside the circle

In CFX-4, structured meshes are used to mesh geometries. The structure refers to an ordered arrangement of the grid cells in the physical domain. Structured meshes consist of rectangular-shaped elements in 2D and cubic-shaped meshes in 3D. In CFX, the user performs the surface meshing on the geometry while the pre-processor performs the volume meshing.

Figure 4.7 gives a schematic of the initial geometry (Geometry 1) of the sedimentation funnel. The funnel cone was 400 mm high with a 450 mm diameter base and inlet, outlet and overflow diameters of 12.7 mm diameter. The overflow is positioned 100 mm from the cone base.

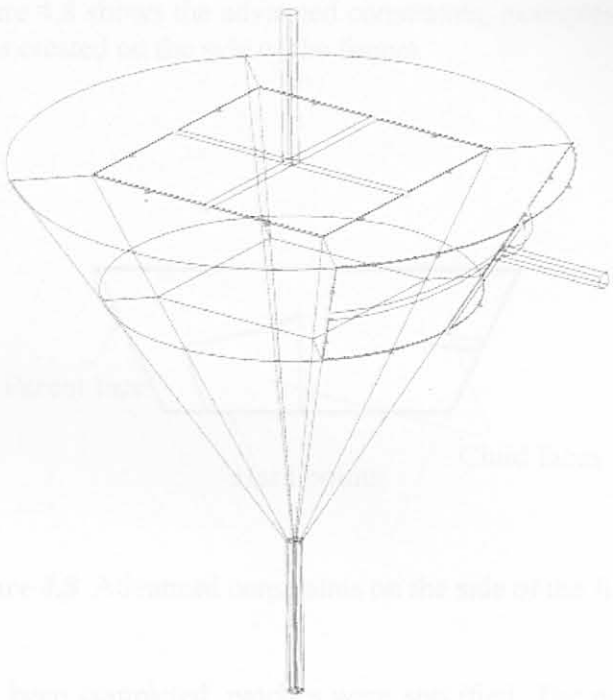

Figure 4.7 Schematic of the initial geometry

The geometry was created in a number of stages. The outlet pipe was created from a square surface inside a circle. This surface was extruded to form the outlet pipe and then further extruded to form the body of the funnel. The reason that this inner rectangular pipe is required is so that the geometry can be topologically correct. The inlet pipe was created by transforming the outlet pipe. Once the inlet pipe was attached to the funnel upper surface, additional surfaces could be created to ensure the geometry was topologically correct. To complete the geometry, a surface from the outlet was transformed and then projected onto the main body. The transformed and the projected surfaces were joined.

In CFX-4.3, if a smaller face, known as the child face, is attached to a larger face known as the parent face, constraints must be used to define this relationship. For the funnel geometry, constraints were required as more than one face from the inlet and overflow pipes constrained the surface face.

To create the constraints, a set of subordinate surfaces completely covering the parent face were created. This meant that areas on the parent face were defined as surfaces. What are termed hard curves and hard points were then created at the intersection of the edge of each subordinate surface and the parent face. These hard points are used by CFX-Build to describe the geometric association between two curves which are coincident but of different lengths. The hard points force a mesh node to occur at each hard point when the surfaces are meshed. (During the meshing which is described below, it is required, when using constraints, to firstly mesh all the subordinate surfaces, then the parent faces and then the other surfaces in the model.) For the

funnel application, Figure 4.8 shows the advanced constraints, examples of the child and parent faces and the hard points created on the side of the funnel.

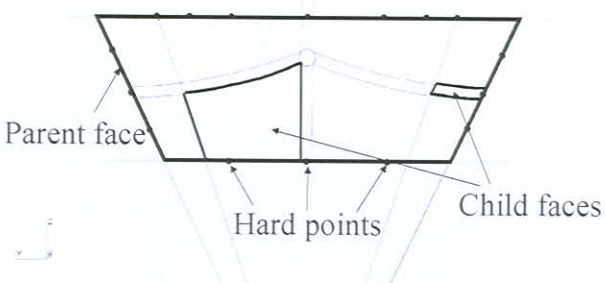

Figure 4.8 Advanced constraints on the side of the funnel

Once the geometry had been completed, patches were specified. The patches are used to name and to specify the location of any surface on which to apply boundary conditions e.g. an inlet, mass flow boundary and solid region. The location, name and type of patch is specified in CFX-Build. In the CFX-4 command file, the boundary conditions e.g. velocity at an inlet applied to each patch are specified. Patches are applied to whole surfaces or whole geometric solids to ensure that they are grid-independent. Patches were specified for the inlet, outlet and overflow. The remainder of the surfaces can either be specified, or the default is taken as a wall.

Once patches have been specified, the geometry can be meshed. CFX-4.3 uses the multi-block grid methodology. The method involves the use of an unstructured set of blocks which are attached to one another. On each of these blocks there is a structured grid. Meshes are prepared in two stages. Firstly, CFX-Build is used to generate surface meshes. This is an interactive process. (This is where, for example, mesh seeds can be specified and the constraint surfaces meshed.) The non-interactive program VOLMSH is then used to generate grids in 3D regions. For the funnel application, mesh seeds were used as shown in Figure 4.9 for various parts of the geometry. Mesh seeds were used to prevent too many cells from being formed, to ensure that the aspect ratio (cell height to width) of cells is relatively uniform (as close as possible to 1) and to ensure that the mesh is created correctly.

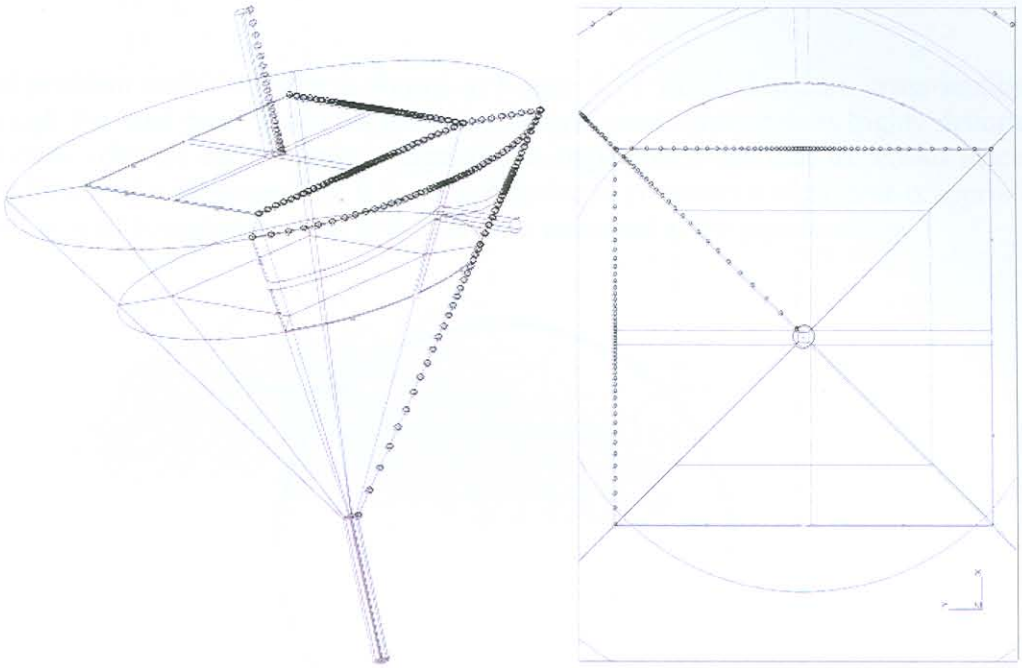

Figure 4.9 Mesh seeds in the geometry

Once Geometry 1 had been meshed, the limitations of using structured meshing became apparent. Because of the ratio of the outlet pipe to the funnel size, the mesh became very fine towards the base of the funnel as the cells were propagated downwards. This effect is shown in Figure 4.10. This results in an extremely fine mesh in relation to other areas of the geometry. If the coarser areas of the mesh at the top of the funnel were to be refined, this would result in a large number of cells with an over refinement in areas where it would not be required. (The aspect ratio is not close to 1.)

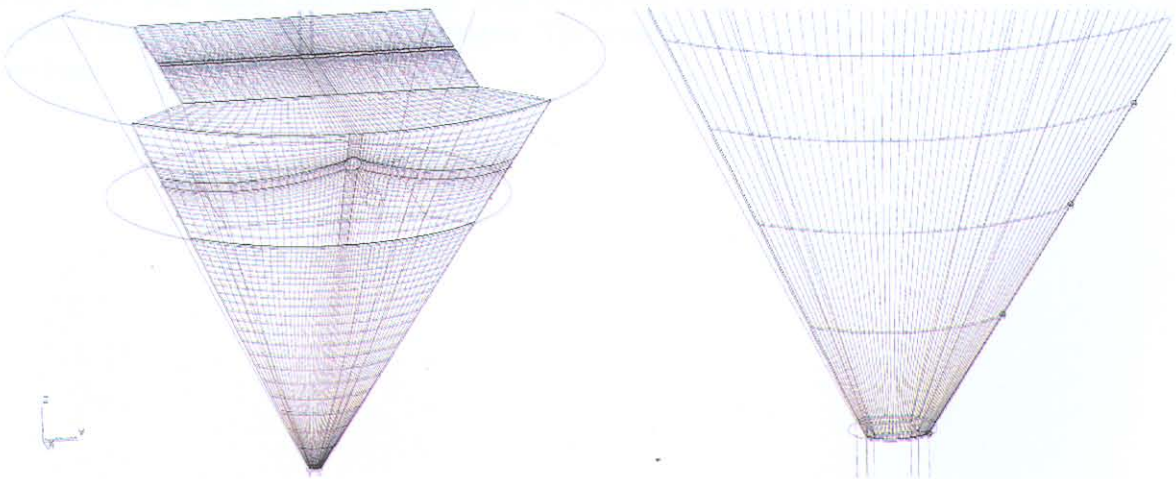

Figure 4.10 Poor mesh created at base of the funnel

A second problem with the mesh is shown in Figure 4.11 which depicts a cross-sectional grid slice through the inlet pipe. It can be seen that the grid inside the circle is highly distorted. The corner control volumes each contain a large obtuse angle which can lead to serious inaccuracies in the prediction of wall properties. It is good practice to construct a mesh that is approximately orthogonal at wall boundaries. (This distortion also occurred in the pipe overflow.)

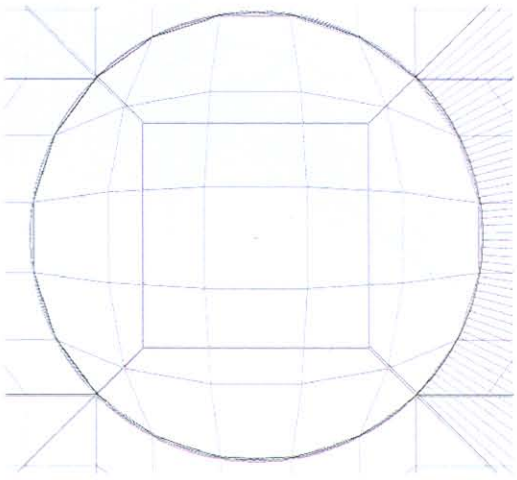

Figure 4.11 Obtuse angles created inside the inlet and overflow pipes

The results obtained from such a grid may not be accurate. It was decided to investigate this geometry using larger pipe diameters. (The original geometry is investigated later in this chapter using unstructured grids in CFX-5.3.)

A schematic of the new geometry (Geometry 2) is given in Figure 4.12. In this configuration, the funnel cone was again 400 mm high with a 450 mm diameter base, but the inlet, outlet and overflow diameters are 75 mm in diameter. The overflow is again positioned 100 mm from the cone base.

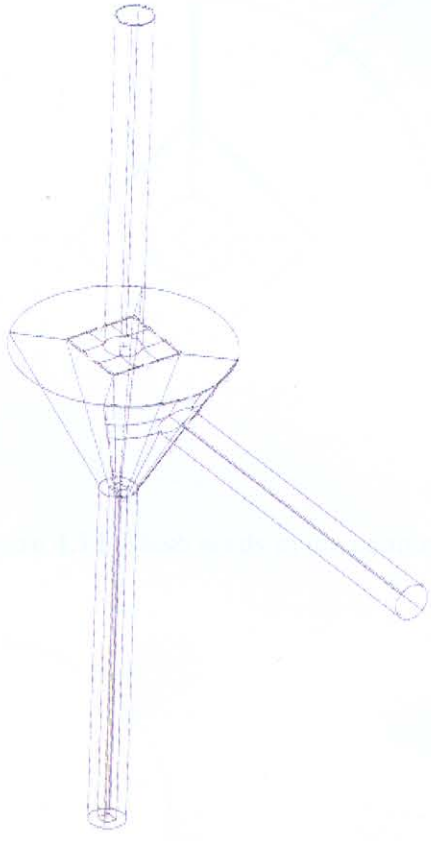

Figure 4.12 Schematic of the second geometry dimensions

The geometry was constructed in a similar manner, constraints and patches were specified, mesh seeds created (see Figure 4.13) and the geometry meshed. The mesh appeared improved at the areas of concern as shown in Figure 4.14 although there is still some distortion on the circular inlet.

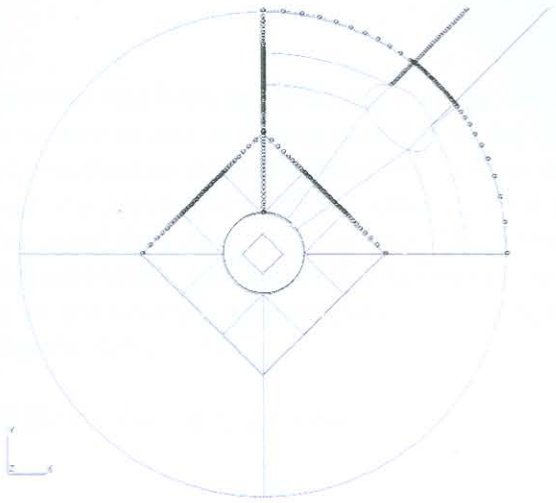

Figure 4.13 Mesh seeds in the geometry

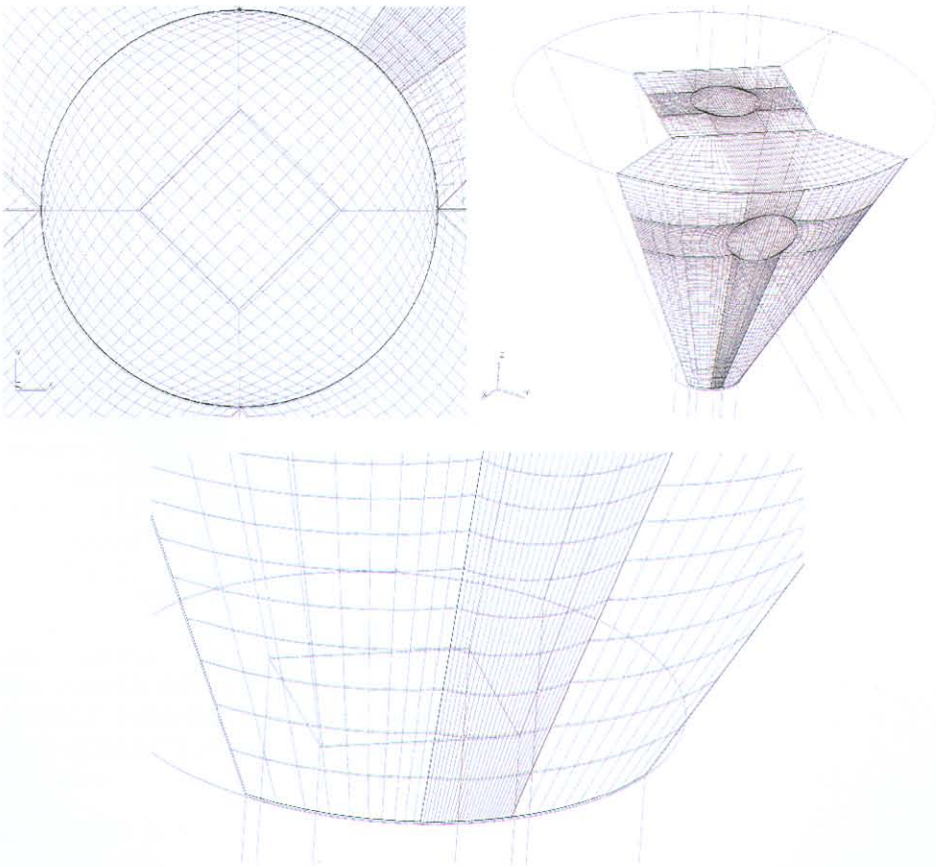

Figure 4.14 Improved mesh of Geometry 2

3.1.2 Solver

Once the geometry of the problem has been specified and meshed, the details of the topology and the grid coordinates can be written to disk in a form readable by the Frontend of the Solver. The Frontend converts the input specification of the problem from a form convenient for the user into a form designed for efficient execution and performs detailed error checking. The problem is specified in a single data file using the Command Language. The Command Language is a set of English-like commands, subcommands, and associated keywords. In the Interactive Frontend, CFX-Setup, this data file is constructed automatically via a graphical user interface. This command file is then used by the Solver. [33]

An example of a Command file for Geometry 2 follows:

```
>>CFX4
  >>OPTIONS
    THREE DIMENSIONS
    BODY FITTED GRID
    CARTESIAN COORDINATES
    TURBULENT FLOW
    ISOTHERMAL FLOW
    INCOMPRESSIBLE FLOW
    STEADY STATE
    USE DATABASE
>>MODEL DATA
  >>MATERIALS DATABASE
    >>SOURCE OF DATA
      PCP
    >>FLUID DATA
      FLUID 'WATER'
      MATERIAL TEMPERATURE 2.7300E+02
      MATERIAL PHASE 'LIQUID'
  >>TITLE
    PROBLEM TITLE 'FUNNELEX4'
  >>PHYSICAL PROPERTIES
    >>STANDARD FLUID
      FLUID 'WATER'
      STANDARD FLUID REFERENCE TEMPERATURE 2.7300E+02
    >>FLUID PARAMETERS
      VISCOSITY 1.0000E-03
      DENSITY 1.0000E+03
>>SOLVER DATA
  >>PROGRAM CONTROL
    MAXIMUM NUMBER OF ITERATIONS 400
    MASS SOURCE TOLERANCE 1.0000E-03
  >>DEFERRED CORRECTION
    K START 0
    K END 200
    EPSILON START 0
    EPSILON END 200
>>MODEL BOUNDARY CONDITIONS
  >>INLET BOUNDARIES
    PATCH NAME 'INLET'
    NORMAL VELOCITY 1.0000E+00
    TURBULENCE INTENSITY 3.7000E-02
```

```
    DISSIPATION LENGTH SCALE 7.5000E-02
  >>PRESSURE BOUNDARIES
    PATCH NAME 'PRESS_OVERFLOW'
    PRESSURE 0.0000E+00
  >>PRESSURE BOUNDARIES
    PATCH NAME 'PRESS_OUTLET'
    PRESSURE 0.0000E+00
  >>WALL BOUNDARIES
    PATCH NAME 'WALL'
>>STOP
```

3.1.3 CFX-Analyse

CFX-Analyse is used to produce the main graphics output. The Solver writes the results to disk files, and these are read by CFX-Analyse. Figure 4.15 shows the output in CFX-Analyse for vector plots of the flow. From this figure it can be seen that the flow entering the funnel may be detrimental as it may disturb the settling of the magnetite particles in the magnetic field.

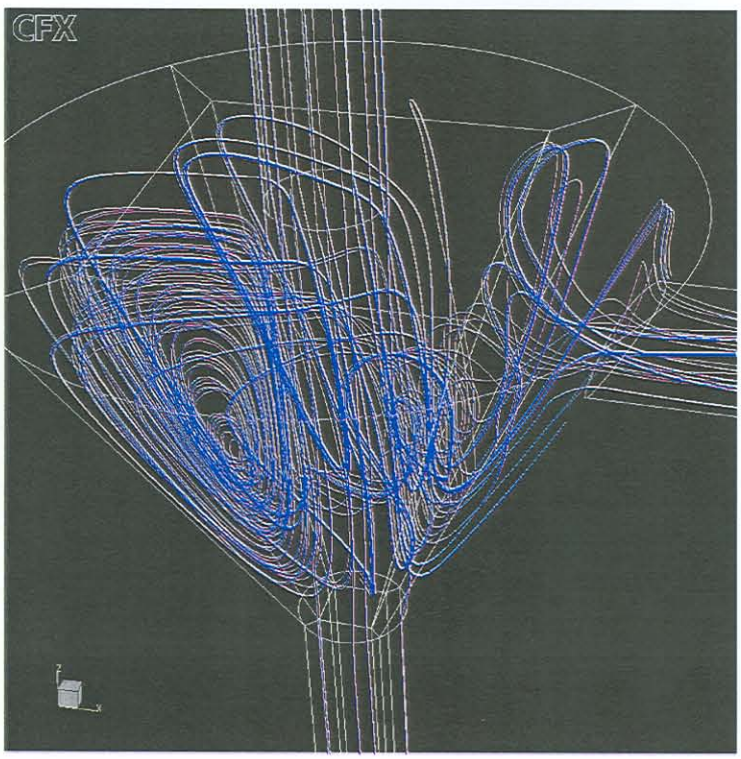

Figure 4.15 Output in CFX-Analyse for vector plots of the flow

3.2 CFX-5.4.1

Because of the limitations in terms of meshing geometries in CFX-4, the CFD study of the sedimentation funnels was performed in CFX-5.

3.2.1 CFX-Build

In CFX-5, unstructured meshes are used to mesh geometries. The unstructured meshes consist of triangular-shaped elements in 2D and tetrahedral-shaped elements in 3D. The advantages of using unstructured meshes are that complex shapes can be meshed relatively easily and the mesh can be easily adapted to give a good solution. CFX-5 is much simpler than CFX-4 in that it is not necessary to construct simple or advanced constraints. Because the mesh structure used by CFX-5 is unstructured, the definition of the position of mesh nodes is not necessary.

In CFX-Build, the mesh is prepared in two stages. Firstly, a surface mesh of triangular elements is generated and secondly a volume mesh of tetrahedral elements (also possibly using prismatic and pyramidal elements) is generated from the surface mesh during the creation of the CFX-5 Definition File. If tetrahedra are used, then a fine surface mesh may be required to avoid generating highly distorted tetrahedral elements at the surface. The mesher overcomes this problem by using prisms to create a mesh that is finely resolved normal to the wall, but coarse parallel to it. This allows the user to grow a series of prismatic elements from triangular elements at the surface to produce a good solution at the model wall where velocity gradients are large normal to the surface. This is termed inflation. This mesh arrangement is beneficial for cost effective analysis. The thickness of the inflation is controlled by the number of layers, the maximum thickness specification, the local element edge length and the inflation thickness multiplier. [33]

Mesh Controls are used to refine the surface and volume mesh in specific regions of the model. Mesh Controls can be:

- a point (region of influence defined by a sphere),
- line (region of influence defined by the cylindrical volume between two spheres),
- triangle (region of influence defined by the prismatic region between three spheres) or
- surface (region of influence defined by the prismatic region between four or more spheres).

Each type of control has certain attributes that should be specified: length scale, radius and expansion factor. [33]

Figures 4.16 and 4.17 show the solids and the meshes that were created for the two geometries in CFX-5. As can be seen from Figure 4.16, the problems that were encountered when structured meshes were used in CFX-4 have been eliminated. The transition from the large funnel to the small outlet pipe results in smooth and even elements being propagated into the outlet pipe. The outlet pipe mesh should be further refined to ensure that the outlet pipe is circular.

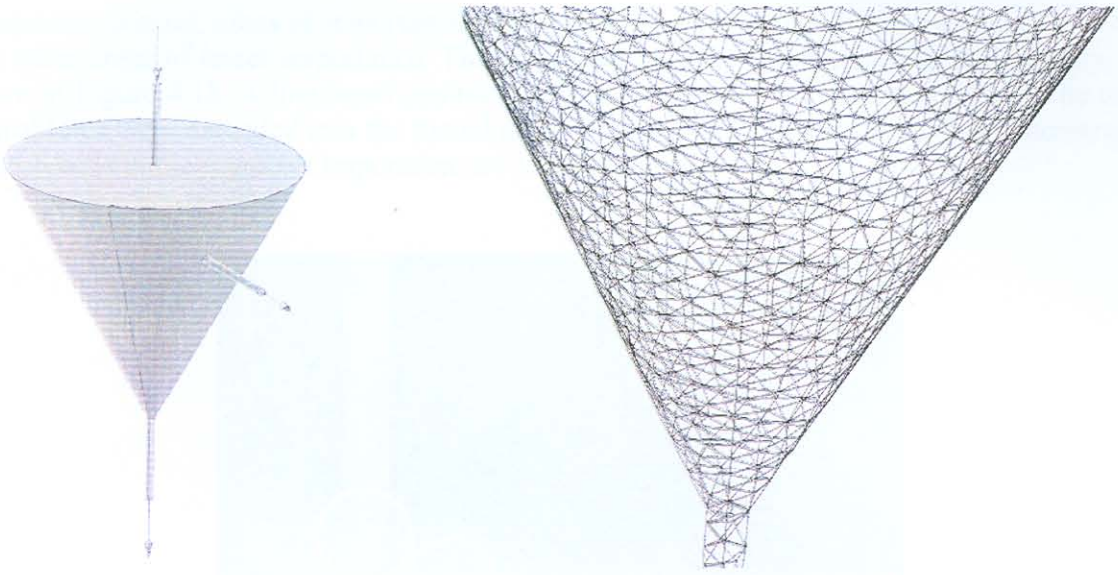

Figure 4.16 Unstructured mesh of Geometry 1

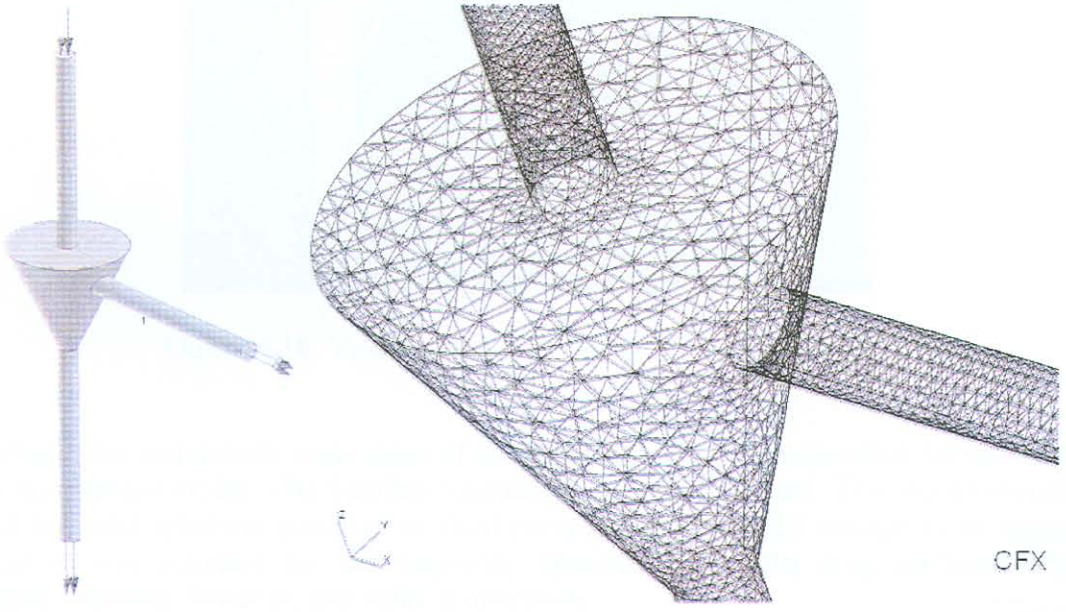

Figure 4.17 Unstructured mesh of Geometry 2

A multi-phase flow case was studied using Geometry 2 in CFX-5.4.1. Initially, to obtain an indication as to whether convergence would be obtained for the multi-phase model, simple flow of particles in a pipe was modelled. Once convergence had been obtained for the multi-phase flow in a pipe, the parameters used for the pipe flow were used to solve the multi-phase flow through the funnel.

Using mesh control, areas of importance that were to be more defined were meshed more finely than other areas of lesser importance. The advantage of using mesh controls for Geometry 2 is shown in Figure 4.18. A line mesh control was used at the inlet, outlet and overflow. The mesh control lines were extended into the funnel to more clearly define these areas. The concentration of mesh cells in the region of importance are visible in Figure 4.18.

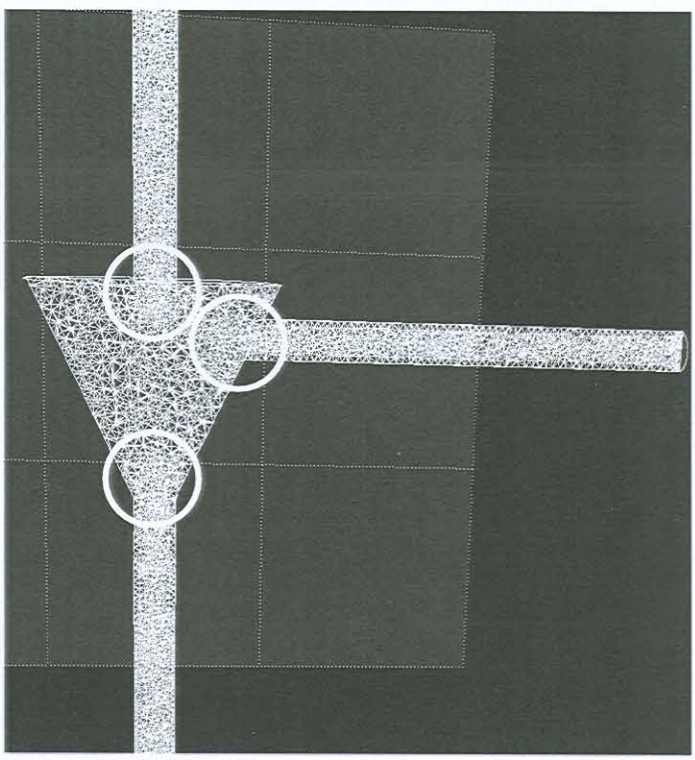

Figure 4.18 Visualisation of mesh control for Geometry 2

The particle size and density were some of the parameters that were specified for the magnetite for the multi-phase model. The Schiller-Naumann model was selected. This model should only be used for solid spherical particles, or fluid particles that are small enough to be considered spherical as was assumed for the magnetite. Specification of the drag coefficient was an alternative selection, however, this value is unknown.

3.2.2 Solver

The solver proceeds as for the CFX-4 solver. Residuals are plotted and the solution proceeds either until convergence is reached or stops if the solution becomes unstable.

3.2.3 CFX-Visualise

Initially, obtaining convergence using the multi-phase flow proved to be difficult. The magnetite particle size was specified as 10 nm. Particles of such a size would not behave differently from

the fluid in which they were contained. The correct solution to this problem would only be obtained once the magnetic field were incorporated into the model as the particles would then be acted upon by an additional external body force. To obtain an indication of the particle movement, it was decided to model the multi-phase flow using magnetite particles of 1 mm in size.

Figure 4.19 shows the water and magnetite velocities obtained using a mesh with 123 906 elements and mesh control. With an increase in the number of mesh cells, the solution obtained improves and so does the definition of the velocity plots. It is impractical, however, to increase the number of elements indefinitely as the computational time increases. A compromise must be reached between accuracy of solution and mesh refinement.

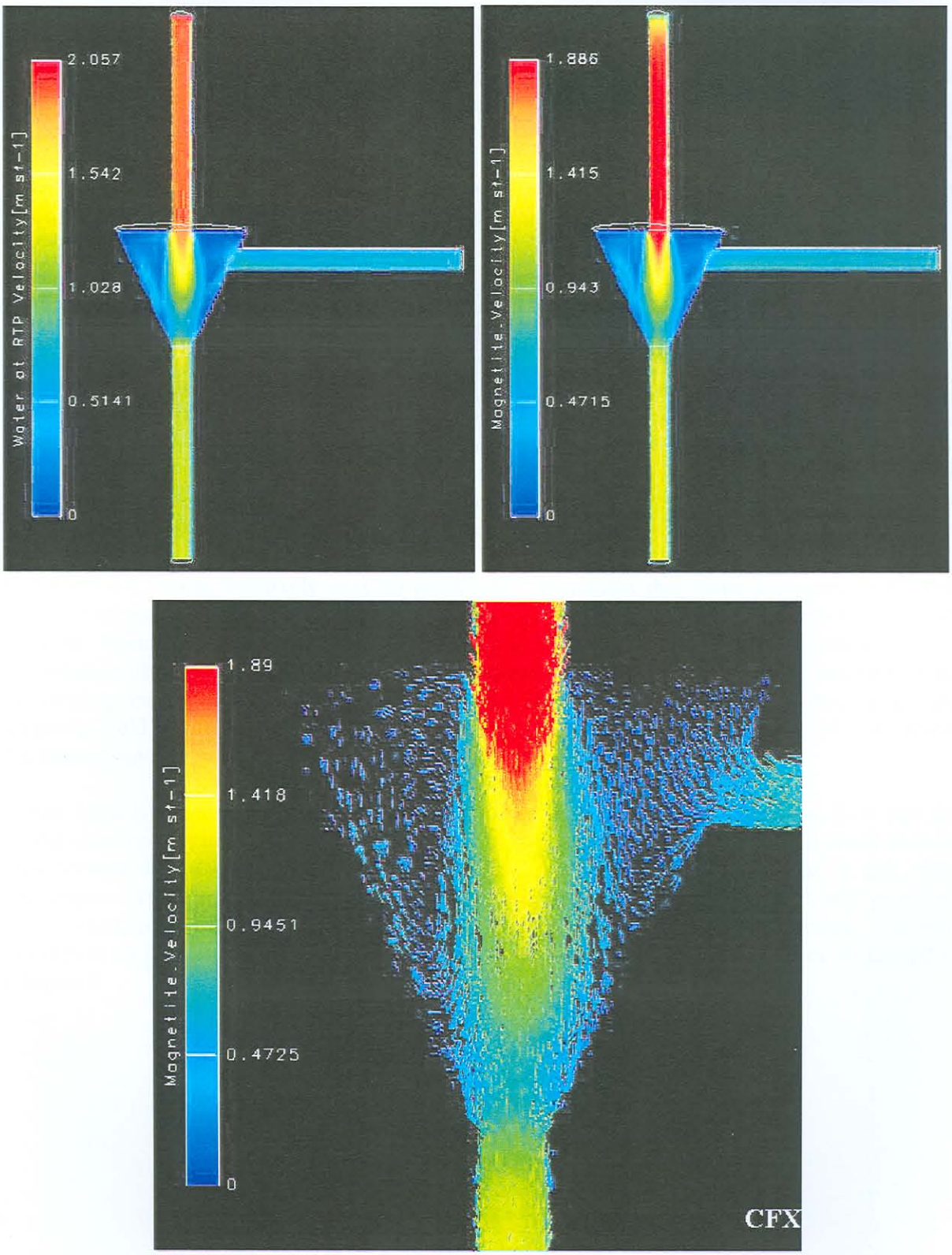

Figure 4.19 Flow visualisation for multi-phase flow in the funnel with mesh control

The results obtained for the multi-phase flow problem in CFX-5 seem reasonable. The vector plots of velocity show the magnetite particles entering the funnel at a high speed and slowing down at the outlet. The vector plots again show, however, that the contents of the funnel are mixed by the inflowing liquid as was seen in CFX-4. It is noted that the magnetite velocity is lower than the water velocity. This may be owing to drag forces experienced by the particles (these results were obtained for the large particle size).

4. CONCLUSIONS AND RECOMMENDATIONS

In this CFD study, a base case funnel containing only water was modelled using CFX-4.3. It was found that because structured mesh creation requires a geometry that is topologically correct, this may complicate simple geometries. Modelling of complex geometries is difficult in CFX-4 as the creation of structured meshes is not easy. From preliminary results obtained from CFX-4, it appears that the inflowing liquid churns up material that may have settled at the base of the funnel. A possible method to eliminate this would be to insert a baffle plate at the funnel entrance.

In CFX-5.4.1, it was relatively easy to mesh both geometries that were attempted in CFX-4. Simple and complex geometries can be solved in CFX-5, largely owing to the method of mesh creation. Unstructured grids are more suitable for difficult geometries. The streamline plots of the solution obtained in CFX-5 confirmed the results obtained in CFX-4. It was realised, when performing the multi-phase flow modelling that it would be necessary to incorporate the magnetic field if the correct solid particle size is to be used. Without the additional body force, the nanometre size particles follow the flow of the main fluid.

It was initially recommended that the funnel geometry be modified such that the flow into the funnel does not disturb the particles at the base of the funnel. The magnetic field could then be incorporated into the model and the four funnels in series be modelled as a unit once convergence on an optimised funnel has been obtained. However, a new concept was proposed as an alternative to the sedimentation funnels and the CFD study was suspended. The new concept is called the wet high intensity magnetic separator (WHIMS) and will be discussed in Chapter 5.

CHAPTER 5

PRECIPITATION: WASHING OF ULTRAFINE MAGNETITE PARTICLES USING A HIGH GRADIENT MAGNETIC WASHING DEVICE

1. INTRODUCTION

As mentioned in Chapter 4, ultrafine magnetite particles are produced during a precipitation reaction which forms part of the ferrofluid production process. The additional steps involved in the process which include the washing and concentration of these particles are extremely difficult. Initially the concept of four sedimentation funnels in series was investigated to perform this function and preliminary CFD modelling conducted to determine the funnels' effectiveness. The application of the concept of sedimentation funnels would require much additional work. An alternative method was investigated. This chapter documents the method selected to achieve the concentration and washing of the particles and discusses the qualitative method used to evaluate the equipment that was designed. A patent has been applied for for the concept as discussed in subsequent sections.

2. SELECTION OF A MAGNETIC SEPARATION TECHNIQUE

According to [34], magnetic separation is generally used:

- for magnetic filtration which involves the recovery of either a liquid or a solid with the magnetisable solid or liquid discarded respectively,
- for the removal of a strongly magnetisable material from a less strongly magnetisable material or
- for the concentration of a valuable strongly magnetisable material from a less strongly magnetisable material.

In the production of ferrofluids, magnetite is required to be separated from an aqueous salt solution. As mentioned in Chapter 2, magnetite adopts a ferrimagnetic ordering in a magnetic field. (In the magnetic field, the atoms magnetised in one direction have a greater effective magnetic moment than those magnetised in the opposite direction as shown in Figure 5.1.) [34]

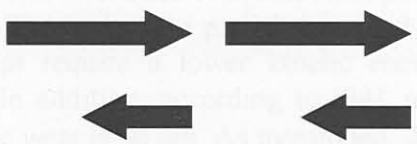

Figure 5.1 Schematic representation of spin arrangements for a ferrimagnetic ordering

There are many different types of magnetic separation technologies and the selection of the most suitable technique is not a simple task. A suggested starting point is to consider the particle size distribution. The average particle diameter of the precipitated magnetite is 10 nm. It is suggested that in the case where the magnetic particles are smaller than 75 μm, a wet separation technique is most suitable. Fine magnetic particles are usually recovered by wet intensity magnetic separators and it was therefore proposed that a wet high intensity magnetic separator (WHIMS) be used in the washing process of the nanometre-sized magnetite particles during the production of ferrofluid. [34]

3. WET HIGH INTENSITY MAGNETIC SEPARATOR DESIGN

The WHIMS is a vessel containing a magnetisable matrix which is surrounded by a magnet e.g. solenoid electromagnet. The procedure used for the WHIMS is analogous to that of deep bed filtration with the magnetic force assisting in particle capture. Sections 3.1 to 3.4 mention points that are relevant to the performance of the WHIMS. [34]

3.1 Matrix

The choice of a matrix is dependent on a number of factors: size, shape, height, loading, magnetic properties, matrix material, wear and clogging. [34]

Matrices can be characterised by their filling factor or by their porosity. A typical filling factor for expanded metal is 0.12 to 0.27 whilst that for wire mesh is in the region of 0.15 to 0.25. The matrix height should be as low as possible in order to minimise the height of the coil. The largest magnetic force should be used which implies the largest possible magnetic field. The total magnetic induction in the vicinity of the matrix element is given by the superposition of the background magnetic induction and the induction due to the matrix element. [34]

The finest possible matrix compatible with the particle size should be used to trap the maximum volume of particles. The ratio of the matrix element radius ($r_{matrix\ element}$) to the particle radius ($r_{particle}$) should preferably be between 100 and 500 but larger than 10. This is so as not to cause mechanical straining owing to particle retention which occurs when $\frac{r_{matrix\ element}}{r_{particle}} < 10$. [34]

The matrix material may be subject to abrasive, adhesive and erosive wear. Erosive wear is a function of incident conditions, characteristics of the medium passing through the matrix and the matrix material characteristics. The higher the particle size and velocity, the higher the erosive wear. Particles that are angular require a lower kinetic energy than spherical particles to penetrate the matrix material. In addition, according to [34], at 10 m/s, the threshold particle diameter so as to prevent erosive wear is 30 μm. As mentioned, the magnetite particles that are to pass through the WHIMS have an average particle diameter of approximately 10 nm and a low linear flow rate through the matrix (of the order of 1 m/s). In addition, the shape of the particles is predominantly spherical. It can therefore be expected that there should not be any problems as

a result of erosive wear. An additional consideration in terms of erosive wear is the possible impact of the fluid on the matrix at the WHIMS inlet. For the application of magnetite washing, the inlet velocity at the nozzle is greater than that through the WHIMS. The liquid inlet is situated at a certain height above the mesh and the liquid does not impact directly on the mesh. The spray pattern of the nozzle is such that the liquid is distributed over the surface of the mesh. There will therefore not be any localised erosive wear on the mesh.

More serious in this application than the possibility of wear caused by the particles is the possibility of corrosion caused by the aqueous salt solution. The magnetite suspension contains chlorides which can be highly corrosive to certain metals or alloys. The WHIMS vessel should preferably be manufactured from plastic and the matrix coated to minimise the effects of corrosion whilst at the same time not affecting the magnetic properties of the matrix.

Blockage of the matrix can be minimised by:

- matching the matrix to the particle size distribution of the feed,
- by using a matrix material of low remanent polarisation (The remanent polarisation refers to a certain permanent magnetisation which remains when the magnetic field is removed. It is a function of the type of material used for the matrix – the removal of particles from the matrix will be promoted if the remanent polarization of the mesh is as low as possible.) and
- by cleaning the matrix with air or water jets. [34]

3.2 Flow velocity

The efficiency of separation is greatly affected by the flow velocity in the matrix. For successful magnetic separation, the magnetic force must be greater than the sum of all competing forces. An increase in flow velocity results in an increase in hydrodynamic drag thereby reducing separation efficiency. A compromise must therefore be reached between product recovery and throughput. The fluid shear stress on the deposited particles should be as low as possible whilst attaining a suitable throughput. [34]

3.3 Feed rate

For a continuous separation process, the higher the feed rate, the higher the throughput through the separator. This is thus an important factor in determining the cost-effectiveness of the separator. If the matrix is not flooded and the loading has not been exceeded, the interstitial velocity through the matrix is high at low or moderate feed rates. The erosion force on the deposited particles will be large. Recovery will increase with increase in flow rate because, at high feed rates, when the matrix is flooded, the interstitial velocity decreases. The grade of recovered material may, however, be lower as the content of non-magnetic material in the final product may increase. [34] For the application that was tested, the throughput was taken to be fixed. In a practical application, the WHIMS filling time, the washing cycle time and the number of washes and the flushing time would be variable.

3.4 Rinsing and flushing

For the production of ferrofluid, non-magnetic particles and salts should be rinsed from the precipitate for reasons described in Chapter 4. An increase in the volume of rinse water will usually result in a decrease in the recovery of the magnetic particles but an increase in the concentration of magnetite particles in the final product. It has been found, however, that a point is reached where increasing the volume of rinse water results in a negligible effect on the recovery of the desired material. After an initial improvement in flushing of particles from a matrix with increase in flushing velocity, a point is reached where particle removal increases only slightly with an increase in velocity. [34]

It has also been found that the removal of particles from the mesh can be dependent on the pH of the flushing water. The optimum pH is dependent on the surface properties of the captured material. Electric double-layer and London-type Van der Waals interactions probably represent the residual forces that prevent complete flushing of the matrix. [34] If the electrostatic attraction between the adsorbed particles and the matrix is neutralised, it is more likely that particles will be flushed from the matrix. Flush water of low or high pH for example will provide positive or negative charge respectively to achieve this charge neutralisation. In addition, a high pressure can be used for flushing to mechanically remove the particles from the matrix. High pressure flushing may also be required as there may be a stray magnetic field and a remanent magnetisation of the matrix. [34]

A specified volume of water is used to flush the magnetic material from the matrix. In practice, for the manufacture of ferrofluid, this volume of flush water would be recirculated through the WHIMS with the field removed so as to minimise the resultant suspension volumes. [34]

3.5 Selection of parameters for WHIMS design

3.5.1 Selection of the matrix and magnetic field strength

Optimum selection of the type of matrix and of the magnetic field strength is critical for correct and trouble-free operation of the WHIMS. Standard procedures [34] for such a selection cannot be applied to ultrafine magnetite in view of its high magnetisation and, at the same time, very small particle size.

In order to better understand the problem, a few preliminary experiments were carried out at Mintek using their laboratory WHIMS. The following combinations of the matrix type and the field strength were used:

- A mild steel woven mesh matrix of 5 mm aperture and 2 mm thick wire was placed in the residual magnetic field of the WHIMS electromagnet (170 G). Most of the magnetite was captured by the matrix but it was extremely difficult to flush the magnetite from the matrix. [35]
- An austenitic stainless steel expanded metal matrix was placed in the field of 9 kG. Not all of the magnetite was captured on the mesh. Once the field was switched off, it was easy to flush the magnetite from the matrix (at the residual field of 170 G). [35]

It thus became clear that in order to achieve capture of all the magnetite with a subsequent efficient wash from the matrix, a coarse ferromagnetic matrix with a low filling factor placed in a modest magnetic field should be used. Based on this philosophy, a solenoid magnet that could generate a magnetic field of 800 to 1000 G was designed and manufactured, based on the specifications summarised in Table 5.1. Coarse matrices shown in Figure 5.2, arranged with a low filling factor were manufactured. [35]

Table 5.1 Properties of the solenoid electromagnet

Property	Description
Inside diameter	240 mm
Outer diameter	Approximately 560 mm
Height of winding	120 mm
Number of turns	2500
Wire	Copper, diameter 2.5 mm
Length of wire	Approximately 3200 m
Resistance of winding	Approximately 10 ohm
Operating current	Maximum 10 A
Voltage	Maximum 100 V
Maximum magnetic field	800 G
Steel cladding	4 mm thick mild steel

Three types of mesh were manufactured for test work (as shown in Figure 5.2). They consist of circular sections of:

- an expanded metal sheet with 8 mm X 20 mm diamond shape openings, a gap of 2 mm between openings and a thickness of 1.2 mm (this mesh will be referred to as Mesh 1),
- a galvanised woven wire screen with a 10 mm aperture and a wire of 4 mm diameter (this mesh will be referred to as Mesh 2) and
- a high carbon woven wire screen with a 5 mm aperture and a wire of 3.15 mm diameter (this mesh will be referred to as Mesh 3).

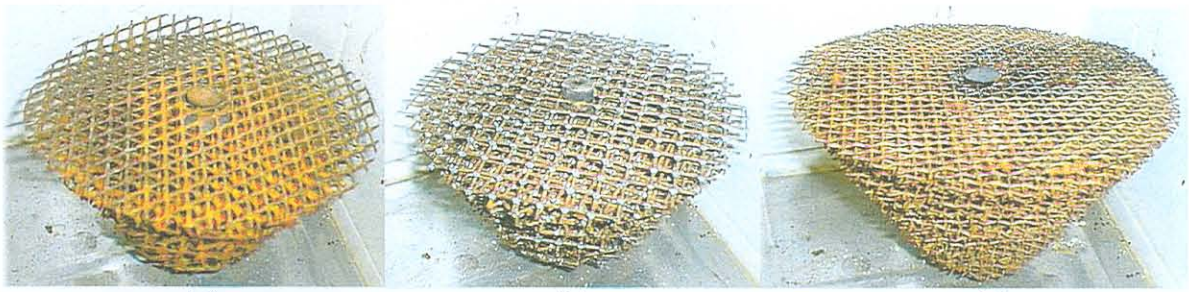

(a) (b) (c)

Figure 5.2 (a) Mesh 1, (b) Mesh 2 and (c) Mesh 3

The ratio of the matrix element and particle radii for all the mesh types is greater than the minimum recommended ratio of 10.

3.5.2 Physical arrangement of the WHIMS

The physical arrangement of the WHIMS consists of a funnel-shaped container, a section of which is surrounded by a solenoid electromagnet (see schematic cross section in Figure 5.3) and contains a magnetisable matrix. The solenoid generates a magnetic field in the funnel and the presence of the magnetisable matrix results in a high magnetic field gradient in the funnel.

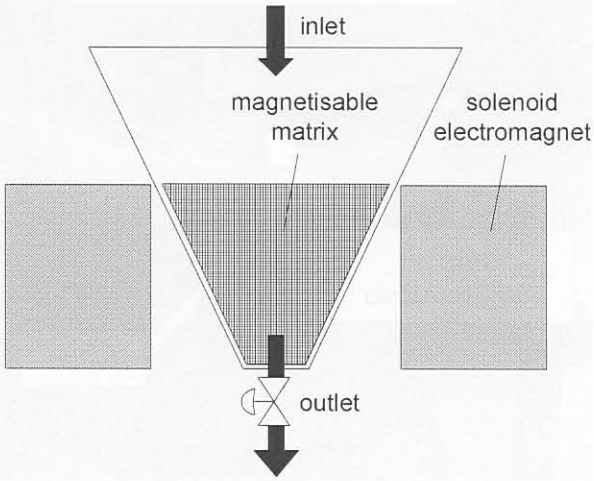

Figure 5.3 Schematic cross section of the WHIMS

A photograph of the current embodiment of the WHIMS is given in Figure 5.4 with the positioning of the matrix inside the funnel shown in Figure 5.5.

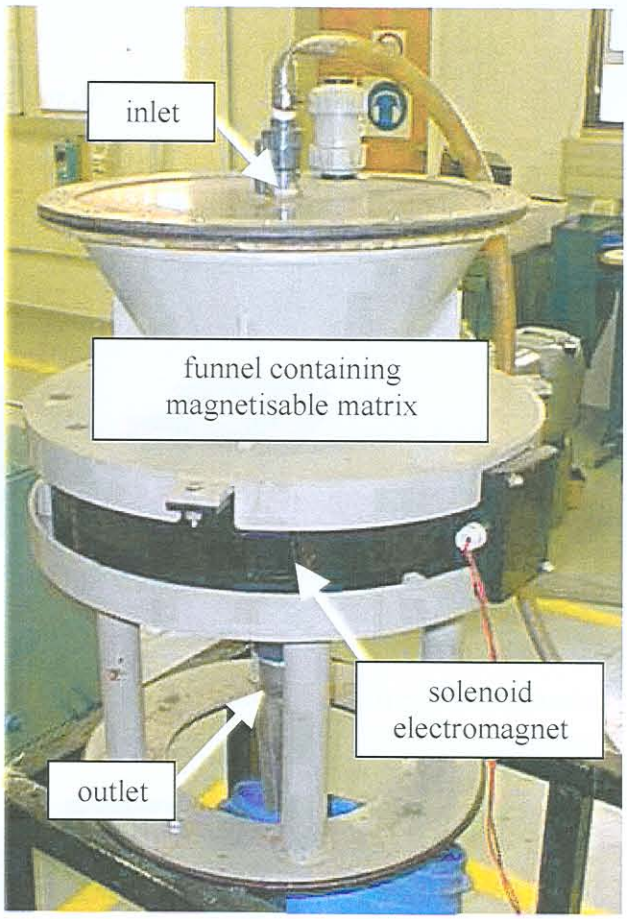

Figure 5.4 Photograph of WHIMS showing electromagnet

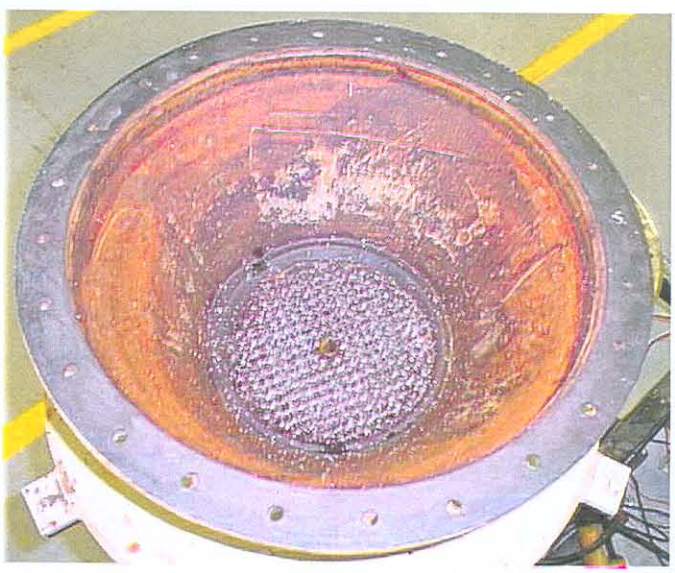

Figure 5.5 Internal view of WHIMS showing magnetisable matrix

3.5.3 Selection of spray nozzle

Two types of full cone nozzles were used for the test work. They are the FullJet and SpiralJet spray nozzle (shown in Figure 5.6) which give spray patterns as shown in Figure 5.7.

(a) (b)

Figure 5.6 (a) FullJet and (b) SpiralJet nozzles

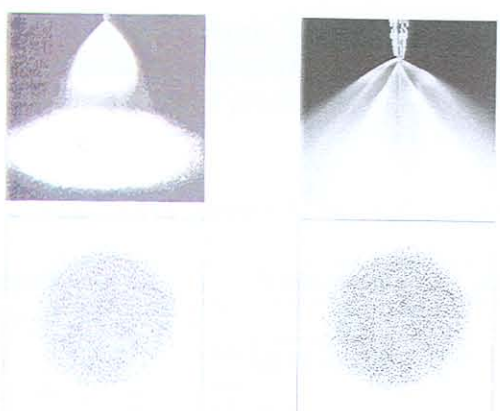

(a) (b)

Figure 5.7 Spray pattern produced by the (a) FullJet and (b) SpiralJet full cone nozzles

The SpiralJet nozzle has a larger free passage and allows for a larger capacity through the nozzle while providing complete coverage of the zone to be rinsed. It was found that the SpiralJet nozzle could flush material more efficiently from the matrix than the FullJet during preliminary test work. This nozzle was therefore used for the remainder of the testwork.

3.6 Proposed operation

A mixture of magnetite and water containing salts produced from precipitation of iron salt solution with ammonium hydroxide solution, will be passed to the WHIMS. The magnetite will be trapped on the magnetised matrix when the current to the solenoid is switched on. Water can then be passed through the matrix to wash the precipitate and remove the dissolved salts. In addition, it is likely that non-magnetic particles will be washed from the mixture. Large particles may also be washed off the matrix because of the higher force exerted on them owing to shear. Once the field has been removed, the magnetite particles can be washed off the matrix into a smaller volume of water than that in which they were originally contained and thus be concentrated.

4. EXPERIMENTAL

The WHIMS had to be tested to determine whether or not it would be suitable for the purposes of washing and concentrating the magnetite. Furthermore, a qualitative estimation of the suitability of the three mesh types was to be determined. The efficiency of the particle capture of the mesh types and the particle retention on the mesh once the magnetic field had been removed had to be determined for each mesh. The results from this investigation would be used to select the most suitable mesh for operation.

A precipitate mixture was made for the test work. Table 5.2 gives the volumes that were used for the laboratory test work. A breakthrough loading was not determined as the manufacture of large volumes of precipitate in the laboratory is not practical.

Table 5.2 Volumes of reagent to be used for the test work

Reagent	Volume for test work (l/h)
$FeCl_3$ solution (43%)	0.72
$FeSO_4.7H_2O$	0.50 kg in 2 litres H_2O
NH_4OH solution (25%)	1.72

The ferrous sulphate was allowed to dissolve for 10 minutes before the ferric chloride was added. The ammonium hydroxide solution was then added rapidly to the iron solution at high stirrer speed and the resulting precipitate mixture stirred for 10 minutes.

The experimental procedure was as follows:

- Samples of 50 ml were taken from the initial precipitate mixture. These samples were labelled "a" and were used to determine the initial magnetite suspension concentration i.e. the mass of magnetite per volume of mixture as indicated by eq. (5.1). (This was performed by evaporation of the liquid and determination of the magnetite mass as explained below.)

$$Initial\ magnetite\ conc. = \frac{mass\ of\ magnetite}{volume\ of\ mixture} \quad (5.1)$$

- The initial precipitate mixture was added to the WHIMS with the current switched on.
- The mixture was allowed to drain from the WHIMS (with a certain volume of magnetite being retained on the mesh).
- The magnetite in the mixture that drains from the WHIMS while the current to the solenoid is switched on is taken to waste. This magnetite is therefore considered to be "lost". Samples of 50 ml were taken from this drained mixture. These samples, labelled "b" were used to determine the percentage magnetite that would be lost using that particular mesh as shown by eq. (5.2).

$$\%\ magnetite\ lost = \frac{conc.\ of\ magnetite\ in\ underflow\ with\ solenoid\ current\ switched\ on}{initial\ magnetite\ conc.} * 100 \quad (5.2)$$

- The current to the coils was then switched off and the mixture recirculated through the WHIMS for one minute to flush the magnetite from the matrix. The mixture that was recirculated contained the magnetite that had been "lost" in the previous step.
- After flushing, a volume of magnetite will possibly remain on the matrix as a result of the stray magnetic field, remanent polarization of the matrix and electrostatic attraction of the particles and the mesh. This magnetite may be detrimental to the process as it will result in clogging of the matrix. Samples of 50 ml of the mixture that was flushed from the matrix were taken. These samples which were labelled "c" were used to determine the percentage magnetite that was retained on the mesh after rinsing and flushing as shown by eq. (5.3).

$$\%\ magnetite\ retained = 100 - (\frac{conc.\ of\ magnetite\ in\ underflow\ with\ solenoid\ current\ switched\ off}{initial\ magnetite\ conc.} * 100) \quad (5.3)$$

- The filling of the WHIMS, the draining and the recirculating and flushing was repeated four times for each of the three mesh types (resulting in samples 1 to 4 and "a" to "c"). Between each of the repeats, the matrix was removed from the funnel and washed to ensure that the matrix was clean for the next run. The initial magnetite concentration (sample "a") for repeats 2 to 4 was taken as the concentration calculated for the percentage magnetite retained of the previous run (sample "c").
- The samples were dried in an oven and the mass of magnetite in each sample determined using a scale. The percentage magnetite lost or retained was then determined for each mesh.

The experimental setup showing the container into which the mixture was drained and the recirculation pump is shown in Figure 5.8.

Figure 5.8 Experimental setup

5. RESULTS AND CONCLUSIONS

As mentioned in Section 4, the aim of the test work was to determine whether or not the WHIMS would be suitable for the purposes of washing and concentrating the magnetite and to obtain a preliminary indication of which mesh is most suitable for the application.

The magnetite concentration in each 50 ml sample at each run is given in Table 5.3. As explained in Section 4, the percentage magnetite lost is the magnetite that is not retained by the mesh when the current to the solenoid is switched on. This percentage was determined from the sample of the underflow from the WHIMS when the current to the coil was on. The percentage magnetite retained is the magnetite that is held on the mesh when it is supposed to have been removed during the rinsing and flushing cycle. This percentage was determined from the difference between the initial magnetite concentration and the magnetite concentration of the underflow sample taken when the current had been switched off and the matrix flushed. The average percentage magnetite lost or retained for each mesh is given in the last line of Table 5.3.

Table 5.3 Magnetite losses and retention in the matrices

	Mesh 1			Mesh 2			Mesh 3		
Sample	**Fe_3O_4 conc. (g/l)**	**Fe_3O_4 lost (%)**	**Fe_3O_4 retained (%)**	**Fe_3O_4 conc. (g/l)**	**Fe_3O_4 lost (%)**	**Fe_3O_4 retained (%)**	**Fe_3O_4 conc. (g/l)**	**Fe_3O_4 lost (%)**	**Fe_3O_4 retained (%)**
1a	138.52			128.05			60.96		
1b	13.16	9.50		23.73	18.53		0.98	1.61	
1c	126.78		8.47	120.75		5.67	50.64		16.94
2a	126.78			120.75			50.64		
2b	52.46	41.31		25.40	21.03		0.49	0.97	
2c	113.94		10.14	117.62		2.60	40.19		20.64
3a	113.94			117.62			40.19		
3b	44.89	39.39		34.66	29.48		0.53	1.31	
3c	129.66		13.89	80.23		31.76	32.39		19.41
4a	129.66			80.23			32.39		
4b	41.97	32.39		16.67	20.77		0.48	1.50	
4c	108.68		16.14	60.96		24.03	22.91		29.27
Ave (%)		**30.65**	**12.16**		**22.45**	**16.01**		**1.35**	**21.56**

The initial value for Mesh 1 (run 1) for the amount of magnetite lost is significantly lower than the subsequent three values. It could be that even though the mesh was cleaned between repeats, some magnetite was still attached to portions of the mesh because of the remanent magnetisation and less surface area was therefore available for the attachment of additional magnetite. The magnetite retained also seemed to increase over time. This could also be because of the remanent magnetisation of the matrix. The magnetite retained on Mesh 2 also appeared to increase over time while the magnetite lost and retained on Mesh 3 was relatively constant.

It was found from the test work that the WHIMS will function effectively in the washing and concentration of the magnetite precipitate. As can be seen from the results, Meshes 1 and 2 behave in a similar fashion in the WHIMS while Mesh 3 loses the least amount of magnetite. Although a minimum loss of magnetite is desirable, the amount of magnetite retained on this mesh is high (approximately 22%). There is a possibility that this mesh may clog relatively easily and quickly if used in practice. Although Meshes 1 and 2 may not clog as easily as Mesh 3, they lose more than 20% of the magnetite.

6. RECOMMENDATIONS

The mass of magnetite lost is critical in producing ferrofluid of a suitable quality. The percentage magnetite retained on the three types of mesh is similar for all three cases, however, Mesh 3 exhibits the lowest loss of magnetite. It is recommended that Mesh 3 be used initially for the washing of magnetite on a larger scale. It is suspected that the outlet flow rate from the WHIMS during washing cycles could be increased with a lower loss of precipitate when using Mesh 3 as compared to the other mesh types. This implies that a greater number of washing cycles could be performed in a certain cycle time per volume if the WHIMS were used in a process that

manufactures ferrofluid continuously. It is further recommended if Mesh 3 is used, that the flushing time for rinsing magnetite from the mesh be increased. If the flushing time is increased, it may be possible to wash Mesh 3 better.

If it is found that Mesh 3 clogs easily and it is not possible to remove the magnetite, Mesh 2 should be used instead. Mesh 2 loses less magnetite than Mesh 1 whilst retaining a similar percentage as Mesh 1. The flushing time when using Mesh 2 may be lower than that required to flush Mesh 3. This allows for a slower draining time or outlet velocity from the mesh which may decrease the percentage magnetite loss. The outlet velocity for the testwork was approximately 3 l/min. If this flow rate is reduced, the entrainment of magnetite out of the WHIMS may be reduced. There will be a compromise between an increase in flushing time versus a slower draining time and the number of washing cycles that can be performed. This is because the volume of the WHIMS is fixed and a washing cycle must occur within a specified period of time. Increasing both the flushing time and decreasing the outlet time may require a larger funnel.

For illustration, examples of the outlet flow rate that would be required with a specific number of washing cycles and a set flushing time are shown in Figure 5.9 (the results are represented by a curve, however, only discrete numbers of washing cycles can be performed). These scenarios are for a washing cycle with the following factors:

- an estimated total filling rate and water addition rate of 0.5 min each,
- the WHIMS has an operating volume of approximately 13 litres,
- there is a total throughput of 74 l/h in the system,
- six cycles are performed per hour (i.e. 10 minutes per cycle) and
- 12.3 litres of mixture are handled per cycle.

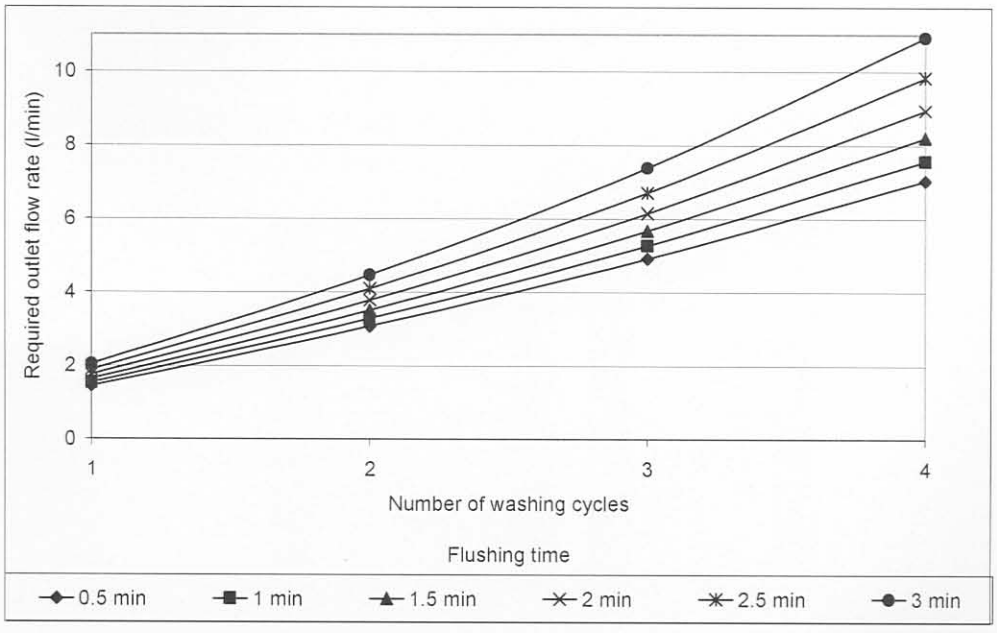

Figure 5.9 Illustration of possible scenarios for the WHIMS cycles for use in a continuous ferrofluid manufacturing process

When the actual filling rate and water addition rate have been determined, various flushing rates and numbers of washing cycles can be tested to determine the optimum manufacturing procedure.

If the current is switched on when the magnetite is added to the WHIMS, it is observed that the precipitate sometimes accumulates at the top of the WHIMS. This may be advantageous as precipitate entrained from the top of the mesh may still settle on the matrix as it travels through the matrix. It may also be disadvantageous as the surface area of the matrix will not be used to its full extent and material accumulating at the top of the matrix will not be held firmly. Furthermore, this could lead to premature blocking of the matrix. It is therefore recommended that the mixture be added to the WHIMS with the current switched off at first. Once the funnel is full, the current can be switched on. This will ensure a more even distribution of magnetite within the mesh.

CHAPTER 6

SURFACTANT STABILISATION

1. INTRODUCTION

The requirements to ensure stability against settling were discussed in Chapter 2. Amongst others, a repulsive force is required to overcome the London-type Van der Waals attractive forces. The mechanism of steric repulsion is introduced by coating the particles with long chain molecules which act as elastic bumpers. Adjacent particles may compress the adsorbed layer surrounding each particle. [7]

Mackor obtained an expression for the repulsive energy for flat surfaces onto which a molecule is adsorbed. The molecule is said to consist of a polar head and a tail. The number of molecules adsorbed onto the surface is such that under the influence of thermal motions, the tail rod can take up any hemispherical orientation. The expression for this energy is given by eq. (6.1) with the graphical illustration of the scenario given in Figure 6.1. [7]

$$\frac{E_f}{kT} = \begin{cases} \xi(1-\dfrac{s}{2\delta}), & \dfrac{s}{2\delta} \le 1 \\ 0 & \dfrac{s}{2\delta} > 1 \end{cases} \qquad (6.1)$$

where ξ is the surface concentration of the absorbed molecules, s is the surface to surface separation, k is the Boltzmann constant, E_f is the repulsion energy per unit area of the flat surface and δ is the length of the absorbed molecule.

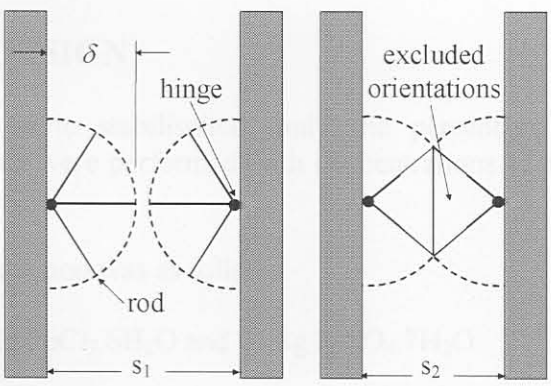

(a) $s_1 > 2\delta$ (b) $s_2 < 2\delta$

Figure 6.1 Illustration of steric repulsion

In Figure 6.1 (a), where the separation between surfaces is greater than twice the length of the tails, there will be no repulsion. In Figure 6.1 (b) the volume available to the tails is reduced and a gaslike repulsion pressure is produced. [7]

Oleic acid is a common dispersing agent in the manufacture of ferrofluids. The oleic acid has a double bond at the ninth carbon position. The double bond is rigid and allows no free rotation to occur. Consequently, the likelihood of neighbouring molecules nesting together and crystallising is greatly reduced. [7]

Reimers and Khalafalla [36] performed investigations into the relationship between the quantity of magnetic material dispersed and the saturation magnetisation. Their results indicated that there is an optimum point where magnetic fluids have the highest magnetisation dependent on the quantity of dispersing agent. For oleic acid, they found this volume percent to be in the region of 8.5 to 10%. In their investigations, the magnetisation seemed to drop off after a certain percentage of dispersing agent had been added (this was for different dispersing and carrier agents). In later work Reimers and Khalafalla (in the production of relatively dilute fluids of 0.045 volumetric packing fraction) found that when manufacturing an aqueous magnetic liquid there was no loss in magnetisation with increase in dispersing agent. However, a scum-like substance appeared on the surface of the liquid when additional dispersing agent was used. [37] In other words, it appeared that a maximum was reached where additional surfactant proved to be detrimental to the fluid manufacture.

From experimental investigations in the laboratory in the past, higher percentages of oleic acid seemed to result in fluids of higher magnetisation with 12% being a common percentage that has been used. This, however, has not been quantified. It was decided to perform an investigation into the effect of the volume of the dispersing agent on the saturation magnetisation of the fluid. In this experimental work, much greater volumes of magnetite were required to be suspended: it was attempted to obtain a volumetric packing fraction of 0.1 as opposed to 0.045 as obtained by Khalafalla and Reimers.

2. EXPERIMENTAL DESIGN

For the investigation into steric stabilisation, only the percentage surfactant added was investigated. Four experiments were performed with concentrations of 8, 10, 12 and 14% oleic acid.

The method of ferrofluid production was as follows:

1. Add 400 ml water to 31.8g $FeCl_3.6H_2O$ and 21.8g $FeSO_4.7H_2O$.
2. Stir for 3 minutes.
3. Rapidly add NH_4OH solution at a stirrer speed of 1050 rpm. Stir for five minutes.
4. Add the oleic acid-kerosene mixture and reduce the stirrer speed to 650 rpm. The four different combinations were as follows:

- 2.2 and 27 ml (run 1),
- 3 and 26 ml (run 2),
- 3.5 and 26 ml (run 3) and
- 4 and 25 ml (run 4) respectively.

5. The mixture is heated to 68°C over approximately 10 minutes but not maintained at this temperature for any length of time.
6. Remove from stirrer and allow the mixture to settle and cool on a barium ferrite magnet. The aqueous and organic layers can then be separated.
7. Centrifuge for 30 minutes.
8. Dilute to 0.98 g/cm^3.
9. Measure the saturation magnetisation.

3. RESULTS

As the percentage oleic acid increased, the volume of magnetite remaining suspended above the ferrofluid appeared to decrease. At 14%, however, suspended magnetite was still visible. Table 6.1 gives the results for the experimental runs.

Table 6.1 Results for experimental runs

Run number	Percentage oleic acid (%)	Density (g/cm^3)	Saturation magnetisation (Gauss)
1	8	0.9762	149.3
2	10	0.9716	158.7
3	12	0.9750	161.5
4	14	0.9718	203.8

A plot of the saturation magnetisation versus the percentage oleic acid is given in Figure 6.2. A straight line has been fitted to these points.

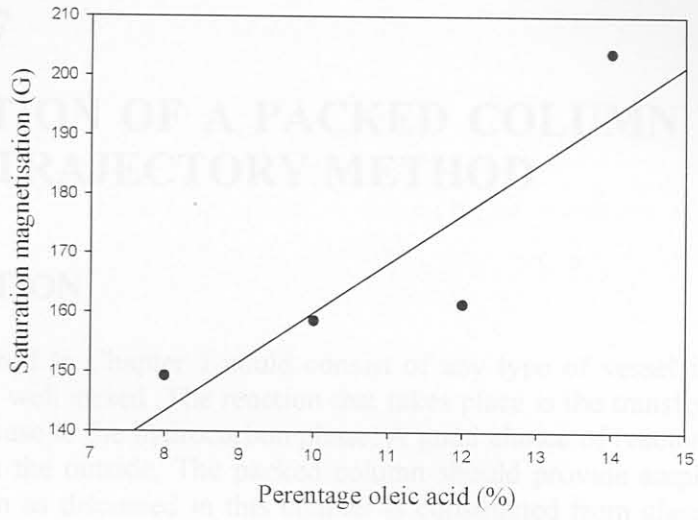

Figure 6.2 Plot of saturation magnetisation versus percentage oleic acid

4. DISCUSSION

As shown in Figure 6.2, as the percentage oleic acid increases, the trend is that saturation magnetisation increases. It is likely that the additional surfactant allows more magnetite particles to be coated. The uncoated magnetite particles remain in the aqueous phase and these particles are lost when the aqueous-hydrocarbon phases are separated. It does not appear that a maximum saturation magnetisation has been reached. Additional oleic acid should be added to see if a maximum can be reached.

5. CONCLUSIONS AND RECOMMENDATIONS

For this brief investigation into steric stabilisation, as the percentage oleic acid increased, the volume of magnetite remaining suspended above the ferrofluid appeared to decrease. It would have been interesting to measure the viscosity of the fluids after each run. It is possible that too high a percentage of oleic acid would result in a fluid of unacceptably high viscosity. It appears that different saturation magnetisations are also obtained using different peptizing times. [36] The fluid should therefore possibly have been maintained at a certain temperature for a certain period of time instead of simply reaching the desired temperature and removing it from the heat source. In addition, it is recommended that an estimate be made of the volume of oleic acid molecules required to coat a magnetite particle of a certain diameter. An initial estimate of the maximum percentage surfactant required could then be established.

CHAPTER 7

OPTIMISATION OF A PACKED COLUMN USING THE DYNAMIC TRAJECTORY METHOD

1. INTRODUCTION

Reactor 6 as described in Chapter 1 could consist of any type of vessel in which the mixture could be heated and well mixed. The reaction that takes place is the transferral of solid particles from the aqueous phase to the hydrocarbon phase. A good choice of reactors would be a packed column heated from the outside. The packed column should provide ample area for the phase transfer. The column as discussed in this chapter is constructed from glass and is packed with glass beads which provide a large surface area for reaction. In order to achieve the phase transfer, heat is required to be input into the system. The column would therefore be heated via electrical heating bands wound around the shell. To obtain the maximum heat transfer at the maximum allowable temperature, the surface area in the column should be at a maximum.

The condition for the optimum temperature progression in a given type of reactor is that the system should be maintained at a temperature where the rate is a maximum. [38] The peptization reaction is endothermic i.e. heat is required to be input into the reaction mixture for most efficient phase transfer. For endothermic reactions, a rise in temperature increases both the equilibrium conversion and the rate of reaction. The maximum possible temperature should thus be used in the process (subject to constraints e.g. no liquid should be boiled off in the process). The heat is transferred to the mixture via the glass beads. The conduction rate (q) is given by eq. (7.1):

$$q = -kA\frac{dT}{dx} \tag{7.1}$$

where k is the thermal conductivity, A is the cross sectional area and $\frac{dT}{dx}$ is the temperature gradient.

From eq. (7.1) it can be seen that to obtain the maximum heat transfer at the maximum allowable temperature, the surface area in the column should be at a maximum.

This chapter documents the procedure of mathematical optimisation using the dynamic trajectory method to determine the optimum column geometry for maximum heat transfer. In this investigation, the reliability of the optimisation algorithm is also tested.

2. AN OVERVIEW OF MATHEMATICAL OPTIMISATION

Mathematical optimisation involves converting a verbal description of a problem into a well-defined mathematical statement. This transcription occurs in three steps: [39]

- identifying the set of variables that describe the system,
- establishing a criterion called the objective function f to determine whether or not a given design is better than another and
- specifying the set of constraints governing the system.

The optimisation problem has the following general mathematical form: [40]

$$\underset{\text{with respect to } x}{\textit{minimise}}\ f(\mathbf{x}),\ \mathbf{x} = (x_1, x_2, \ldots, x_n) \in R^n \tag{7.2}$$

and is subject to the following constraints:

$$g_j(\mathbf{x}) \leq 0 \quad j = 1,2,\ldots,m \tag{7.3}$$

$$h_j(\mathbf{x}) = 0 \quad j = 1,2,\ldots,r < n \tag{7.4}$$

where $f(\mathbf{x})$, $g_j(\mathbf{x})$ and $h_j(\mathbf{x})$ are scalar functions of $\mathbf{x}$.

$f(\mathbf{x})$ is the objective function where $\mathbf{x} = (x_1, x_2, \ldots x_n)$ represents the vector of the design variables i.e. all the possible solutions

$g_j(\mathbf{x})$ represents the jth inequality constraint

$h_j(\mathbf{x})$ represents the jth equality constraint0

The vector $\mathbf{x}$ that minimises $f(\mathbf{x})$ subject to the given constraints is denoted by $\mathbf{x}^*$ with the corresponding optimum function value $f(\mathbf{x}^*)$.

The values of $f(\mathbf{x})$, $g_j(\mathbf{x})$ and $h_j(\mathbf{x})$ at any point, $\mathbf{x} = (x_1, x_2, \ldots x_n)$, may be obtained from analytical known formulae, from a computational process or from measurements of the physical process.

Solving engineering optimisation problems may be difficult for a number of reasons: [40]

- evaluation of the objective and constraint functions may be computationally very expensive,
- numerical noise may exist in the objective and constraint functions,
- there may be discontinuities in the functions,
- the objective and constraint functions may possess areas where they are undefined and
- the problem to be solved may have more that one local minimum.

In order to address these problems, a number of different optimisation algorithms and methods have been developed. For this optimisation problem, the dynamic trajectory methods for unconstrained minimisation by Snyman (also called the "leap-frog" method) will be used. The code LFOPCV3 (leap-frog algorithm for constrained problems) used in the problem was modified for the application. [40]

3. DYNAMIC TRAJECTORY METHOD FOR UNCONSTRAINED MINIMISATION

The basic dynamic trajectory model is based on the following argument:

Assume a particle of unit mass in an n-dimensional conservative force field, with the potential energy at $\mathbf{x}$ given by $f(\mathbf{x})$. The particle can "roll" up or down a "hill". The hill represents the function. The objective is for the particle to roll down to the bottom of the hill i.e. to a minimum. At $\mathbf{x}$, the force on the particle is given by $\mathbf{a} = \ddot{\mathbf{x}} = -\nabla f(\mathbf{x})$. For the time interval [0,t], the conservation of energy holds

$$\frac{1}{2}\|\dot{\mathbf{x}}(t)\|^2 - \frac{1}{2}\|\dot{\mathbf{x}}(0)\|^2 = -[f(\mathbf{x}(t)) - f(\mathbf{x}(0))] \tag{7.5}$$

$$\frac{1}{2}\|\dot{\mathbf{x}}(t)\|^2 - \frac{1}{2}\|\dot{\mathbf{x}}(0)\|^2 = f(\mathbf{x}(0)) - f(\mathbf{x}(t)) \tag{7.6}$$

or
$$\frac{1}{2}\|\dot{\mathbf{x}}(t)\|^2 + f(\mathbf{x}(t)) = \frac{1}{2}\|\dot{\mathbf{x}}(0)\|^2 + f(\mathbf{x}(0)) \tag{7.7}$$

$$\|\mathbf{x}\| = \|(x_1, x_2, \ldots, x_n)\| = \sqrt{x_1^2 + x_2^2 + \ldots + x_n^2} \tag{7.8}$$

let
$$\frac{1}{2}\|\dot{\mathbf{x}}(t)\|^2 = T(t) \tag{7.9}$$

and
$$\frac{1}{2}\|\dot{\mathbf{x}}(0)\|^2 = T(0) \tag{7.10}$$

then
$$T(t) + f(t) = T(0) + f(0) = constant \tag{7.11}$$

or
$$\Delta f = -\Delta T \tag{7.12}$$

From (7.11) it can be seen that as long as T increases, the potential energy f decreases as the particle rolls down the hill (function) with increasing velocity, moving to a region of lower potential energy. This is the basis of the dynamic trajectory algorithm.

The dynamic trajectory method has the following properties:

- It uses only function gradient information and no explicit line searches are performed to determine the value of the function at a particular point. The method is robust and can handle discontinuities in functions and gradients and steep valleys in terms of the shape of the function.
- This algorithm seeks a low local minimum and can therefore be used in a methodology for global optimisation.
- The method is, however, not as efficient on smooth and near quadratic functions as some of the more classical optimisation methods. [40]

3.1 Basic algorithm for unconstrained problems

For unconstrained problems i.e. where no constraints exist and all points $\mathbf{x}$ are feasible where the function is defined, the code LFOP1(b) may be used. With $f(\mathbf{x})$ defined and a starting point, $\mathbf{x}(0) = \mathbf{x}^0$ given, the dynamic trajectory is computed by solving the initial value problem:

$$\ddot{\mathbf{x}} = -\nabla f(\mathbf{x}(t)) \tag{7.13}$$

$$\dot{\mathbf{x}}(0) = 0 \tag{7.14}$$

$$\mathbf{x}(0) = \mathbf{x}^0 \tag{7.15}$$

In computing the trajectory, $\dot{\mathbf{x}}(t)$ must be monitored because as long as T (which is $\frac{1}{2}\|\dot{\mathbf{x}}(t)\|^2$) increases, $f(\mathbf{x}(t))$ decreases. When $\|\dot{\mathbf{x}}(t)\|$ decreases i.e. the particle starts rolling up the hill (function), an interfering strategy must be applied to extract some energy to increase the likelihood of descent of the particle to the bottom of the hill.

In practice the numerical integration of the initial value problem by the "leap-frog" method is performed as follows:

$$\mathbf{x}^{k+1} = \mathbf{x}^k + \mathbf{v}^k \Delta t \tag{7.16}$$

$$\mathbf{v}^{k+1} = \mathbf{v}^k + \mathbf{a}^{k+1} \Delta t \tag{7.17}$$

where $\mathbf{a}^k = -\nabla f(\mathbf{x}^k)$ and $v^0 = \frac{1}{2} a^0 \Delta t$ for k=0, 1, 2, ... and time step Δt.

A typical interfering strategy would be as follows:

If $\|\mathbf{v}^{k+1}\| \geq \|\mathbf{v}^k\|$ continue, else

set $\mathbf{v}^k = \dfrac{\mathbf{v}^{k+1} + \mathbf{v}^k}{4}$ and $\mathbf{x}^k = \dfrac{\mathbf{x}^{k+1} + \mathbf{x}^k}{2}$ to compute a new $\mathbf{v}^{k+1}$ before continuing.

3.2 Basic algorithm for constrained problems

In certain problems, constraints are imposed on the feasible region via expressions (7.3) and (7.4). When constraints exist, the unconstrained optimisation algorithm LFOP1(b) can be applied to the constrained problem if this problem is reformulated in terms of the penalty function formulation. $P(\mathbf{x})$, the penalty function, is a combination of the original function and the constraints i.e.

Minimise $P(\mathbf{x})$ (7.18)

where $P(\mathbf{x}) = f(\mathbf{x}) + \sum_{i=1}^{m} \rho_i h_i^2(\mathbf{x}) + \sum_{j=1}^{r} \beta_j g_j^2(\mathbf{x})$ (7.19)

and $\rho_i >> 0$ $\beta_j = \begin{cases} 0 & \text{if } g_j(\mathbf{x}) \le 0 \\ \mu_j >> 0 & \text{if } g_j(\mathbf{x}) > 0 \end{cases}$ (7.20)

ρ_i and μ_j are penalty parameters. Often $\rho_i = \mu_j =$ constant $= \rho$ for all i and j and the penalty function is then denoted by $P(\mathbf{x}, \rho)$ where typically, $\rho = 10^4$.

The code used for constrained optimisation is LFOPCV3. LFOPCV3 is the application of LFOP1(b) to the penalty function formulation. There are three phases in this code as described below.

In the first phase, the overall penalty parameter $\rho = \rho_0$ is set to equal 10^2. Using some $\mathbf{x}^0$, LFOP1(b) is applied to $P(\mathbf{x}, \rho_0)$ to give $\mathbf{x}^*(\rho_0)$.

In the second phase, $\mathbf{x}^0 = \mathbf{x}^*(\rho_0)$. The penalty parameter is increased, $\rho = \rho_1 = 10^4$ and LFOP1(b) is applied to $P(\mathbf{x}, \rho_1)$ to give $\mathbf{x}^*(\rho_1)$. The active constraints are identified $i_a = 1,2,...n_a$; $g_{i_a}(\mathbf{x}^*(\rho_1)) > 0$.

In the third phase, $\mathbf{x}^0 = \mathbf{x}^*(\rho_1)$ and LFOP1(b) is used to minimise $P_a(\mathbf{x}, \rho_1) = \sum_{i=1}^{m} \rho_1 h_i^2(\mathbf{x}) + \sum_{i_a=1}^{n_a} \rho_1 g_{i_a}^2(\mathbf{x})$ (including active constraints) to give $\mathbf{x}^*$.

The derivatives of the objective function and the constraints are again required as for the unconstrained problem (Section 3.1).

4. PACKED COLUMN PROBLEM DEFINITION

The total available surface area in the packed column (assuming all surface areas are at the same temperature) is a function of the area of one bead (a_{bead}) multiplied by the total number of beads (n_{beads}). (The contact area between the beads and between the beads and the column wall has not been included. Furthermore, the inner surface area of the column has been excluded. Additional comments regarding this exclusion are given in Section 7.)

$$Total\ surface\ area = n_{beads} a_{bead} \tag{7.21}$$

where

$$a_{bead} = \pi d_{bead}^2 \tag{7.22}$$

and d_{bead} represents the bead diameter.

The number of beads can be calculated as the volume in the column occupied by the beads divided by the volume of one bead (with the voidage taken into consideration). The volume of a single bead is given by

$$v_{bead} = \frac{\pi d_{bead}^3}{6} \tag{7.23}$$

ε is the voidage in the column i.e. the volumetric fraction that is not occupied by beads but through which liquid can flow. A common value selected for the voidage is 0.4 [41]. (1- ε) therefore represents the volumetric fraction occupied by the beads (V_{beads}). The height of the column is H_{column} and ϕ_{column} is the diameter of the column.

$$V_{beads} = \frac{\pi \phi_{column}^2 H_{column}(1-\varepsilon)}{4} \tag{7.24}$$

The number of beads (n_{beads}) is given by:

$$n_{beads} = \frac{V_{beads}}{v_{bead}} = \frac{3\phi_{column}^2 H_{column}(1-\varepsilon)}{2d_{bead}^3} \tag{7.25}$$

The surface area is therefore given by:

$$Total\ surface\ area = n_{beads} a_{bead} = \frac{3\pi\phi_{column}^2 H_{column}(1-\varepsilon)}{2d_{bead}} \tag{7.26}$$

It was assumed that the diameter and height of the column would be restricted by space limitations if the column were to be used in an application on a plant and glass columns of diameter between 0.1 and 1 metre and heights of between 0.5 and 3 metres were considered. The size of glass beads that were considered is in the range of 5 to 75 mm.

The following equations are obtained when translating into inequality constraints:

$$0.1 \leq \phi_{column} \leq 1 \tag{7.27}$$

$$0.5 \leq H_{column} \leq 3 \tag{7.28}$$

$$0.005 \leq d_{bead} \leq 0.075 \tag{7.29}$$

Rearranging eqs (7.27) to (7.29) gives

$$\phi_{column} - 1 \leq 0 \tag{7.30}$$

$$0.1 - \phi_{column} \leq 0 \tag{7.31}$$

$$H_{column} - 3 \leq 0 \tag{7.32}$$

$$0.5 - H_{column} \leq 0 \tag{7.33}$$

$$d_{bead} - 0.075 \leq 0 \tag{7.34}$$

$$0.005 - d_{bead} \leq 0 \tag{7.35}$$

A further important parameter is the time required for the mixture to react and for the reaction to go to completion. Experimental work has indicated that a residence time (τ) of approximately 15 minutes is required to ensure that the solid particles are transferred in the reaction. It has also been noticed that the residence time should be less than 30 minutes in order to prevent the reaction mixture from becoming viscous.

The residence time, τ, (in hours) can be determined from eq. (7.36) where $V_{liquid\ in\ column}$ is the volume through which liquid can flow in the column, and Q is the volumetric flow rate through the column. The volumetric flow rate for this investigation was taken to be 58 l/h ($1.6*10^{-5}$ m^3/s).

$$\tau = \frac{V_{liquid\ in\ column}}{Q} = \frac{\pi \phi_{column}^2 H_{column} \varepsilon}{4Q} \tag{7.36}$$

Taking the residence times into account gives

$$\frac{15}{60} \leq \frac{\pi \phi_{column}^2 H_{column} \varepsilon}{4Q} \leq \frac{30}{60} \tag{7.37}$$

or, rearranged,

$$\frac{15}{60} \frac{4Q}{\pi \varepsilon} \leq \phi_{column}^2 H_{column} \leq \frac{30}{60} \frac{4Q}{\pi \varepsilon} \tag{7.38}$$

Often the optimum length to diameter ratio of vessels is in the range of 2.5 to 5. [42] It was decided that the ratio of the column height to the diameter should be at least less than 3/2 which gives a value in the same area as the recommended ratio. The equation indicating this proportion is given by

$$\frac{\phi_{column}}{H_{column}} \leq \frac{2}{3} \tag{7.39}$$

or

$$\frac{\phi_{column}}{H_{column}} - \frac{2}{3} \leq 0 \tag{7.40}$$

The constraints in terms of the geometry limitations are taken into account and an additional constraint arises, namely that the diameter of the glass beads must be less than that of the column.

$$d_{bead} \leq \phi_{column} \tag{7.41}$$

or

$$d_{bead} - \phi_{column} \leq 0 \tag{7.42}$$

5. DEFINITION OF OBJECTIVE FUNCTION AND CONSTRAINTS

The design variables chosen for this problem are the column diameter, the diameter of the glass beads and the height of the column. The diameter of the glass beads is orders of magnitude smaller than the diameter and height of the column. This variable should therefore be scaled. [40]

Let

$$x_1 = \phi_{column} \tag{7.43}$$

$$x_2 = 100 * d_{bead} \tag{7.44}$$

$$x_3 = H_{column} \tag{7.45}$$

The design variables are substituted into eq. (7.26) to give

$$f(\mathbf{x}) = \frac{300\pi x_1^2 x_3 (1-\varepsilon)}{2x_2} \tag{7.46}$$

5.1 Reaction excluding residence time and column proportion

Initially, for interest, the simple case for reaction where the residence time and column proportion are not taken into account was considered.

The objective is to maximise the surface area for reaction and heat transfer. This is equivalent to minimising the negative of the objective function:

$$\text{Minimise } f(\mathbf{x}) = -\frac{300\pi x_1^2 x_3 (1-\varepsilon)}{2x_2} \tag{7.47}$$

The objective function must be minimised subject to the following inequality constraints from eqs (7.30), (7.31), (7.34), (7.35), (7.32), (7.33) and (7.42).

$$\begin{aligned}
g_1(\mathbf{x}) &= x_1 - 1 \le 0 \\
g_2(\mathbf{x}) &= 0.1 - x_1 \le 0 \\
g_3(\mathbf{x}) &= x_2 - 7.5 \le 0 \\
g_4(\mathbf{x}) &= 0.5 - x_2 \le 0 \\
g_5(\mathbf{x}) &= x_3 - 3 \le 0 \\
g_6(\mathbf{x}) &= 0.5 - x_3 \le 0 \\
g_7(\mathbf{x}) &= x_2 - 100x_1 \le 0
\end{aligned} \tag{7.48}$$

The derivatives of the objective function with respect to the three design variables are given by

$$\frac{\partial f}{\partial x_1}(\mathbf{x}) = -\frac{300\pi x_1 x_3(1-\varepsilon)}{1x_2}$$
$$\frac{\partial f}{\partial x_2}(\mathbf{x}) = \frac{300\pi x_1^2 x_3(1-\varepsilon)}{2x_2^2} \tag{7.49}$$
$$\frac{\partial f}{\partial x_3}(\mathbf{x}) = -\frac{300\pi x_1^2(1-\varepsilon)}{2x_2}$$

The derivatives of the inequality constraints are given by

$$g_1'(\mathbf{x}) = 1$$
$$g_2'(\mathbf{x}) = -1$$
$$g_3'(\mathbf{x}) = 1$$
$$g_4'(\mathbf{x}) = -1$$
$$g_5'(\mathbf{x}) = 1 \tag{7.50}$$
$$g_6'(\mathbf{x}) = -1$$
$$g_7'(\mathbf{x}, x_1) = -100$$
$$g_7'(\mathbf{x}, x_2) = 1$$

5.2 Reaction including residence time and column proportion

For the case where the residence time and the column proportion were taken into account, the equation for the objective function remained the same but additional inequality constraints were added. The inequality constraint for the residence time is derived as shown by

$$\frac{15}{60}h * \frac{4}{\pi\varepsilon} * 58\frac{l}{h} * \frac{1}{1000\frac{l}{m^3}} \le \phi_{column}^2 H_{column} \le \frac{30}{60}h * \frac{4}{\pi\varepsilon} * 58\frac{l}{h} * \frac{1}{1000\frac{l}{m^3}} \tag{7.51}$$
$$\frac{0.058}{\pi\varepsilon} \le x_1^2 x_3 \le \frac{0.116}{\pi\varepsilon}$$

or

$$x_1^2 x_3 - \frac{0.116}{\pi\varepsilon} \le 0 \tag{7.52}$$

$$\frac{0.058}{\pi\varepsilon} - x_1^2 x_3 \le 0 \tag{7.53}$$

The additional inequality constraints are given by

$$g_8(\mathbf{x}) = x_1^2 x_3 - \frac{0.116}{\pi\varepsilon} \leq 0$$
$$g_9(\mathbf{x}) = \frac{0.058}{\pi\varepsilon} - x_1^2 x_3 \leq 0 \qquad (7.54)$$
$$g_{10}(\mathbf{x}) = \frac{x_1}{x_3} - \frac{2}{3} \leq 0$$

The derivatives of the objective function remain the same.

The derivatives of the additional inequality constraints are given by

$$g_8'(\mathbf{x}, x_1) = 2x_1 x_3$$
$$g_8'(\mathbf{x}, x_3) = x_1^2$$
$$g_9'(\mathbf{x}, x_1) = -2x_1 x_3$$
$$g_9'(\mathbf{x}, x_3) = -x_1^2 \qquad (7.55)$$
$$g_{10}'(\mathbf{x}, x_1) = \frac{1}{x_3}$$
$$g_{10}'(\mathbf{x}, x_3) = -\frac{x_1}{x_3^2}$$

6. RESULTS

The objective function, equations for the inequality constraints, derivatives of the objective function with respect to the design variables and derivatives for the constraints were entered into LFOPCV3. A portion of the Fortran source code for the investigation into the optimisation of the surface area with residence time and geometric constraints is given in the appendix.

6.1 Reaction excluding residence time and column proportion

The number of variables was specified as three. The initial guess was chosen as X(1) = 0.3 (column diameter = ϕ_{column} = 0.3 m), X(2) = 0.5 (bead diameter = d_{bead} = 5 mm) and X(3) = 1.5 (column height = H_{column} = 1.5 m). The number of inequalities was specified as 7 (as given by eq. (7.48)) and the number of equalities as zero. The penalty function parameters were specified as 10^2 for (ρ_0) and 10^4 for (ρ_1). The tolerance, XTOL was specified to be 10^{-9} and EG (the value against which the gradient vector of the penalty function is compared) set to 10^{-8}. The maximum step size was set to be 1 and the maximum number of iterations was set at 100 000.

The objective function was input into SUBROUTINE FUN of LFOPCV3 and the inequality constraints were input into SUBROUTINE CONIN. SUBROUTINE CONEG for equality

constraints was left blank. The gradient vectors of the objective function and the inequality constraints were input into SUBROUTINE GRADF and SUBROUTINE GRADC respectively while SUBROUTINE GRADH (for the gradient vectors of the equality constraints) was left blank.

The solution was found to converge in 295 iterations. The optimum for the surface area was found where $x_1^* = 1$; $x_2^* = 0.5$ and $x_3^* = 3$. This means that the column diameter is equal to 1 m; the bead diameter is equal to 5 mm and the height is equal to 3 m. The resultant surface area was found to be 1696.5 m^2 and the number of beads required is 21 600 000. Figure 7.1 shows the plots of the values of the variables at each iteration.

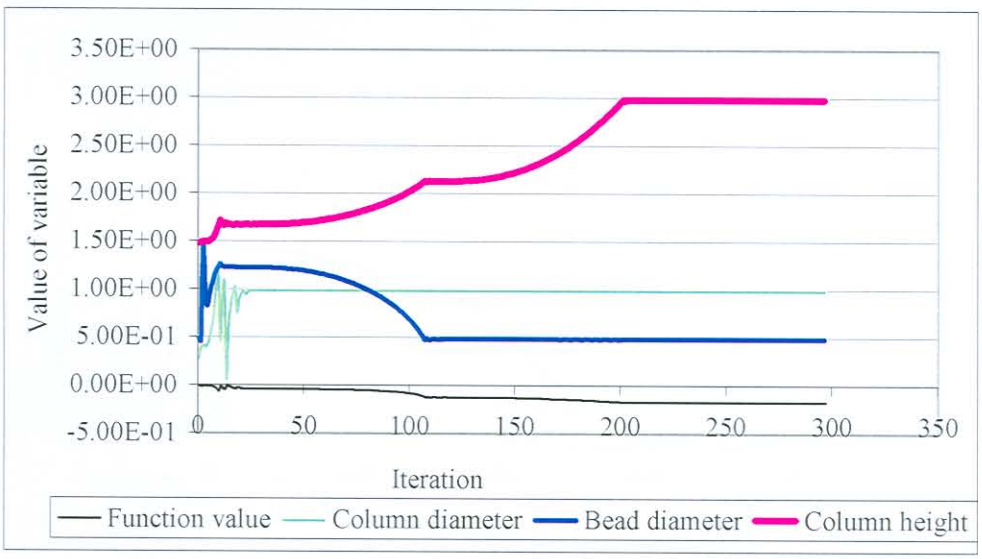

Figure 7.1 Plots of the values of the variables at each iteration

These results make sense as the largest column with the smallest bead size would give the greatest area. A larger column would be able to accommodate a larger number of beads and more beads of a smaller size would fit into the column giving a greater surface area for reaction.

6.1.1 Investigation into the effect of different starting conditions

Different starting conditions were chosen to determine whether or not the solution converged to the same answer and whether or not the minimum of the previous solution was a local or a global minimum. These starting conditions along with the number of iterations required to obtain convergence are shown in Table 7.1. Figures 7.2, 7.3 and 7.4 show the plots of the values of the variables at each iteration for run 1, 2 and 3 respectively.

For all runs, the same solution is obtained. For run 1, arbitrary initial values were selected for the three variables. In run 2, the initial variables are those furthest away from the solution. The solution is obtained in 1688 iterations which is greater than the 388 and the 102 required for

conditions 1 and 3 respectively. The solution converged relatively quickly in run 3 as the starting conditions chosen were those values of the converged solution.

Table 7.1 Values of the variables for different starting conditions

Run no.	Starting value for variable			Iteration
	X(1)	X(2)	X(3)	
1	1	2	1	388
2	0.1	7.5	0.5	1688
3	1	0.5	3	102

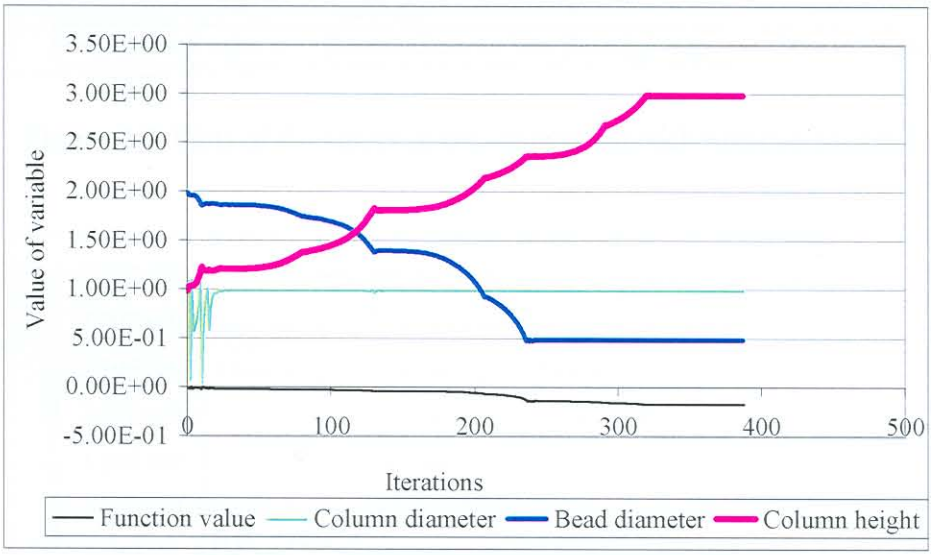

Figure 7.2 Plots of the values of the variables at each iteration for run 1

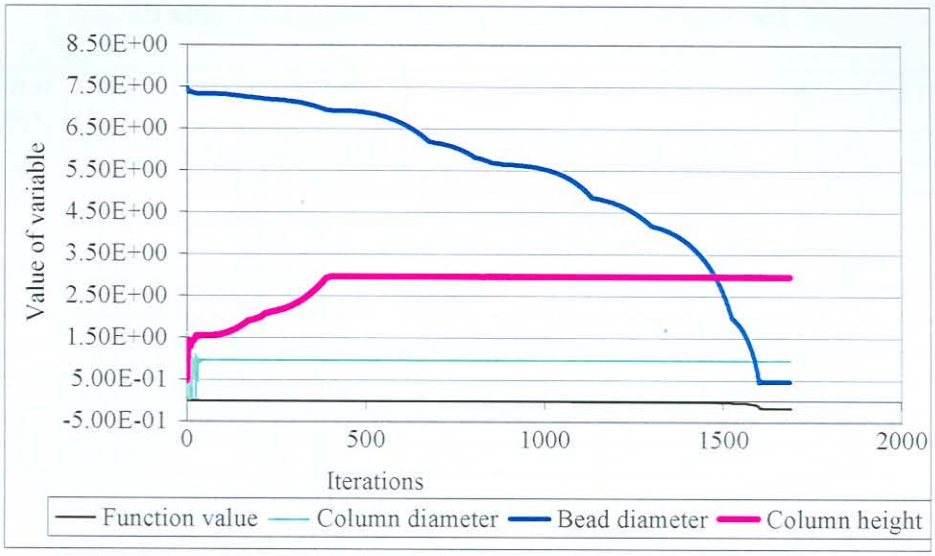

Figure 7.3 Plots of the values of the variables at each iteration for run 2

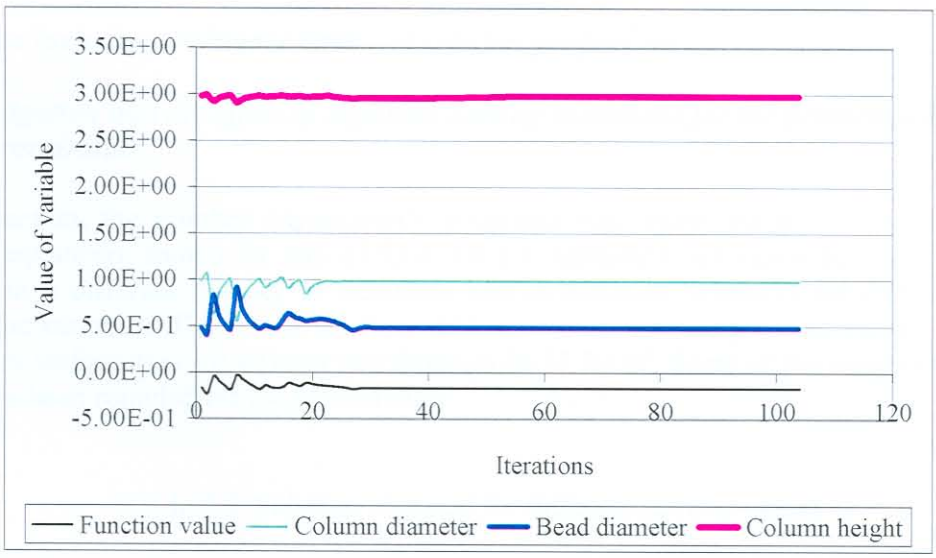

Figure 7.4 Plots of the values of the variables at each iteration for run 3

6.1.2 Investigation into the effect of changing the step size, DELT

The effect of changing the step size, DELT and with X(1) = 1, X(2) = 0.5 and X(3) = 3 was investigated. The results are given in Table 7.2. The results are rounded off where necessary for presentation in the table.

Table 7.2 Effect of DELT on the solution obtained

DELT	Iterations	Obj. func.	Final x-values			Final inequality constraint function values						
		F	X(1)	X(2)	X(3)	C(1)	C(2)	C(3)	C(4)	C(5)	C(6)	C(7)
100	1075	-0.17	1	0.5	3	$2.7e^{-11}$	-0.9	-7	$2.7e^{-11}$	$4.5e^{-12}$	-2.5	-99.5
10	153	-0.17	1	0.5	3	$5.8e^{-9}$	-0.9	-7	$5.8\ e^{-9}$	$9.6\ e^{-10}$	-2.5	-99.5
1	102	-0.17	1	0.5	3	$-1.0e^{-9}$	-0.9	-7	$-1.0e^{-9}$	$-1.6e^{-10}$	-2.5	-99.5
0.1	107	-0.17	1	0.5	3	$8.5e^{-9}$	-0.9	-7	$8.6e^{-9}$	$1.4e^{-9}$	-2.5	-99.5
0.01	76	-0.17	1	0.5	3	$1.8e^{-10}$	-0.9	-7	$1.8e^{-10}$	$2.9\ e^{-11}$	-2.5	-99.5
0.005	57	-0.17	1	0.5	3	$5.2e^{-9}$	-0.9	-7	$5.3e^{-9}$	$8.7e^{-10}$	-2.5	-99.5
0.004	49	-0.17	1	0.5	3	$5.6e^{-9}$	-0.9	-7	$5.6e^{-9}$	$9.3e^{-10}$	-2.5	-99.5
0.001	49	-0.17	1	0.5	3	$1.0e^{-8}$	-0.9	-7	$1.0e^{-8}$	$1.7e^{-9}$	-2.5	-99.5
0.0001	109	-0.17	1	0.5	3	$1.0e^{-8}$	-0.9	-7	$1.0e^{-8}$	$1.7e^{-9}$	-2.5	-99.5
0.00001	474	-0.17	1	0.5	3	$-3.7e^{-12}$	-0.9	-7	$-3.7e^{-12}$	$-6.2e^{-13}$	-2.5	-99.5

The solution converged to the same final value for the objective function value with the minimum number of iterations for DELT equal to 0.004. The same number of iterations was required for DELT equal to 0.001 but DELT equal to 0.004 gave the lowest value for the final inequality constraint function values.

6.2 Reaction including residence time and column proportion

6.2.1 Investigation into the effect of different starting conditions for the problem with inequality constraints

For this reaction, the number of inequality equations was increased to 10 (as given by the additional equations shown in eqs (7.53)). DELT remained set equal to 1. The solution converged in a different number of iterations and to different solutions for differing starting values for the variables. The results for these different conditions are given in Tables 7.3 and 7.4. The resultant surface area for all runs was found to be 52.20 m^2. Some of the values in Tables 7.3 and 7.4 have been rounded off for presentation.

Table 7.3 Solution obtained for different starting values

Run no.	Starting value for variable			Iterations	Obj. func.	Final x-values		
	X(1)	X(2)	X(3)		F	X(1)	X(2)	X(3)
1	0.3	0.5	1.5	126	-0.00522	0.25	0.5	1.5
2	1	2	1	394	-0.000249	-0.038	0.5	3
3	0.1	7.5	0.5	18974	-0.00522	0.39	0.5	0.61
4	1	0.5	3	122	-0.00522	0.18	0.5	2.88
5	0.39	0.5	0.61	230	-0.00522	0.38	0.5	0.64
6	0.38	0.5	0.64	373	-0.00522	0.38	0.5	0.64

Table 7.4 Values for the final inequality constraint functions

Run no.	Final inequality constraint function values									
	C(1)	C(2)	C(3)	C(4)	C(5)	C(6)	C(7)	C(8)	C(9)	C(10)
1	-0.75	-0.14	-7	$-1.4e^{-9}$	-1.5	-1.4	-24	$-4.2e^{-9}$	$-4.6e^{-2}$	-0.50
2	-1	0.14	-7	$4.3e^{-4}$	$1.2e^{-3}$	-2.9	4	$-8.8e^{-2}$	$4.2e^{-2}$	-0.69
3	-0.61	-0.28	-7	$7.2e^{-11}$	-2.4	-0.81	-38	$9.8e^{-11}$	$-4.6e^{-2}$	$-3.0e^{-2}$
4	-0.82	$-7.9e^{-2}$	-7	$7.5e^{-13}$	-0.12	-2.8	-17	$5.4e^{-12}$	$-4.6e^{-2}$	-0.60
5	-0.63	-0.28	-7	$1.5e^{-10}$	-2.4	-0.62	-38	$2.1e^{-10}$	$-4.6e^{-2}$	$-7.1e^{-2}$
6	-0.62	0.28	-7	$2.0e^{-11}$	-2.4	-0.6	-37	$2.8e^{-10}$	$-4.6e^{-2}$	$-7.4e^{-2}$

Run 2 did not appear to reach a solution as two of the final inequality constraint function values were contravened (C(2) and C(7)). It appears that a number of different local optima were obtained in this problem. This probably comes about as a result of the flexibility in the design for the column proportion. There are a number of different possible combinations for the optimum surface area for a column diameter to height ratio of less than 2/3. Runs 5 and 6 converged to approximately the same answer possibly as a result of the similar starting variables.

6.2.2 Investigation into the solution obtained with one equality constraint and inequality constraints

The effect of adding the ratio of column diameter to height as an equality constraint instead of an inequality constraint was investigated. The ratio was set to 2/3. The number of inequality equations was decreased to 9 and the number of equality constraints to 1. The equality constraint is given by

$$h_1(\mathbf{x}) = \frac{x_1}{x_3} - \frac{2}{3} = 0 \tag{7.56}$$

For these conditions, DELT remained set equal to 1. The solution converged in 157 iterations for starting values of X(1) = 0.3, X(2) = 0.5 and X(3) = 1.5. The optimum for the surface area was found where $x_1^* = 0.39480761$; $x_2^* = 0.5$ and $x_3^* = 0.59221141$. This means that the column diameter is equal to approximately 0.39 m; the bead diameter is equal to 5 mm and the height is equal to approximately 0.59 m. The resultant surface area was found to be 52.20 m^2. The values of the final inequality constraints were:

C(1) = –0.61
C(2) = -0.29
C(3) = -7
C(4) = $6.5e^{-10}$
C(5) = -2.4
C(6) = -0.49
C(7) = -39
C(8) = $1.2e^{-10}$
C(9) = $-4.6e^{-2}$

for the nine equations respectively. The final equality constraint function value was $-5.6e^{-9}$.

6.2.3 Investigation into the effect of changing the step size, DELT with inequality and one equality constraint

The effect of changing DELT and with starting values of X(1) = 0.3, X(2) = 0.5 and X(3) = 1.5 was investigated. The results are given in Tables 7.5 and 7.6. Some of the results are rounded off where necessary for presentation in the table.

Table 7.5 Effect of DELT on the solution obtained

Run no.	DELT	Iteration	Obj. func.	Final x-values		
				X(1)	X(2)	X(3)
1	100	407	-0.00522	0.39	0.5	0.59
2	10	508	-0.00522	0.39	0.5	0.59
3	5	179	-0.00522	0.39	0.5	0.59
4	1	157	-0.00522	0.39	0.5	0.59
5	0.1	195	-0.00522	0.39	0.5	0.59
6	0.01	268	-0.00522	0.39	0.5	0.59
7	0.001	1288	-0.00522	0.39	0.5	0.59
8	0.0001	11122	-0.00522	0.39	0.5	0.59

Table 7.6 Values for the final inequality constraint functions

Run no.	Final inequality constraint function values									Fin. equal constr. funct.
	C(1)	C(2)	C(3)	C(4)	C(5)	C(6)	C(7)	C(8)	C(9)	H(1)
1	-0.61	-0.29	-7	$3.0e^{-10}$	-2.4	-0.49	-39	$5.6e^{-10}$	$-4.6e^{-2}$	$-1.7e^{-9}$
2	-0.61	-0.29	-7	$4.1e^{-10}$	-2.4	-0.49	-39	$-2.2e^{-10}$	$-4.6e^{-2}$	$7.4e^{-10}$
3	-0.61	-0.29	-7	$6.7e^{-10}$	-2.4	-0.49	-39	$9.8e^{-10}$	$-4.6e^{-2}$	$-4.5e^{-9}$
4	-0.61	-0.29	-7	$6.5e^{-10}$	-2.4	-0.49	-39	$1.2e^{-10}$	$-4.6e^{-2}$	$-5.6e^{-10}$
5	-0.61	-0.29	-7	$-3.1e^{-10}$	-2.4	-0.49	-39	$4.5e^{-11}$	$-4.6e^{-2}$	$-1.1e^{-9}$
6	-0.61	-0.29	-7	$-3.1e^{-10}$	-2.4	-0.49	-39	$2.1e^{-10}$	$-4.6e^{-2}$	$-1.1e^{-9}$
7	-0.61	-0.29	-7	$-4.9e^{-10}$	-2.4	-0.49	-39	$4.9e^{-10}$	$-4.6e^{-2}$	$-1.6e^{-9}$
8	-0.61	-0.29	-7	$3.5e^{-10}$	-2.4	-0.49	-39	$7.6e^{-11}$	$-4.6e^{-2}$	$-3.9e^{-9}$

Figure 7.5 gives the plot of the values of the variables at each iteration for the DELT that gives the lowest number of iterations. This is run 4 where DELT equals 1. The fact that the fewest iterations are obtained when DELT is less than 10 and greater than 0.99 can possibly be explained by the following. DELT should be of the same order of magnitude as the "diameter" of the region if interest [43] i.e. $DELT = \sqrt{N} * variable - range$ where N is the number of variables. DELT can be calculated to be in the region of:

$$\sqrt{3}*1-0.9=0.8$$
$$\sqrt{3}*3-2.5=2.7 \qquad (7.57)$$
$$\sqrt{3}*5-7=1.7$$

for the column height and diameter and bead diameter respectively (taking a random value for the variable in the range provided).

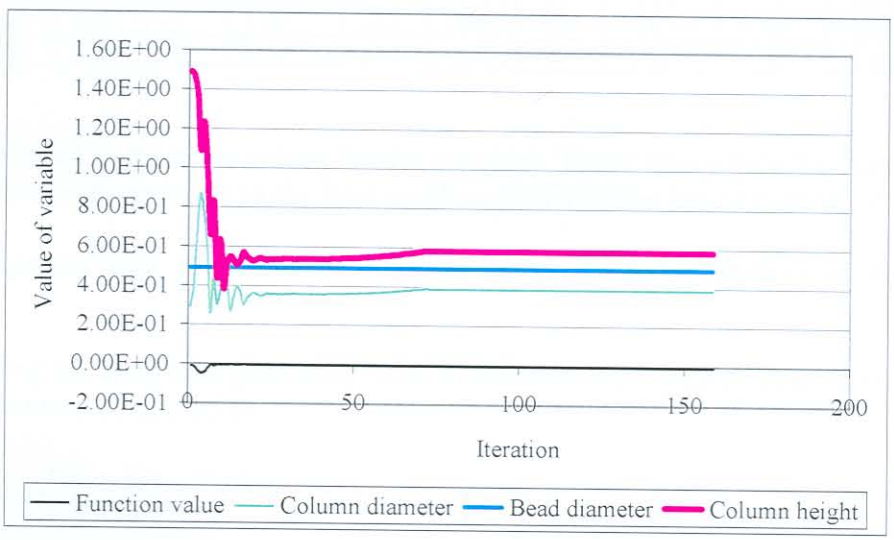

Figure 7.5 Plots of the values of the variables at each iteration

6.2.4 Investigation into the effect of different starting conditions with one equality constraint and inequality constraints

With the new system of equations and with DELT equal to 1, solutions were obtained for differing starting values for the variables. The results for these different conditions are given in Tables 7.7 and 7.8. Once again, the resultant surface area was found to be 52.20 m^2 for all runs. Some of the values in Table 7.7 have been rounded off for presentation.

Table 7.7 Solution obtained for different starting values

Run no.	Starting value for variable			Iterations	Obj. func.	Final x-values		
	X(1)	X(2)	X(3)		F	X(1)	X(2)	X(3)
1	0.3	0.5	1.5	157	-0.00522	0.39	0.5	0.59
2	1	2	1	1360	-0.00522	0.39	0.5	0.59
3	0.1	7.5	0.5	32845	-0.00522	0.39	0.5	0.59
4	1	0.5	3	189	-0.00522	0.39	0.5	0.59
5	0.39	0.5	0.59	352	-0.00522	0.39	0.5	0.59

Table 7.8 Values for the final inequality constraint functions

Run no.	Final inequality constraint function values									Fin. equal constr. funct.
	C(1)	C(2)	C(3)	C(4)	C(5)	C(6)	C(7)	C(8)	C(9)	H(1)
1	-0.61	-0.29	-7	$6.5e^{-10}$	-2.4	-0.49	-39	$1.2e^{-10}$	$-4.6e^{-2}$	$-5.6e^{-10}$
2	-0.61	-0.29	-7	$1.4e^{-10}$	-2.4	-0.49	-39	$2.8e^{-10}$	$-4.6e^{-2}$	$1.05e^{-10}$
3	-0.61	-0.29	-7	$5.8e^{-11}$	-2.4	-0.49	-39	$4.1e^{-11}$	$-4.6e^{-2}$	$-8.8e^{-10}$
4	-0.61	-0.29	-7	$3.5e^{-10}$	-2.4	-0.49	-39	$7.1e^{-10}$	$-4.6e^{-2}$	$-1.6e^{-10}$
5	-0.61	-0.29	-7	$2.1e^{-10}$	-2.4	-0.49	-39	$-4.8e^{-10}$	$-4.6e^{-2}$	$-1.6e^{-9}$

All runs converged to the same values for the variables. Those runs where the starting values of the variables were chosen close to the final x-values exhibited the lowest number of steps.

6.2.5 Investigation into the solution obtained using finite differences to determine the gradients

Instead of using the analytical gradients, finite differences were used to determine the gradients i.e. the gradient was computed as:

$$f'(x) = \frac{f(x+\Delta x) - f(x)}{\Delta x} \tag{7.58}$$

The solution obtained using this method was then compared to that obtained when using the analytical gradients.

With starting values of X(1) = 0.3, X(2) = 0.5 and X(3) = 1.5, 203 iterations were required to obtain a solution when finite differences were used to calculate the gradients with Δx (the step size used to find the gradient) or DELX equal to 10^5. Figure 7.6 gives the plot of the values of the variables at each iteration for DELT equal to 1 (see Table 7.5). This value resulted in the lowest number of iterations required for run 4. The solution obtained is the same as that obtained for the gradients by the analytical derivatives.

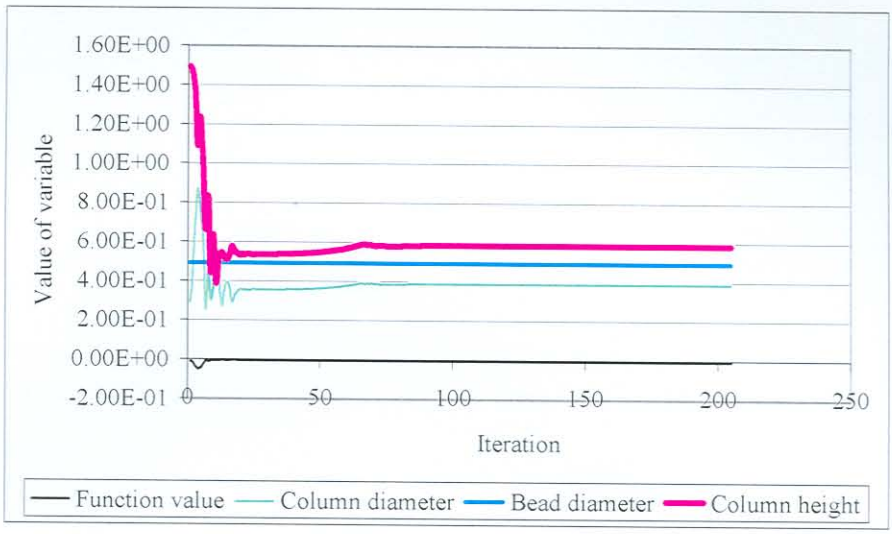

Figure 7.6 Plots of the values of the variables at each iteration

The value of DELX was varied to determine the effect on the number of iterations required to obtain the solution. The results are given in Table 7.9.

Table 7.9 Effect of DELX on iterations required to obtain solution

Run no.	Size of DELX	Iteration
1	$1e^{-6}$	157
2	$1e^{-5}$	157
3	$1e^{-4}$	161
4	$1e^{-3}$	201
5	$1e^{-2}$	203
6	$1e^{-1}$	195
7	0.5	848
8	1	848
9	10	149
10	100	133

All runs converged to the same solution. As the size of DELX decreased (below 1), the number of iterations required to reach the solution also decreased possibly because the value of the gradient was more accurate and the solution was approached more quickly. Figure 7.7 gives the plot of the values of the variables at each iteration for DELX equal to 10^{-5} that gives the lowest number of iterations.

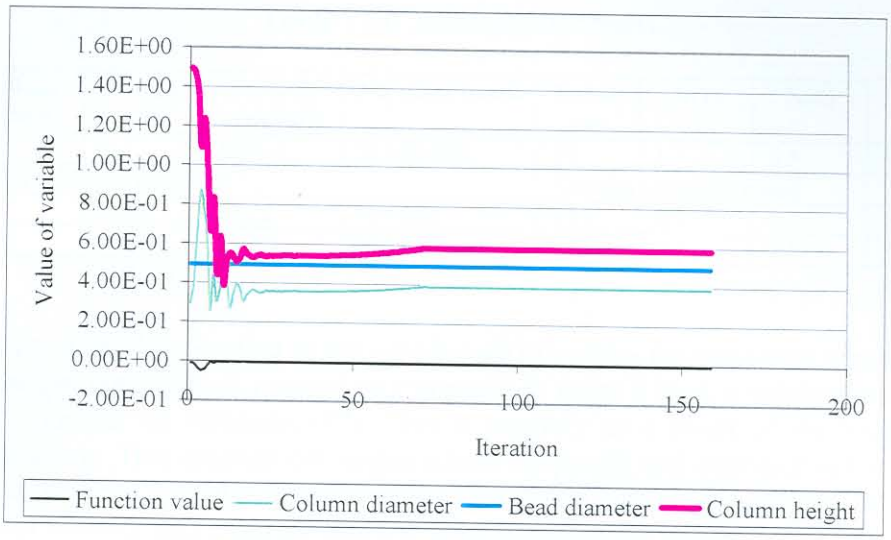

Figure 7.7 Plots of the values of the variables at each iteration

As DELX increased above 1, the number of iterations required for convergence also decreased. This is probably because, as the gradient is calculated, the constraints are encountered and the solution is forced to convergence more quickly.

7. CONCLUSIONS AND RECOMMENDATIONS

A number of investigations were conducted to determine what the dimensions of a packed column should be to obtain maximum heat transfer at the maximum allowable temperature for the manufacture of ferrofluid. The solutions obtained with the least number of steps for the various cases considered are summarised in Table 7.10.

1 = Optimisation where the residence time and geometric column height to diameter constraint is ignored
2 = Optimisation where the residence time and geometric column height to diameter constraint is taken into consideration as an inequality constraint
3 = Optimisation where the residence time is considered and the geometric column height to diameter constraint is taken as an equality consideration
4 = Optimisation where the residence time is taken into account, geometric column height to diameter constraint is taken as an equality consideration and finite differences are used to calculate derivatives

Table 7.10 Summary of results

	ϕ_{column} (m)	d_{bead} (mm)	H_{column} (m)	Surface area (m^2)	No. glass beads	Iterations	X(1)	X(2)	X(3)	DELT
1	1	5	3	1696.5	21 600 000	57	1	0.5	3	0.004
2	Various valid solutions obtained					Various variables tested				
3	0.39	5	0.59	52.22	664 630	157	0.3	0.5	1.5	1
4	0.39	5	0.59	52.22	664 630	157	0.3	0.5	1.5	1

From the results it can be seen that in the simple case (1) where the residence time and geometric diameter to height constraint is ignored as compared to cases 2 to 4, a solution is obtained with the minimum number of iterations (57). This is possibly as a result of the lower number of constraint equations. This solution converges where the height and diameter of the column are a maximum and the bead diameter is a minimum. This would provide the greatest surface area thus promoting heat transfer and ensuring that the solid particles are transferred from the aqueous to the organic phase. The residence time in this case if the values of the variables obtained as a solution are substituted back into the equations would, however, result in a completely unacceptable residence time of more than 16 hours. The resultant product would be viscous and much of the organic phase may have evaporated.

When including the residence time considerations and the height to diameter ratio as an inequality constraint, various valid solutions were obtained for different starting values of the variables. This is because there are a number of combinations of height to diameter that would be below 2/3 that would still give the same surface area and acceptable residence time. (In fact, from calculations, it is seen that for the solutions obtained in Table 7.3, the residence time is a maximum.) In further work that was conducted but not reported in this dissertation, it was found that when the inner surface area was included, different starting conditions converged to one solution where a maximum was obtained for the inner surface area.

When the height to diameter ratio is included as an equality constraint and when finite differences are used for calculation of the gradient, the solution is obtained in 157 iterations when DELT equals 1. The column diameter would be approximately 0.39 m, the height would be approximately 0.59 m and the bead diameter 5 mm. The bead diameter is at its smallest size to give the largest surface area. The surface area available for reaction is approximately 52.22 m^2. With the additional constraints, there is approximately 32 times less surface area available for reaction and heat transfer.

An area for further study would be to consider the number of beads required to fill the column to be a discrete value. The bead diameter could also be considered a discrete variable, as the glass beads are available commercially in certain specific sizes. The problem could be reformulated accordingly. The column height and diameter are relatively flexible as a glass blower could manufacture a column to a required specification. It would, however, be cheapest to purchase a standard commercially available glass column. In addition, experimental verification of the computed results would prove interesting.

CHAPTER 8

PROJECT SUMMARY, CONCLUSIONS AND RECOMMENDATIONS

In this dissertation an attempt was made to explain and offer a more detailed understanding of some of the basic aspects of ferrofluids and key parameters involved in their manufacture. This was performed because, although the process for ferrofluid synthesis appears to be relatively simple, many of the steps in the manufacture are not understood fully.

In Chapter 3, parameters that could affect the production of magnetite were discussed and an investigation was conducted to confirm what the preferred conditions are for the production of magnetite. From the investigations, it appears that magnetite is produced through the formation of green rust complexes. The green rusts are produced from ferrihydrites and iron (II) ions. Magnetite is then produced by the dehydroxylation of the green rusts. The following parameters favour the formation of magnetite: high pH, rapid addition of ammonium hydroxide solution, a rapid stirrer speed and sufficient ammonium hydroxide to ensure that the pH is in the correct range for the dehydroxylation of green rusts and for the prevention of formation of non-magnetic oxides.

In Chapter 4, the CFD software, CFX was used to determine the suitability of sedimentation funnels for the washing and concentration of the magnetite precipitate. A base case funnel containing only water was modelled using CFX-4.3. From preliminary results obtained from CFX-4, it appears that the inflowing liquid churns up material that may have settled at the base of the funnel. A possible method to eliminate this would be to insert a baffle plate at the funnel entrance. The streamline plots of the solution obtained in CFX-5 confirmed the results obtained in CFX-4. It was realised, when performing the multi-phase flow modelling that it would be necessary to incorporate the magnetic field if the correct solid particle size is to be used. Without the additional body force, the nanometre size particles follow the flow of the main fluid. It was initially recommended that the funnel geometry be modified such that the flow into the funnel does not disturb the particles at the base of the funnel. The magnetic field could then be incorporated into the model. The four funnels in series could then be modelled as a unit once convergence on an optimised funnel has been obtained. A new concept was, however, proposed as an alternative to the sedimentation funnels and the CFD study was suspended.

In Chapter 5, the WHIMS was discussed as an alternative to the method of the sedimentation funnels for the washing and concentration of magnetite precipitate. A prototype of the WHIMS was built to determine whether or not it would be suitable for this purpose. Furthermore, a qualitative estimation of the suitability of three mesh types was determined. It was found from the test work that the WHIMS will function effectively in the washing and concentration of the magnetite precipitate. The percentage magnetite retained on the three types of mesh is similar for all three cases, however, Mesh 3 (a high carbon woven wire screen with a 5 mm aperture and a wire of 3.15 mm diameter) exhibits the lowest loss of magnetite. It is recommended that Mesh 3 be used initially. It is suspected that the outlet flow rate from the WHIMS during washing cycles

could be increased with a lower loss of precipitate when using Mesh 3 as compared to the other mesh types. This implies that a greater number of washing cycles could be performed in the allowable cycle time per volume if the WHIMS were used in a process that manufactures ferrofluid continuously. It is further recommended if Mesh 3 is used, that the flushing time for rinsing magnetite from the mesh be increased. If the flushing time is increased, it may be possible to wash Mesh 3 better. If it is found that Mesh 3 clogs easily and it is not possible to remove the magnetite, Mesh 2 (a galvanised woven wire screen with a 10 mm aperture and a wire of 4 mm diameter) should be used instead. Mesh 2 loses less magnetite than Mesh 1 (an expanded metal sheet with 8 X 20 mm diamond shape openings, a gap of 2 mm between openings and a thickness of 1.2 mm) whilst retaining a similar percentage as Mesh 1. The flushing time when using Mesh 2 may be lower than that required to flush Mesh 3. This allows for a slower draining time or outlet velocity from the mesh which may decrease the percentage magnetite loss. The outlet velocity for the testwork was approximately 3 l/min. If this flow rate is reduced, the entrainment of magnetite out of the WHIMS may be reduced. There will be a compromise between an increase in flushing time versus a slower draining time and the number of washing cycles that can be performed. This is because the volume of the WHIMS is fixed and a washing cycle must occur within a specified period of time. Increasing both the flushing time and decreasing the outlet time may require a larger funnel.

In Chapter 6, the stability requirements in terms of particle coating with surfactant were discussed. The investigation into the optimum quantity of surfactant required for steric stabilisation showed that as the percentage oleic acid increases, the volume of magnetite remaining suspended above the ferrofluid appears to decrease. It is possible, however, that too high a percentage of oleic acid would result in a fluid of unacceptably high viscosity. It is recommended that an estimate be made of the volume of oleic acid molecules required to coat a magnetite particle of a certain diameter. An initial estimate of the maximum percentage surfactant required could then be established.

In the final chapter, Chapter 7, the use of a packed column for the peptization stage of the ferrofluid production was investigated. This chapter documented the procedure of mathematical optimisation using the dynamic trajectory method to determine the optimum dimensions of such a column that would result in maximum heat transfer. Various scenarios were investigated. It was found that in the simple case where the residence time and geometric diameter to height constraint is ignored the solution converges where the height and diameter of the column are a maximum and the bead diameter is a minimum. This would provide the greatest surface area thus promoting heat transfer and ensuring that the solid particles are transferred from the aqueous to the organic phase. The residence time in this case if the values of the variables obtained as a solution are substituted back into the equations would, however, result in a completely unacceptable residence time of over 16 hours. The resultant product would be viscous and much of the organic phase may have evaporated. When including the residence time considerations and the height to diameter ratio as an inequality constraint, various valid solutions were obtained for different starting values of the variables. This is because there are a number of combinations of height to diameter that would be below 2/3 that would still give the same surface area and acceptable residence time. When the height to diameter ratio is included as an equality constraint and when finite differences are used for calculation of the gradient, it is found that the column diameter would be approximately 0.39 m, the height would be approximately 0.59 m and the

bead diameter 5 mm. The bead diameter is at its smallest size to give the largest surface area. The surface area available for reaction is approximately 52.22 m^2. With the additional constraints, there is approximately 32 times less surface area available for reaction and heat transfer. An area for further study would be to consider the number of beads required to fill the column to be a discrete value. The bead diameter could also be considered a discrete variable, as the glass beads are available commercially in certain specific sizes. The problem could be reformulated accordingly. The column height and diameter are relatively flexible as a glass blower could manufacture a column to a required specification. It would, however, be cheapest to purchase a standard commercially available glass column.

In summary then, various aspects and key parameters of ferrofluid manufacture were discussed and investigated in this dissertation. Additional information was provided regarding the preferred parameters for the formation of magnetite, precipitate washing and concentration, the volume of surfactant required for coating magnetite particles and the optimum method for heat transfer in the peptization reaction. This information clarifies some of the aspects in the production of this fascinating substance.

REFERENCES

1. Jakubovics, J. P. (1994) *Magnetism and Magnetic Materials*, 2nd edition, The Institute of Materials, Cambridge University Press
2. Young, H. D. (1992) *University Physics*, 8th edition, Addison-Wesley Publishing Company, 770-771, 821-825
3. Krüger, L. (2002) *Preparation of ferrofluids - part 1: Magnetic properties of ultrafine magnetite particles*, De Beers Consolidated Mines, DebTech Technical Note 2002-03-11
4. Svoboda, J. (2002) Magnetism and magnetic properties, Personal communication, De Beers Consolidated Mines, DebTech Research Department
5. Department of Geological Sciences at the Mackay School of Mines, University of Nevada, Reno (2002) Types of magnetism http://mines.unr.edu/geology/Home/faculty_pages/Geol333/Types of Magnetism.ppt [October 2002]
6. Charles, S. W. and Popplewell, J. (1980) Ferromagnetic liquids, *Ferromagnetic Materials: A handbook on the properties of magnetically ordered substances*, Mag-16, 2, North-Holland Publishing Company, Amsterdam, 509-559
7. Rosensweig, R. E. (1985) *Ferrohydrodynamics*, Cambridge University Press
8. Wolfram Research Resource Library (2002) http://scienceworld.wolfram.com/chemistry/SpinelStructure.html [October 2002]
9. Buske, N., Sonntag, H. and Götze, T. (1984) Magnetic Fluids – their Preparation, Stabilisation and Applications in Colloid Science, *Colloids and Surfaces*, 12, 195-202
10. Dan's Data (2001) Rare earth magnets for fun and profit http://www.dansdata.com/magnets.htm#ff [October 2002]
11. Carolina Biological Supply Company (2002) http://www.carolina.com/physics/index.asp [October 2002]
12. Farkas, J. (1983) A Pilot-Plant Process for Manufacturing Kerosene-Base Ferromagnetic Fluid, *Separation Science and Technology*, 18 (9), 787-802
13. Svoboda, J. *et al.* (1996) *Experimental Investigation of Ferrohydrostatic Separation and Development of its Control System*, De Beers Consolidated Mines, Diamond Research Laboratory Report
14. Murariu, V. (2002) De Beers Consolidated Mines, Presentation for DebTech Technical Seminar
15. Nogita, S., Takashi, I., et al. (1977) Recovery of Nonferrous Metals using Magnetic Fluid Techniques, *Hitachi Review*, 26, 4, 139-144
16. Gribanov, N. M., Bibik, E. E., et al. (1990) Physico-Chemical Regularities of Obtaining Highly Dispersed Magnetite by the Method of Chemical Condensation, *Journal of Magnetism and Magnetic Materials*, 85, Elsevier Science Publishers, 7-10
17. Rosensweig, R. E., *Magnetic Fluids*, 124-132
18. Krüger, L. (2002) *Preparation of ferrofluids - part 2: Colloidal stabilisation of ultrafine magnetite particles*, De Beers Consolidated Mines, DebTech Technical Note 2002-03-12
19. Vibrating Sample Magnetometer Model LDJ 9600 Operation Manual (1997) LDJ Model Electronics, Inc., 1280 E. Beaver Rd, Troy, Michigan 48083, USA
20. Baran, A. S. (1999) *Determination of particle size distribution in ferrofluids from magnetisation curve*, De Beers Consolidated Mines, DebTech Technical Note 1999-01-08
21. Cornell, R. M. and Schwertmann, U. (1997) *The Iron Oxides*, John Wiley & Sons

22. Misawa, T., Hashimoto, K. and Shimodaira, S. (1973) *J. Inorg. Nucl. Chem.*, 35, 4167-4174
23. Krüger, L. (2002) *Preparation of ferrofluids - part 3: Synthesis of ferrofluid*, De Beers Consolidated Mines, DebTech Technical Note 2002-03-20
24. Sugimoto, T. and Matijevic, E. (1980) *J. Colloid Interface Sci.*
25. Regazzoni, A. E., Blesa, M. A. and Maroto, A. J. G. (1983) *J. Colloid Interface Sci.*
26. Blesa, M. A. and Matijevic, E. (1989) *J. Colloid Interface Sci.*
27. Reimers, G. W. *et al.* (1974) *Production of magnetic fluids by peptization techniques*, US Patent 3,843,540
28. Krüger, L. (2002) Mechanism of magnetite formation, Personal communication, De Beers Consolidated Mines, DebTech Research Department
29. Jolivet J. P., Tronc E. et al. (1994) Formation of Magnetic Spinel Iron Oxide Solution, *NATO ASI Series E Applied sciences*, 260, 45-48, Kluwer
30. Fraunhofer Institute for Manufacturing and Advanced Materials (2001) Diagram of sedimentation funnels, Wiener Straße 12, 28359 Bremen, Germany
31. Fofana, M. (2001) Modeling of sedimentation funnel, De Beers Consolidated Mines, DebTech Research Department
32. Craig, K. (2001) Computational Fluid Dynamics MBV 780, Department of Mechanical and Aeronautical Engineering, University of Pretoria
33. CFX (2001) Help files
34. Svoboda, J. (1987) Developments in Mineral Processing, *Magnetic Methods for the Treatment of Minerals*, 8, Amsterdam: Elsevier Science Publishers B.V.
35. Vatta, L. L. and Svoboda, J. (2002) *Preparation of ferrofluid part 6: Washing of ultrafine magnetite particles using a high gradient magnetic washing device*, De Beers Consolidated Mines, DebTech Technical Note 2002-03-12
36. Reimers G. W. and Khalafalla S. E. (1972) Preparing magnetic fluids by a peptizing method, *Bureau of Mines Innovative Processes in Extractive Metallurgy Program Technical Progress Report*, 59, U.S. Department of the Interior, Twin Cities Metallurgy Research Center
37. Khalafalla S. E. and Reimers G. W. (1980) Preparation of dilution-stable aqueous magnetic fluids, *IEEE Transactions on Magnetics*, Mag-16, 2, 178-183
38. Levenspiel, O. (1972) *Chemical Reaction Engineering*, 2nd edition, John Wiley and Sons, New York, 219 – 221
39. Snyman, J. and Craig, K. (1999) *Practical Mathematical Optimisation for Engineers and Scientists*, Multidisciplinary Design Optimisation Group, Department of Mechanical and Aeronautical Engineering, University of Pretoria
40. Snyman, J. (2001) Mathematical Optimisation MWO 780 notes, Department of Mechanical and Aeronautical Engineering, University of Pretoria
41. Levenspiel, J. M. (1981) *Chemical Engineering Kinetics*, 3rd edition, Mc-Graw Hill Book Company, 334
42. Seider, W. D., Seader, J. D. and Lewin, D. R. (1999) *Process Design Priniciples Synthesis, Analysis and Evaluation*, Wiley & Sons, New York
43. Snyman, J. (1997) LFOPCON Version 3 – LFOPCV3 General Mathematical Programming Code, Department of Mechanical and Aeronautical Engineering, University of Pretoria

APPENDIX

Source code for optimisation of surface area with residence time and geometric constraints

```
C**** SPECIFY NUMBER OF VARIABLES N ***********************************C
C                                                                       C
      N=3
C                                                                       C
C*****SPECIFY STARTING POINT (INITIAL GUESS) : X(I), I=1,N ************C
C                                                                       C
      X(1)=0.38016051d0
      X(2)=0.5d0
      X(3)=0.63872483d0
C                                                                       C
C*****SPECIFY NUMBER OF INEQUALITIES NI (NI=0 IF NONE)*****************C
C                                                                       C
      NI=10

C                                                                       C
C*****SPECIFY NUMBER OF EQUALITIES NE   (NE=0 IF NONE)*****************C
C                                                                       C
      NE=0
C                                                                       C
C***********************************************************************C
C               ONLY REQUIRED FOR CONSTRAINTS                           C
C     SPECIFY PENALTY FUNCTION PARAMETERS : XMU & XMUMAX                C
C                                                                       C
C     STANDARD SETTINGS :  XMU=100.0  ;  XMUMAX=10000.0                 C
C                                                                       C
C***********************************************************************C
C                                                                       C
      XMU=1.D2
      XMUMAX=1.D4
C                                                                       C
C***********************************************************************C
C     SPECIFY CONVERGENCE CRITERIA TOLERANCES : EG & XTOL               C
C                                                                       C
C     CODE TERMINATES IF                                                C
C               || X(CURRENT STEP) - X(PREVIOUS STEP)|| < XTOL          C
C     OR                                                                C
C               || GRADIENT VECTOR OF PENALTY FUNCTION || < EG          C
C***********************************************************************C
C                                                                       C
      XTOL=1.D-9
      EG=1.0D-8
C                                                                       C
C***********************************************************************C
C     SET MAXIMUM STEP SIZE : DELT                                      C
C                                                                       C
C     DELT SHOULD BE OF THE SAME ORDER OF MAGNITUDE AS THE "DIAMETER"   C
C     OF THE REGION OF INTEREST : DELT = SQRT(N)*VARIABLE-RANGE         C
C***********************************************************************C
C                                                                       C
      DELT=1
C                                                                       C
C***********************************************************************C
C     SPECIFY MAXIMUM NUMBER OF STEPS PER PHASE (THREE PHASES: 0,1&2)   C
C     ONE STEP = EVALUATION OF ONE SET OF GRADIENTS = ONE DER CALL      C
C***********************************************************************C
C                                                                       C
      KMAX=100000
C                                                                       C
C***********************************************************************C
C    IPRINT CONTROLS PRINTING : PRINTING OCCURS EVERY ]IPRINT] STEPS.   C
C         IPRINT=KMAX+1:PRINTING ON STEP 0 AND ON EXIT ONLY.            C
C     VALUES OF X SUPPRESSED ON INTERMEDIATE STEPS IF IPRINT.LT.0       C
C***********************************************************************C
```

```
C                                                                       C
      IPRINT= 10
C                                                                       C
C***********************************************************************C
C     USER SPECIFIED SUBROUTINE                                         C
C                                                                       C
      SUBROUTINE FUN(N,X,F)
C                                                                       C
C     COMPUTE OBJECTIVE FUNCTION : F                                    C
C                                                                       C
C***********************************************************************C
      implicit real*8 (a-h,o-z), integer (I-N)
      real pi,epsilon,a,vb,V,num,SA
      dimension X(N)

      pi=3.141595d0
      epsilon = 0.4d0

      F =(-1.d0*3*pi*(X(1)**2.d0)*X(3)*(1.d0-epsilon))/(200.d0*X(2))
      return
      end

C***********************************************************************C
C     USER SPECIFIED SUBROUTINE                                         C
C                                                                       C
      SUBROUTINE CONIN(N,NI,X,C)
C                                                                       C
C     COMPUTE INEQUALITY CONSTRAINT FUNCTIONS                           C
C                                                                       C
C***********************************************************************C
      IMPLICIT REAL*8 (A-H,O-Z),INTEGER(I-N)
      real pi,X1min,X1max,X2min,X2max,X3min,X3max
      DIMENSION X(N),C(NI)

      pi=3.141595d0
      epsilon = 0.4d0

      X1min = 0.1d0
      X1max = 1.0d0
      X2min = 0.5d0
      X2max = 7.5d0
      X3min = 0.1d0
      X3max = 3.0d0

      C(1)  = X(1) - X1max
      C(2)  = X1min - X(1)
      C(3)  = X(2) - X2max
      C(4)  = X2min - X(2)
      C(5)  = X(3) - X3max
      C(6)  = X3min - X(3)
      C(7)  = X(2) - 100*X(1)
      C(8)  = (X(1)**2)*X(3) - 0.116/(pi*epsilon)
      C(9)  = 0.058/(pi*epsilon) - (X(1)**2)*X(3)
      C(10) = X(1)/X(3) - (2d0/3d0)


      RETURN
      END
C***********************************************************************C
C     USER SPECIFIED SUBROUTINE                                         C
C                                                                       C
      SUBROUTINE CONEQ(N,NE,X,H)
C                                                                       C
C     COMPUTE EQUALITY CONSTRAINT FUNCTIONS                             C
C                                                                       C
C***********************************************************************C
      IMPLICIT REAL*8 (A-H,O-Z),INTEGER(I-N)
      DIMENSION X(N),H(NE)
C
c-----------no eq constr
c
```

```
      RETURN
      END
C*********************************************************************C
C     USER SPECIFIED SUBROUTINE                                       C
C                                                                     C
      SUBROUTINE GRADF(N,X,GF)
C                                                                     C
C     COMPUTE THE GRADIENT VECTOR OF THE OBJECTIVE FUNCTION W.R.T.    C
C     THE VARIABLES X(I) : GF(I),I=1,N                                C
C                                                                     C
C*********************************************************************C
      IMPLICIT REAL*8 (A-H,O-Z),INTEGER(I-N)
      DIMENSION delx(N),X(N),GF(N),Xst(N)
      open(unit=3,file='history.out',status='unknown')
      pi=3.141595d0
      epsilon = 0.4d0
c start save to output
      F =(-1.d0*3*pi*(X(1)**2.d0)*X(3)*(1.d0-epsilon))/(200.d0*X(2))
      f0=F
      write(3,123)f0,X(1),X(2),X(3)
c   to save to output
      GF(1) = -1.d0*3.d0*pi*X(1)*X(3)*(1-epsilon)/(100d0*X(2))
      GF(2) = 3d0*pi*(X(1)**2)*X(3)*(1-epsilon)/(200d0*(X(2)**2))
      GF(3) = -1d0*3d0*pi*(X(1)**2)*(1-epsilon)/(200d0*X(2))
  123 FORMAT(4E13.6)
      RETURN
      END
C                                                                     C
C*********************************************************************C
C     USER SPECIFIED SUBROUTINE                                       C
C                                                                     C
      SUBROUTINE GRADC(N,NI,X,GC)
C                                                                     C
C     COMPUTE THE GRADIENT VECTORS OF THE INEQUALITY CONSTRAINTS CJ   C
C     W.R.T. THE VARIABLES X(I) : GC(J,I), J=1,NI I=1,N               C
C                                                                     C
C*********************************************************************C
      IMPLICIT REAL*8 (A-H,O-Z),INTEGER(I-N)
      DIMENSION X(N),GC(NI,N),Xst(N)

      GC(1,1)  =  1d0
      GC(2,1)  = -1d0
      GC(3,2)  =  1d0
      GC(4,2)  = -1d0
      GC(5,3)  =  1d0
      GC(6,3)  = -1d0
      GC(7,1)  = -100d0
      GC(7,2)  =  1.d0
      GC(8,1)  =  2d0*X(1)*X(3)
      GC(8,3)  =  X(1)**2
      GC(9,1)  = -2d0*X(1)*X(3)
      GC(9,3)  = -1d0*(X(1)**2)
      GC(10,1) =  1d0/X(3)
      GC(10,3) = -1d0*X(1)/(X(3)**2)

      RETURN
      END
C                                                                     C
C*********************************************************************C
C     USER SPECIFIED SUBROUTINE                                       C
C                                                                     C
      SUBROUTINE GRADH(N,NE,X,GH)
C                                                                     C
C     COMPUTE THE GRADIENT VECTORS OF THE EQUALITY CONSTRAINTS HJ     C
C     W.R.T. THE VARIABLES X(I) : GH(J,I), J=1,NE I=1,N               C
C                                                                     C
C*********************************************************************C
      IMPLICIT REAL*8 (A-H,O-Z),INTEGER(I-N)
      DIMENSION X(N),GH(NE,N)
C
c--------------no eq
```

```
C
      RETURN
      END
C                                                                       C
C*************************************************************************C
C                            FINISH                                       C
C*************************************************************************C
```